TD

Computing Self-Sustainment Voltages in High Pressure Air

DOCTORAL THESIS

Rui Manuel dos Santos Almeida
DOCTORATE IN PHYSICS

UNIVERSIDADE da MADEIRA
A Nossa Universidade
www.uma.pt

October | 2024

Computing Self-Sustainment Voltages in High Pressure Air

DOCTORAL THESIS

Rui Manuel dos Santos Almeida
DOCTORATE IN PHYSICS

SUPERVISORS
Mikhail S. Benilov
Pedro G. C. Almeida

Dedicated to my parents Clarinda and Hermínio,
who's loving care I will never be able to repay.

Acknowledgements

I want to thank both my supervisors for guiding this research to its fruitful outcome. I'm grateful to Professor Mikhail Benilov as my former university teacher and senior colleague, for laying out a clear work-path and for invaluable contributions and discussions, as well as for his balanced measure between demanding results and extending helpful advice. Above all I appreciate his patience, as I have put it through thorough testing. I'm grateful to my second supervisor, Professor Pedro Almeida, as my former university student, I'm sure a peculiar situation(!), for his enduring support and insight, his constant readiness to help and for refocusing, time and again, my efforts when I strayed off-track. Also, a special thanks to him for drawing me back to the academia to do science. On several occasions have they alluded to medieval torture instruments, but somehow I came out unscathed. I highly value both their friendship.

I have reveled in the privilege of being able to work in the challenging but friendly environment they have promoted in the IPFN research group at Madeira University.

I further want to thank Professor Naidis for his collaboration, in particular his always prompt readiness to clarify issues and for all his helpful suggestions. A special thanks to Diego and Nuno from whose far vaster numerical experience with COMSOL, I've received valuable help on innumerable occasions during the research. I would also like to thank my colleagues, Nelson and Mário, for their companionship and friendly words in our weekly meetings, whether in discussing physics or software issues.

To my wife, Tânia for her support and for sometimes having to cope with my alienated presence. To João and David my two beloved sons who, though shining from afar, fill me with contentment. Though in the firm grip of ignorance as I cling to appearances as real, I aspire to recognize all as 'the illusory display of the unity of unborn emptiness and interdependent origination'. To this vision I pay homage.

Preamble

The work leading to this thesis was performed within activities of:

- Projects Pest-OE/UID/FIS/50010/2019, UIDP/50010/2020 and UIDB/50010/2020 of IPFN - Instituto de Plasmas e Fusão Nuclear, supported by FCT - Fundação para a Ciência e Tecnologia, I.P.
- Research Fellowship PlasMa/BI/2019-3 under project PlasMa-M1420-01-0145-FEDER-000016 *PlasMa: teoria e simulação avançada de plasmas relevantes para aplicações energéticas*, co-financed by the Operational Program of the Autonomous Region of Madeira 2014-2020.
- Research Fellowship BI/2023-2 in the framework of the projects of IPFN - Instituto de Plasmas e Fusão Nuclear, supported by the Industrial Project *Modes of current transfer to cathodes* from the Physics Department of Madeira University.

Most of the results presented in this thesis are published in the following articles:

- P. G. C. Almeida, R. M. S. Almeida, N. G. C. Ferreira, G. V. Naidis, and M. S. Benilov, "Simple computation of ignition voltage of self-sustaining gas discharges", Plasma Sources Science and Technology, vol. 29, no. 12, pp. 125005-1-6 (2020).
- M. S. Benilov, P. G. C. Almeida, N. G. C. Ferreira, R. M. S. Almeida and G. V. Naidis, "A practical guide to modeling low-current quasi-stationary gas discharges: Eigenvalue, stationary, and time-dependent solvers", Journal of Applied Physics, vol. 130, no. 12, pp. 121101 (2021).
- R. M. S. Almeida and P. G. C. Almeida and G. V. Naidis and M. S. Benilov, "Validation of the Townsend criterion for ignition of volume gas discharges", Plasma Sources Science and Technology, vol. 32, no. 10, pp. 105014 (2023).

Results presented in this thesis were reported at the following conferences:

- R. M. S. Almeida, P. G. C. Almeida, G. V. Naidis and M. S. Benilov,"Self-sustainment voltage calculations in cylindrical device with dielectric spacer at 1 atm", Conference Poster at the '25th Europhysics Conference on Atomic and Molecular Physics of Ionized Gases' (ESCAMPIG 2022), 19-23 July 2022, Paris, France.

- R. M. S. Almeida, P. G. C. Almeida, G. V. Naidis and M. S. Benilov, "Validating Townsend criterion for the ignition of volume electrical discharges", accepted conference poster for the '35th International Conference on Phenomena in Ionized Gases' (ICPIG 2023), 9-14 July, Egmond aan Zee, The Netherlands.
- R. M. S. Almeida, P. G. C. Almeida, G. V. Naidis and M. S. Benilov, "Breakdown characterization in device with dielectric spacer in air at 1 atm", accepted conference poster for the '35th International Conference on Phenomena in Ionized Gases' (ICPIG 2023), 9-14 July, Egmond aan Zee, The Netherlands.
- R. M. S. Almeida, N. G. C. Ferreira, P. G. C. Almeida, G. V. Naidis and M. S. Benilov, "Dynamics of Breakdown along a Dielectric Surface in Air at 1 atm", Book of abstracts of the '26th Europhysics Conference on Atomic and Molecular Physics' (ESCAMPIG 2024), pag. 129-130, 9-13 July 2024, Brno, Czech Republic.
- R. M. S. Almeida, P. G. C. Almeida, H. Kaufmann and M. S. Benilov, "Fast Calculation Tool for Breakdown Voltage in a setup with a Dielectric Surface", Book of abstracts of the '26th Europhysics Conference on Atomic and Molecular Physics' (ESCAMPIG 2024), pag. 304-305, 9-13 July 2024, Brno, Czech Republic.

Resumo

Este trabalho propõe um método para avaliar tensões de disrupção de descargas de baixa corrente e alta pressão em configurações com fraca não-uniformidade do campo.

Todas as configurações estudadas, compostas por dois elétrodos separados por um espaçamento, foram construídas utilizando um pacote de software baseado no método numérico de elementos finitos. As equações do modelo de fluido foram configuradas para modelizar ar a 1 atm presente no espaçamento, com um esquema simplificado de processos químicos de plasma envolvendo eletrões, um ião positivo e três iões negativos.

O critério de Townsend para a determinação da tensão de auto-sustentação é matematicamente alargado a descargas multidimensionais. O critério alargado, baseia-se na análise da descarga ao longo das linhas de campo elétrico. No entanto, o novo critério continua a ser válido apenas para configurações com gases eletronegativos dominados pela deriva.

Este trabalho propõe uma abordagem mais geral para a obtenção da descarga autónoma, válida também para gases eletropositivos e/ou onde a difusão pode ser significativa. Esta abordagem foi designada de 'método de ressonância' e pode ser aplicada a descargas quase-estacionárias de baixa corrente em gases a pressão elevada. O método baseia-se no reconhecimento de que o sistema de equações de fluidos é linear na ignição da descarga e que a sua solução constitui um problema de valores próprios sendo a tensão aplicada o valor próprio. É estabelecido um procedimento sistemático para a obtenção da descarga autónoma. Cada passo baseia-se em cálculos estacionários. O método proposto permitiu investigar a relação entre as tensões de auto-sustentação e de disrupção.

É dada especial atenção a uma configuração simples que modeliza um interruptor. Para esta configuração axissimétrica, o método de ressonância calculou duas tensões de auto-sustentação utilizando duas condições fronteira sobre o dielétrico. A modelização não-estacionária calculou duas tensões de disrupção; a tensão de primeira-disrupção e a de disrupção-repetitiva, resultantes de duas condições iniciais. Os cálculos não-estacionários basearam-se na utilização da tensão de auto-sustentação, previamente calculada pelo método de ressonância. Os resultados mostram que, com condições de fronteira adequadas, as tensões de auto-sustentação concordam com as tensões de disrupção calculadas. Este acordo traduz-se numa redução significativa do tempo computacional necessário para estimar a tensão de disrupção de uma configuração.

Palavras chave: Descargas de baixa corrente quasi-estacionárias. Ignição de

descarga autónoma. Método de ressonância. *Solvers* estacionários. Primeira-disrupção. Disrupção-repetitiva.

Abstract

This work proposes a method for evaluating breakdown voltages of low-current, high-pressure discharges in setups with weak field non-uniformity.

All studied setups, composed of two electrodes separated by a gap, were constructed using a numerical finite element method software package. Fluid model equations were coded to model air at 1 atm filling the gap, with a simplified scheme of plasmachemical processes involving electrons, a positive ion and three negative ions.

The Townsend criterion for determining the self-sustainment voltage, is mathematically extended to multidimensional discharges. The extended criterion is based on analyzing the discharge along electric field lines. The new criterion is still, however, only valid for setups with drift dominated electronegative gases.

This work proposes a more general approach for obtaining the self-sustaining discharge, valid also for electropositive gases and/or where diffusion may be significant. This approach is called the 'resonance method' and is applicable to low-current quasi-stationary discharges in high-pressure gases. The method is based on recognizing that the system of fluid equations is linear at discharge ignition, and that its solution constitutes an eigenvalue problem with the applied voltage being the eigenparameter. A systematic procedure is laid out to obtain the self-sustaining discharge. Each step of the procedure is based on stationary calculations. The proposed method allowed to research the relation between self-sustainment and breakdown voltages.

Special attention is given to a simple setup modeling a circuit-breaker. For this axi-symmetric setup, the resonance method, using two boundary conditions over the dielectric, calculated two self-sustainment voltages. Non-stationary modeling, using two initial conditions, calculated two breakdown voltages; the first-breakdown and repetitive-breakdown voltages. The non-stationary calculations relied on using the self-sustainment voltages as calculated by the resonance method. Results show that, with the proper boundary conditions, the self-sustaining voltages agree well with the obtained breakdown voltages. This agreement translates into a significant reduction of the computational time needed to estimate the breakdown voltage of a setup.

Keywords: Low-current quasi-stationary discharge. Ignition of self-sustaining discharge. Resonance method. Stationary solvers. First-breakdown. Repetitive-breakdown.

Contents

List of Figures

Chapter 1

Introduction

1.1 Gas discharges

In the late nineteenth century, the simple setting of a sealed glass tube with two electrodes and filled with a gas allowed researchers to undertake a systematic experimental study of the behavior of electrical discharges in gases. Johann Wilhelm Hittorf, a German physicist, observed that when a high voltage was applied to a gas-filled tube, an electrical discharge would occur across the electrodes, associated with the ionization of the gas and emission of light. He also observed that the characteristics of the discharge, such as its color and shape, could be influenced by the type of gas and the pressure inside the tube. Building on Hittorf's work, other researchers began to explore the relation between the voltage applied to a gas-filled tube and the characteristics of the resulting discharge. In 1889 Friedrich Pashen found that there was a critical voltage at which the discharge would become self-sustaining. He observed the non-monotonic dependence of this ignition-voltage in parallel-plate gaps with varying gap and pressure. J.J. Thomson identified the observed cathode rays that would make the glass behind the anode glow, as being made up of a new particle, the electron(1897). This was also the time when Thomas Edison perfected a carbon filament between electrodes creating the first durable and economic light bulb (1880). It was a time of prolific experimental developments made by many scientists, the time when electricity started its ever ascending importance, driving society into our electrified modernity.

Coincidence or not, the late nineteenth century also saw the development of powerful theoretical tools for the field of gas discharges. In 1872 Boltzmann derived a nonlinear integro-differential equation capable of describing a weakly ionized gas at the microscopic level. Not long after, in 1903, another set of equations was being used, e.g. [1], to describe the flux of charged particles as composed of a drift term due to an electric field, and a diffusion term due to concentration gradients. These latter

equations were shown by Chapman and Enskog, in 1916-1917, to be derivable from the Boltzmann equation under certain conditions known as the drift-diffusion approximation. The equations of continuity together with the drift-diffusion approximation for the particle flux, still form one of the main resources for studying the transport of charged particles in gases.

The ever increasing demand for electrical power has carried since its inception a challenge: how to prevent breakdown, i.e. prevent a large quantity of charge from abruptly flowing out of a conductor, through an insulator, to a position of lower potential? This challenge is still at the forefront of the technological development. Energy transmission and distribution across long distances, like from renewable offshore wind farms, is done through high voltage direct current (HVDC) cables which can be buried or run over the seabed. The conductor is held at the center of the coaxial cable by dielectric spacers in a gas, this setting is called a Gas Insulated Line (GIL) [2–5]. Another prospective application of HVDC is in More Electrical Aircraft (MEA) research, that aims to develop solutions for more energy efficient and environmentally sustainable commercial flying. In this field, one of the identified enabling technologies is the development of high breakdown-strength insulation materials [6, 7].

When a section of the energy grid of a city, an airport, a heavy industry, wind turbines, down to an individual household appliance, needs to be shut down for whatever reason, a circuit breaker is needed. A circuit breaker is an automatically operated electrical switch designed to protect an electrical circuit from damage caused by overload or short circuit. Its basic function is to detect a fault condition and interrupt current flow. These switches come in different sizes and shapes depending on their purpose. For instance the one in Fig. 1.1 is used in rail infrastructure, automotive factories, stadiums and power generation plants, to mention just a few applications.

Prospects for an ever enhanced performance of these devices require a thorough understanding of the physics of the breakdown phenomenon. What is the proper definition of breakdown, where and how does breakdown happen, what type of insulation breaks down, is it the gas, the dielectric, or both, do the insulator properties vary in time? What range of applied voltages and temperatures are to be considered? It can be a formidable task to detail the kinetics of the gas or the bulk and surface properties of the dielectric and conductor.

1.1.1 Ignition voltage and avalanches

In discharge setups powered by DC voltages that have an electric field that is uniform (like between parallel-plates), or weakly non-uniform, and where the current is low, the discharge is called the Townsend, or dark, discharge. In principle, there exists a

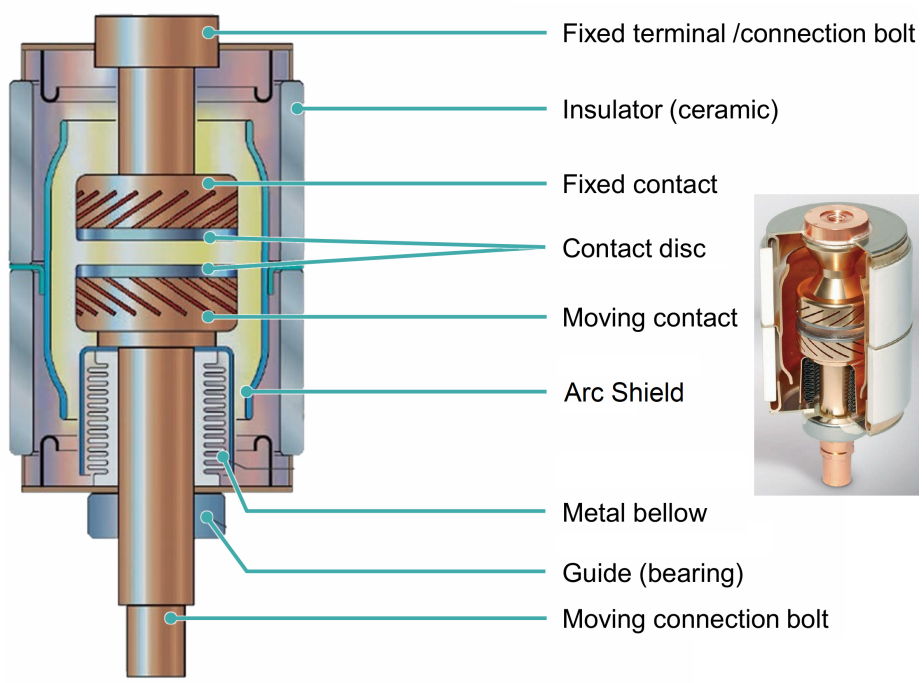

Figure 1.1: Diagram of an industrial low and medium-voltage circuit breaker. Taken from Siemens AG catalog.

minimum voltage at which the discharge becomes self-sustained. This, however, does not mean that the considered setup won't have a stable discharge at lower voltages, it means that for the lowest possible current, this is the lowest possible voltage. Different terms are used for this voltage, like ignition, inception or self-sustainment voltage, and it corresponds to the voltage needed to maintain a steady gain-loss balance of charges.

The physical mechanism in terms of which ignition is explained, is called an avalanche, see Fig. 1.2. One single electron ejected from the cathode or created in the volume, for instance by a cosmic ray, accelerates in the electric field to an energy sufficient to ionize a neutral atom or molecule and, on collision, creates one more electron. Both electrons are again accelerated and repeat the process so that after a distance x there will be $\exp(\alpha x)$ electrons, hence the term 'avalanche'. Here α is the amount of ionizations per unit length. At the ignition-voltage in a uniform field, if a seed electron is created and if it manages to gain energy to start an avalanche, then sufficient positive ions are created that can drift and strike the cathode to eject secondary emission electrons, originating the next avalanche in a positive feedback cycle. As a result of this, sufficient charge can be created to make the discharge sustainable. At ignition however space-charge is negligible and the magnitude of the electric field of the local charges is much lower than the background field due to the electrodes.

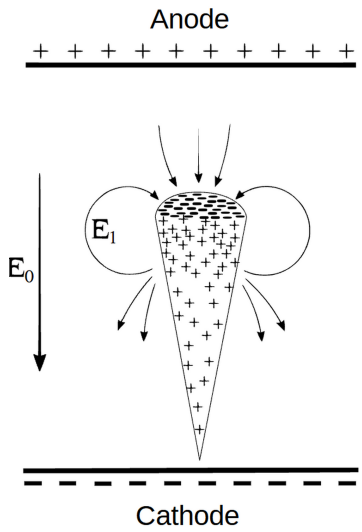

Figure 1.2: Schematic depiction of the avalanche process. '-' represent electrons; '+' positive ions; $\mathbf{E}_0$ background field due to electrodes; $\mathbf{E}_1$ local field due to space-charge. Here $|\mathbf{E}_1| \ll |\mathbf{E}_0|$.

In the simplest configuration of parallel-plates with just positive ions and electrons, neglecting photoionization and diffusion, the following expression for the current can be obtained

$$I = I_0 \frac{\exp(\alpha d)}{1 - \gamma\left[\exp(\alpha d) - 1\right]} \tag{1.1}$$

where I_0 is the electron current leaving the cathode, α the number of ionizations per unit length in the direction of the electric field, γ the effective secondary electron emission coefficient from the cathode, and d the gap distance. The condition for a self-sustained discharge is obtained equating the denominator of (1.1) to zero. The resulting criterion is known as the Townsend criterion and can be written as,

$$\alpha d = \ln\left(1 + \frac{1}{\gamma}\right) \tag{1.2}$$

This criterion depends only on global features of the particular discharge, and it is through the empirical dependence of α on the electric field for the particular gas, that the ignition-voltage can be calculated. The right hand side (rhs) of (1.2) is dependent on γ through a logarithm and can be considered a constant for Townsend discharges. This expression doesn't take into account negative ions nor detachment reactions. For ignition αd is typically within the range $8 - 10$ [8].

Eq. (1.2) cannot be used in cases where the field distribution is not uniform. However, with a slight modification, it can still be used to estimate the ignition-voltage for discharges in setups where the electric field non-uniformity is located at the cathode,

called negative corona discharges. To do this the left hand side (lhs) of Eq. (1.2) has to be rewritten to account for a non-uniform electric field,

$$K = \int_L \alpha d\ell \tag{1.3}$$

where the integration is along the path between the electrodes that maximizes this integral, called the ionization integral. For discharges in setups where the field non-uniformity is at the anode, called positive corona discharges, secondary electrons are mainly created through photoionization in the volume close to the anode tip and not through secondary electron emission from the cathode. Positive coronas have filamentary luminous channels propagating till some distance from the anode tip. For positive coronas the ignition-voltage can be estimated by assigning to K a value in the range $18-20$ [9]. This is an empirical procedure and is therefore subject to significant error.

Early experimentalists noticed that to get a discharge started in a parallel-plate setup in parallel with a voltage source and resistor, an initially higher voltage needed to be applied, 603 V in [10](Chapter XI, sec. 292), which was called the sparking potential. Once the current started to flow, the voltage needed to keep the discharge steady, would drop to 350 V. This would be the ignition, or self-sustainment voltage. The discharge setup is usually in series with a ballast to keep the current low. Charges produced by residual ionization from the environment or cosmic radiation are energized in the electric field, initiating a self-sustained discharge. It was also noted that other sources of ionization like X-Rays, radioactivity, or irradiating the cathode with UV light, could initiate the discharge [10](Chapter X, sec. 233). The purpose is clear: to provide an initial aid to get the discharge started.

1.1.2 Breakdown voltage and streamers

If, in a certain DC powered setup with relatively uniform electric field, the voltage is raised above the ignition-voltage, and if the current is allowed to freely increase, then there will be breakdown. Breakdown is here understood as a process distinct from electron avalanches, mainly because experimentally breakdown was seen to happen much faster than could be accounted for by the avalanche process. Like avalanches, it is a transient situation, however now the applied voltage leads to a dramatic decrease of the setup's resistance, allowing charge to escape the stressed conductor to a lower potential. The lowest voltage that brings about this transition, is called the breakdown or hold-off voltage. The term 'breakdown' means a transition from low- to high-current discharge, accompanied by a sharp decrease of the discharge voltage. Experimentally this transition, which may imply very high final currents, can also be identified by

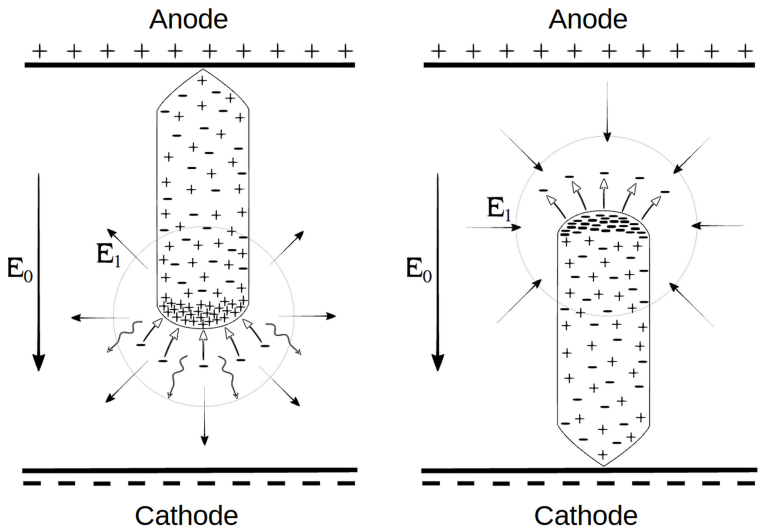

Figure 1.3: Schematic depiction of two types of streamers. a) Positive streamer b) Negative streamer. '-' represent electrons; '+' positive ions; '⇝' represent photons; $\mathbf{E}_0$ background field due to electrodes; $\mathbf{E}_1$ local field due to streamer head. Here $|\mathbf{E}_1| \gtrsim |\mathbf{E}_0|$

high-speed photography as a luminous channel closing the gap and may lead to the degradation of the setup due to joule heating. The physical phenomenon that causes the luminous channel and breakdown is called a streamer. In the case of a setup with a non-uniform field and likewise no restriction on current increase, there may be so called partial discharges with audible crackling sounds, where a streamer only partially bridges the gap. There may also be stable corona discharges at voltages above the ignition-voltage and up to the breakdown voltage. In the field of high-voltage insulation, breakdown is an unwanted destructive process and much of the ongoing research is on how to prevent it, or at least how to design setups that better withstand breakdown. Partial breakdown phenomena or corona discharges, are purposefully exploited in various other industrial applications, such as high-speed printing devices, paint sprayers, photocopiers, ozone generators, systems of air and water cleaning, micromachines and electrostatic microspray, flow control over flight surfaces, in-flight removal of unwanted electric charges from the surface of aircraft or in handling waste or water treatment [8, 11–13], to mention just a few.

The breakdown mechanism was put forth by Meek[14], Loeb[15] and Raether[16]. Successive electron avalanche processes described in Sec. 1.1.1, can give rise to a space-charge buildup with significant distortion of the background electric field in the vicinity of the avalanche head, see Fig. 1.3. This space-charge locally enhances the electric

field, which strongly influences ionization by electron impact and photoionization in front of the avalanche head, that in turn creates more space-charge. This process constitutes a positive feedback, making, under certain conditions, the avalanche head propagate in a fairly autonomous way. It is this formation that is called a streamer. The self-sustained character of a streamer, allows for it to travel into regions where the background field is small. There are positive streamers that move toward the cathode and negative streamers that move toward the anode. In experiment, streamer propagation leaves in its wake a filamentary plasma channel of high conductivity. The transition from avalanche to streamer occurs when the local field created by the space-charge in the streamer head is of the same order of magnitude as the background field. Both positive and negative streamers advance as a result of multiple electron avalanches in the streamer front, but the exact mechanisms are different. Negative streamers advance due to a high outward acceleration of electrons in the negatively charged streamer head, creating numerous electron avalanches directed away from the negative streamer head [14]. Positive streamers, on the other hand, propagate as a result of electrons attracted to the positively charged streamer head. These electrons originate mainly from the region in front of the streamer due to photoionization, producing multiple avalanches directed towards the positive streamer head. Both negative and positive streamers are a type of ionization wave, where propagation is a result of the region in front of the streamer head gradually becoming the region with highest space-charge. Streamer velocities are therefore not directly connected to electron drift, but can vary from electron drift velocity to 10% the speed of light. In air at atmospheric pressure, typical velocities are of the order $0.1-10\,\mathrm{mm/\,ns}$ but vary with the electric field [17–19].

It is standard engineering practice, to estimate the breakdown voltage resorting to the empirical procedure of prescribing to K, in (1.3), a value in the range $18-20$. This is the same range as for positive corona ignition, however for streamer breakdown the electron density should be at least $10^{18}\,\mathrm{m}^{-3}$ [20]. Others have prescribed different values of K to distinguish Townsend avalanche, Streamer, Corona and Arc breakdown discharges [9, 21]. It should be noted that in certain conditions the breakdown voltage coincides with the voltage of ignition of a self-sustaining discharge; e.g., [22].

For air at atmospheric pressure, a typical streamer inception field strength is $26\,\mathrm{kV/\,cm}$. Once a streamer is generated, the critical field needed to keep a positive streamer propagating in air is $4.4\,\mathrm{kV/\,cm}$ [23], and for a negative streamer the critical field is $2-3$ times higher [17, 20]. The growth, decay, and stable propagation of streamers is according to [17] controlled not solely by the external field but also by the physical dimensions of streamers. In particular, the streamer radius required for stable propagation is inversely proportional to the external field, with larger and

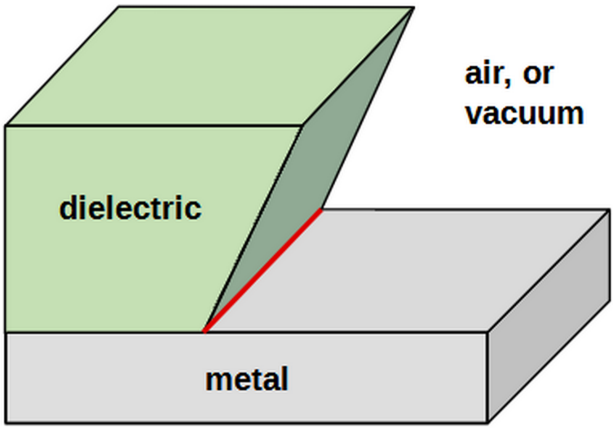

Figure 1.4: Schematic depiction of the triple junction (marked in red) between a dielectric volume, a metal volume, and a gaseous or vacuous volume.

smaller initial radii leading to, respectively, growing and decaying streamers.

1.1.3 Discharges along surfaces, Flashovers

When the setup includes a dielectric along the discharge path between the electrodes, breakdown is also called surface flashover, indicating that a conduction channel was created over the dielectric surface accompanied by the emission of a flash of light. The flashover sequence can generically be subdivided into three stages, an initial stage, a development stage, and the final discharge stage. In the initial stage, surface flashover of an insulator is believed to be due to field emission from the cathode. The emitted amount of electrons increases exponentially in the development stage through ionization, secondary electron emission from the dielectric surface, or other processes. Eventually, the final discharge stage occurs with a complete breakdown. At every stage the shape of the electrodes and insulators and insulator material are considered to be important, in particular for the electric field distribution. There is an overall consensus on the mechanisms operating in the first stage of surface flashover, namely field emission from cathode protrusions or the triple junction, which refer to the area where the insulator, the electrode, and the vacuum or air are in contact, see Fig. 1.4. The type of breakdown mechanism of the last stage, whether in air or in vacuum, is still mainly characterized as of the streamer type.

The way in which a dielectric surface affects phenomena in the gas is dictated by several factors. The normal electric field lines and the normal particle fluxes at dielectric surfaces are affected by accumulated surface-charge. The geometry of the dielectric's surface affects the overall field distribution in the gas. Its material will polarize in the presence of space-charge, thereby exerting an attractive force on the

charges. The dielectric surface can capture electrons, but electrons can also be emitted due to photoemission or ion bombardment. The dielectric will have surface and bulk conductivities, it may be doped with impurities to create charge traps, the surface may be finely polished or have a varying grade of roughness or be a profiled surface. It is therefore clear that the presence of a dielectric surface can significantly affect the discharge characteristics and is a considerable challenge experimentally to prepare and test, as well as numerically to model. In the next sections a few experimental and modelling results are referenced.

Selected experimental and theoretical research

A good review on surface flashover of insulators in vacuum can be found in [24]. For setups with air filled gaps, among the large number of experimental research, some noteworthy results are here highlighted. The surface flashover voltage, or breakdown voltage (BDV) is highest in vacuum, decreases in the pressure range 10^{-5} atm to 10^{-3} atm, to increase again with increasing pressure [25, 26], see Fig. 1.5. Focusing on research done at 1 atm, it was found that the effect of an applied voltage waveform (DC, AC or pulsed) on the BDV, depends on the non-uniformity of the electric field and on the pulse rise time [27]. For a disk dielectric tightly stacked between parallel disk electrodes, Pillai [25] obtained comparable BDVs for AC(peak), DC and the $1.2/50\,\mu$s pulse(peak) voltage forms. Regarding the type of gas, gases that are more electronegative, have higher BDVs, since attachment takes away the needed electrons for the breakdown mechanism [28]. The effect of the dielectric permittivity on the BDV is weak [25]. In a contribution by Sudarshan [27] effects of surface treatments, conditioning and geometries are reviewed. More recently, insulators with a profiled surface, including a shed and knurled surfaces were also seen to be able to increase the BDV[29–32], a result that was attributed to the larger length a streamer has to travel to bridge the gap. To try and understand the obtained results, where the BDV increases (or decreases) in DC conditions, many have resorted to an explanation in terms of surface-charge effects due to charge accumulation on the dielectric surface. A dielectric can also have a bulk space-charge density due to temperature [33] or permittivity gradients, it can trap space-charge close to the surface due to impurities, decreasing the surface flashover voltage with an increase in temperature [34]. A recent extended review of the effect of surface-charge can be found in [35].

In an interesting experiment and theoretical treatment, Pai [36] showed that for breakdown in air at 1 atm between two point electrodes with a dielectric surface parallel to the discharge axis but not touching the electrodes, there is a distance of the dielectric for which the BDV is minimum, i.e., if the dielectric is further from, or closer

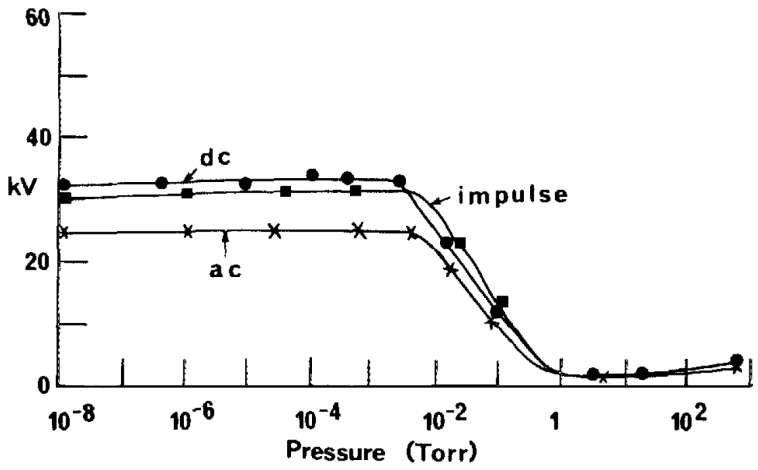

Figure 1.5: Dependence of DC, AC (60 Hz), and impulse flashover voltages on gas pressure in air. Insulator material Teflon 2 mm long, 7.0 mm diameter. Electrode material: stainless steel. From [25].

to, the electrodes, the BDV increases. The reason is attributed to the competition between a volumetric term and an exponential diffusion term in their expression for the BDV. In [27] Sudarshan identifies the main processes that contribute to the flashover event. A total of 22 contributing factors are identified related namely to initial electron production, secondary electron generation processes, charge diffusion, impurity gas production and electric field modifications. Since then, other contributing factors, related mainly to properties of the dielectric, were added, like electron traps [37], and surface and bulk conduction [24, 38, 39].

The most popular theoretical conjectures for breakdown, focus each on one particular mechanism operating during breakdown. The mechanism has to explain how the charges, mainly the electrons, are created to initiate the discharge. These conjectures were initially proposed for vacuum, but the processes are present also in compressed gases. Two popular conjectures are: the secondary electron emission avalanche (SEEA) conjecture where electron emission is due to the impact of electrons or ions on the dielectric, and another is the electron triggered polarization relaxation (ETPR) conjecture where electron emission from the dielectric is related to the emission of trapped electrons from the dielectric. In SEEA some of the electrons emitted from the triple junction strike the surface of the insulator, producing additional electrons by secondary emission. Some of these secondary electrons will somewhat further strike the insulator surface again, producing tertiary electrons. This successive chain of events results in the development of an SEEA, and culminates in a flashover. In ETPR the main mechanism for the intermediate phase of surface flashover is the propagation of electrons in a conduction band of the insulator [24, 37, 38]. The intermediate phase is

explained as being initiated either by the injection of electrons into the insulator by tunnelling at the cathode, or by the excitation of electrons at a point on the surface of the insulator. A significant amount of electrons can be trapped into a $10 - 40\,\mu$m surface layer of the dielectric insulator due to the non-uniformity of the material's susceptibility. The bounding energy of these 'polaron-traps' is expected to be high enough to allow charge fixing as well as low enough to allow charge migration under an electrical perturbation. This mechanism is able to explain the long lifetime of negative or positive surface-charge on the dielectric surface. The injected electrons are then accelerated by the electric field within the insulator. The electrons gain energy and begin participating in inelastic collisions, and as soon as their energy exceeds the band gap of the insulator, they create an electron cascade along the inner dielectric surface. These electrons induce rapid charge detrapping from localized sites and corresponding relaxation of energy of polarization. A fraction of these cascade electrons will be desorbed from the surface, whereupon the external electric field drives them towards the anode. One further conclusion from ETPR is that choosing the 'better' insulator, with higher permittivity, is not the best option to prevent breakdown in view of higher permittivity entailing higher susceptibility, and therefore higher density of trapped charges which can more easily be triggered to participate in breakdown. Reviews discussing other conjectures and aspects of the surface flashover are mentioned in [27, 35, 40, 41].

Selected numerical research

In this concise review we focus on modelling of artificial air in a setup containing a dielectric and subject to DC voltage. Within this still vast category, we look at simulations of streamers done with the conventional system of hydrodynamic equations describing low-current discharges, which comprises equations of conservation and transport of charged particles and the Poisson equation for the electric potential.

In [42] simulations were performed with a dielectric boundary discharge (DBD) plasma actuator at AC voltage, focusing mainly on the electrohydrodynamic force generation process. The geometry was a planar dielectric tightly stacked between an equal sized ground electrode and a planar, but smaller, stressed electrode sunk flat into the dielectric, i.e., the angular aperture into air at the triple junction was 180^o, see Fig. 1.6a. The stressed electrode and dielectric surface were exposed to air at 1 atm, no photoionization was considered. An initial uniform plasma density of $10^7\,\mathrm{m}^{-3}$ was used. Surface streamers would originate close to the triple junction of the stressed electrode and propagate along the dielectric. The effect of the chemical reaction scheme was researched firstly with a simple model including species; e, N_2^+,

O_2^+, O_2^-, O^-. With a more elaborate chemical scheme involving 14 species and 78 reactions they were able to conclude that the cluster ion O_4^+ becomes the dominant ion species influencing the electrohydrodynamic force. In a similar DBD geometry [43], but having an angular aperture into air at the triple junction of 90^o, see Fig. 1.6b, subject to various Gaussian voltage pulses spanning 15 ns, the effect of residual surface-charges on surface streamer evolution and corresponding energy deposition are calculated. The hydrodynamic equations are used with the Poisson equation, photoionization and a 34 reactions scheme, to solve for the densities of 15 species. Dependent on the voltage pulse being negative or positive, negative or positive streamers originate, respectively, at the triple junction and propagate along the dielectric surface with different characteristics. Results showed that the type of pulses that better hold off breakdown, were cyclic negative pulses, where the streamer ignites later and reduces faster its initial velocity, therefore travelling a smaller distance.

A point-to-plane planar geometry in air at 1 atm, with a dielectric tilted 45^o to the plane and touching the HV electrode tip, was studied experimentally and numerically using a 2D domain in [44], see Fig. 1.6c. The author sought to reproduce, through simulation, the interesting experimental observation that, on the dielectric surface, at a certain distance from the HV tip, a streamer would originate and start propagating into the air. This distance would increase with increasing peak voltages. In the experiment, also surface partial streamers were generated successively during the positive rising part of a 4 Hz sinusoidal wave. A simple hydrodynamic description was used, where the gas was simulated by abstract atoms, the reaction scheme included ionization, attachment, recombination, but no photoionization. An initial Gaussian density seed of electrons and positive ions was at the HV tip with a maximum of $10^{16}\,\mathrm{m}^{-3}$ and standard deviation of 200 μm, elsewhere the density was $10^{13}\,\mathrm{m}^{-3}$. With an applied DC voltage of 30 kV and an initial surface-charge concentrated on the dielectric, 0.4 mm away from the HV tip, the author managed to simulate a streamer originating at the charged spot. The spot was 0.1 mm wide with an surface-charge density of 50 $\mathrm{nC/\,cm^2}$.

Simulations with a profiled dielectric surface have been performed [45] where the streamer dynamics on smooth and corrugated flat dielectric surfaces is analyzed in a 2D planar geometry, see Fig. 1.6d. Results, in qualitative agreement with experiments, show a much slower effective streamer velocity along a square corrugated surface, where progression happens due to sequential re-ignition of secondary streamers at neighboring corrugation sites.

Dubinova in [18] uses a cylindrical geometry where a dielectric disk is tightly stacked between two larger disk electrodes in a 150 mbar air gap, where the stressed positive disk had a protrusion into the dielectric bulk, see Fig. 1.6e, while in Li [46] a rectangular geometry is used where a plane dielectric is tightly stacked between

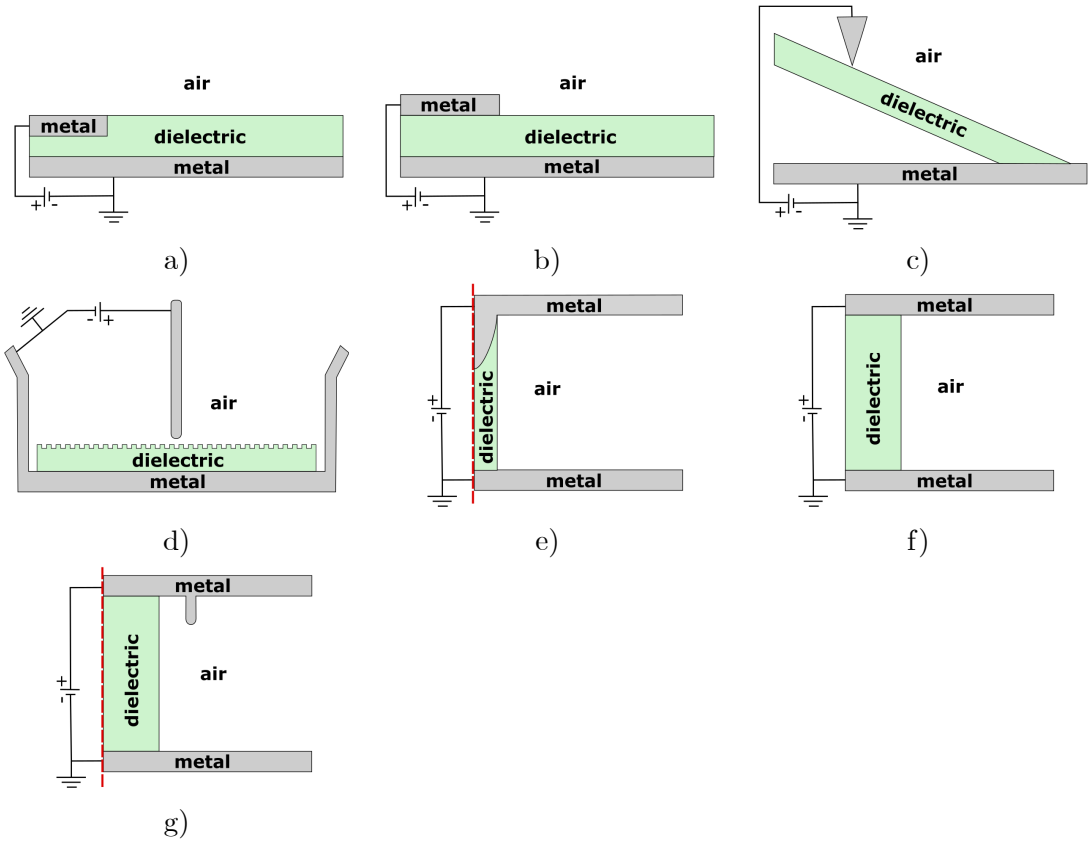

Figure 1.6: Schematic of simulated domains. a) Planar geometry of [42]. b) Planar geometry of [43]. c) Planar geometry of [44]. d) Planar geometry of [45]. e) Cylindrical geometry of [18]. f) Planar geometry of [46]. g) Cylindrical geometry of [28].

two larger plane electrodes in a 1 atm air gap, see Fig. 1.6f. Both these geometries have triple junctions capable of locally enhancing the electric field, however to initiate the positive streamers in the simulations, either a homogeneous high initial electron and positive ion density of $10^{13}\,\mathrm{m}^{-3}$ is used [18], or a high localized density with a maximum of $5 \times 10^{18}\,\mathrm{m}^{-3}$ at the anode is used [46]. For the conditions in the cylindrical geometry of [18] both surface and volume streamers are generated simultaneously. Both works agree that secondary electron emission (SEE) from the dielectric has a negligible effect on streamer dynamics, while the surface's photoemission increases the streamers affinity to the surface, as does a higher permittivity. Conclusions however differ regarding which streamer, surface or volume, has higher velocity; experimental data [47] however favor Li's conclusion of faster surface streamers.

In [28], a similar geometry to [18] is used, but where the protrusion on the HV anode is now close to the dielectric surface and into the air at 1 atm, see Fig. 1.6g. Simulation results show strong branching[1], with the dielectric surface attracting a surface streamer which gains a higher velocity and electron density ($\sim 10^{21}\,\mathrm{m}^{-3}$), when compared to the velocity and electron density ($\sim 10^{19}\,\mathrm{m}^{-3}$) of the volume streamer. It is claimed that branching is caused by the instability of the development of the spatial net charge layer in the streamer head, but is not further discussed. Contrary to results from [18, 46], this research claims that SEE from the dielectric surface, leads to an increased surface streamer velocity. The presented streamer dynamics, in particular its loose attachment to the dielectric surface, is quite different from other results [46]. Since the dielectric radius of 2 mm is relatively small, it is possible that this is related to 'self-repulsion' (a 2D axi-symmetric effect) of the cylindrical streamer observed and discussed in [18].

Review [48] focuses on streamer discharges in atmospheric-pressure non-equilibrium plasmas and contains further references to numerical simulations done for discharges in the presence of dielectrics.

1.2 This work

In the present work we move from the rather peaceful realm of the low current self-sustaining discharge to beyond the quiet '*enchanting beauty*' of a glow discharge, as Raizer [20] put it, to the study of the transient wrathful realm of breakdown.

In doing stationary or non-stationary modelling, the numerical method needs an initial approximation, or initial condition for the non-stationary case, to initiate iterations that will hopefully lead to a converged final state. The most time-consuming

[1] Branching occurs where the streamer-head splits into two. The exact mechanism by which this happens is still a topic of discussion.

step in modelling by means of stationary solvers is, in many cases, finding this suitable initial approximation. For instance, in the calculation of the current-voltage characteristic of a setup, it is very helpful to use the self-sustained state as the starting point. In this work a simple method is proposed to obtain this initial approximation for low-current self-sustaining discharges, called the resonance method. It is a method that implements a theoretical counterpart to the experimental procedure of aiding discharge ignition with an external ionization source in order to obtain a self-sustained discharge.

If the sole interest is obtaining the ignition-voltage of a setup, then it may be possible to use the Townsend criterion. Its applicability is however limited to setups with a weak field non-uniformity and negligible diffusion and photoionization. In this work the Townsend criterion is extended to cases where the limitation on the field non-uniformity is relaxed and where negative ions are taken into account.

In this work a particular point of interest is the relation between the ignition-voltage and the breakdown voltage. The latter has received little attention in the literature. Though there are plenty of studies on the effect of dielectric surfaces on the breakdown voltage, there seem to be no published measurements of the effect of dielectric surfaces on ignition-voltages. Likewise, in a literature search for numerical modelling, no work was found that pursued establishing a connection between the ignition and breakdown voltage. In [20] it is argued that for the DC case, an overvoltage of 10% above the ignition-voltage will trigger breakdown. In the present work a systematic and straightforward procedure to predict the breakdown voltage is presented. It is not based on performing time-consuming, trial and error, non-stationary calculations, but rather relies on stationary calculations within the scope of the resonance method. Other recent research, aimed at predicting the breakdown voltage, have resorted to AI methods of machine learning to identify partial discharges as a precursor to breakdown in HVDC [49], or artificial neural networks [50, 51] to predict the breakdown voltage in polluted outdoor insulators.

Results in this work are for DC powered low current discharge setups where the cathode remains cold, the plasma is in a low ionization degree, and the emission mechanism is an effective secondary electron emission, comprising the combined effect of ion impact, excited particle impact and photoemission. Throughout this work the gas under consideration will be dry air at 1 atm. The kinetic scheme for air was relatively simple, but has proved accurate in reproducing many experimental results. Whenever possible, validation of the modelling results was sought by referencing the available experimental data. Conditions were such that a fluid model of the charged particles was well justified. Throughout this work special attention is given to a simplified setup used to model the circuit breaker shown above in Fig. 1.1. This type

of circuit breakers of industrial interest is known to break down, with the breakdown path running along the insulator. The associated simplified setup has cylindrical symmetry and consists of a dielectric disk tightly stacked between two disk electrodes. With the results of this work, the applicability of the resonance method, designed to calculate self-sustaining states, is broadened to be relevant for breakdown calculations. The work builds on the decades long expertise in this field by the Madeira University research team led by Prof. M. Benilov.

This text is organized into five chapters, the first being this Introduction. In Chap. 2 the fluid model equations are introduced for electrons, an effective positive ion and three negative ions, along with the respective transport coefficients and kinetic scheme. In this chapter a method is proposed for modelling the ignition of a self-sustaining discharge. This method, coined the 'resonance method', was used as an in-house tool of the IPFN research group in Madeira since at least 2016, and is here presented as an expedient systematic stepwise procedure for modelling the ignition of a discharge. Though introduced here in general terms, the resonance method will in subsequent chapters be applied to coaxial cylinders, a point-to-plane geometry and to simple setup containing a dielectric, determining their respective self-sustainment voltage and, on occasion, aid the construction of a particular current-voltage characteristic.

In Chap. 3 an alternative method is proposed to evaluate the self-sustainment voltage in volume discharges of drift dominated electronegative gases. It constitutes an extension of the classical Townsend method to setups not reducible to 1D domains. This approach is numerically less demanding than the resonance method, in that it only requires the solution of the Laplace equation, and integration along electric field lines. The extended method is validated against the resonance method and available experimental data for three selected setups.

In Chap. 4, conditions are proposed for the resonance method to calculate voltages for first-breakdown and for repetitive-breakdowns. The agreement between the latter voltages calculated by the stationary resonance method and by the non-stationary modelling method, is highlighted. The influence of the dielectric permittivity and radius on the calculated voltages was studied. Characteristic time-scales for the formation of self-sustaining discharges with and without surface-charge on the dielectric are also evaluated. Some notes regarding the dynamics of breakdown at low overvoltages are mentioned.

In Chap. 5 conclusions of this work are given and possible directions of future research discussed.

All the modelling results included in this thesis were obtained using COMSOL Multiphysics.

Chapter 2

A practical guide to modelling low-current quasi-stationary gas discharges: Eigenvalue, stationary, and time-dependent solvers

2.1 Introduction

The content of this chapter was adapted from the article [52] published in the Journal of Applied Physics (2021).

The physics of many gas discharge systems has been understood reasonably well by now. High-quality data for evaluation of transport and kinetic coefficients and tools performing such evaluation are publicly available, e.g., LXCat [53] and LoKI [54]. Sophisticated numerical models have been developed for simulation of gas discharge systems. Such models are virtually universally based on time-dependent solvers, which give detailed information on spatiotemporal distributions of plasma parameters and are indispensable for studies of discharges with fast temporal variations, such as high-frequency discharges, pulsed discharges, streamer and spark discharges *etc*; e.g., [20, 55].

Time-dependent solvers can also be used for the computation of steady-state (or, more precisely, quasi-stationary) gas discharges: an initial state of a discharge is specified and its relaxation over time is followed until a steady-state has been attained. An alternative is to use stationary solvers, which solve steady-state equations describing

a steady-state discharge by means of an iterative process unrelated to time relaxation. Stationary solvers offer important advantages in simulations of steady-state discharges. In particular, they are not subject to the Courant–Friedrichs–Lewy criterion or analogous limitations on time stepping. This allows one to speed up simulations, with improvement by orders of magnitude depending on the modelled geometry, and is particularly important for modelling discharges with strongly varying length scales, e.g., corona discharges, where a variation of the mesh element size by orders of magnitude is indispensable. Moreover, stationary solvers allow decoupling of physical and numerical stability. Another useful feature of stationary solvers is their ability to compute patterns of complex behavior that can manifest itself in the modelling of gas discharges even in apparently simple quasi-stationary situations. Time-dependent solvers may not provide important information in such cases. Several such examples referring to the modelling of glow discharges and thermionic arc discharges can be found in [56].

Although most of the popular ready-to-use toolkits for gas discharge simulation employ time-dependent solvers, e.g., nonPDPSIM [57] and Plasma module of commercial software COMSOL Multiphysics®, stationary solvers for gas discharge modelling are provided by Plasimo [58]; COMSOL Multiphysics® provides stationary solvers for general partial differential equations; although the Plasma module of COMSOL Multiphysics® is intended to work with time-dependent solvers, it can still be used with stationary solvers [56].

This work is concerned with modelling of low-current discharges, including the Townsend and corona discharges, the aim being to develop an integrated approach suitable for the computation of the whole range of existence of a quasi-stationary discharge from its inception to a non-stationary transition to another discharge form, such as the transition from the Townsend discharge to a normal glow discharge or the corona-to-streamer transition. It is convenient to divide the task into three steps: (i) modelling of the ignition of a self-sustaining discharge, (ii) modelling of the quasi-stationary evolution of the discharge with increasing current, and (iii) the determination of the current range where a quasi-stationary discharge ceases to exist and the above-mentioned non-stationary transition begins.

From the mathematical perspective, the problem of ignition of self-sustaining discharges is an eigenvalue problem [59]. There are several methods that can be used for its numerical solution. The method of choice, the so-called resonance method, is physics-based and requires solving a boundary-value problem for steady-state linear partial differential equations, which may be routinely done by means of ready-to-use solvers, including commercial ones. Note that, in addition to being of theoretical interest, understanding the ignition of self-sustaining discharges is important for applications: it is a useful reference point in the investigation of breakdown in high-voltage

electrical equipment in low-frequency, e.g., 50 Hz, electric fields, where the time of variation of the applied voltage is much longer than the ion drift time.

The solution describing the ignition of a self-sustaining quasi-stationary discharge, obtained at the first step, may be conveniently extended to higher currents by means of stationary solvers. The most time-consuming step when using stationary solvers is usually finding a suitable initial approximation, which requires intelligent guesswork. Fortunately, in simulations of low-current self-sustaining discharges this step can be performed in a routine way using the resonance method. In this work, such integrated approach is discussed in some detail and examples of its application to corona discharges of different configurations and both polarities can be found in Sec. B of [52].

As the current of a quasi-stationary discharge increases, the discharge will lose stability and a non-stationary transition into another discharge form occurs. The loss of stability against small perturbations may be studied by means of solving the eigenvalue problem resulting from linear stability theory. In [60], this approach was used to study the stability of the Townsend and glow discharges. An alternative approach to investigation of stability is to apply a perturbation to a steady-state solution and to follow the development of the perturbation by means of a time-dependent solver. This approach allows studying stability against both small and finite perturbations. For an example illustrating the application of this approach to a positive point-to-plane corona, see Sec. V of [52].

The outline of this chapter is as follows. A model of low-current discharges in high-pressure gases is briefly described in Sec. 2.2. Computation of initiation of self-sustaining gas discharges is considered in Sec. 2.3. The eigenvalue problem, which governs the discharge initiation, is formulated and its solution is obtained by the resonance method. An integrated approach for calculation of low-current quasi-stationary discharges, which is based on a combination of the resonance method and stationary solvers, is discussed in Sec. 2.4. A brief summary is given in Sec. 2.5. In order not to overload this chapter, some material has been combined into three Appendixes: Appendix A, where the boundary conditions for drift-diffusion equations are briefly discussed; Appendix B, concerned with plasmachemical processes and transport coefficients of low-current discharges in high-pressure air; and Appendix C, where the effective reduced temperature of a pair of ion species in high electric fields is briefly discussed.

2.2 A model of low-current discharges in high-pressures gases

Mathematical ideas discussed in this work apply to both hydrodynamic and kinetic models of gas discharges. For brevity, here the consideration is restricted to the conventional system of hydrodynamic equations describing low-current discharges in high-pressure gases, which comprises equations of conservation and transport of charged particles, excited states, and radicals produced in the discharge, and the Poisson equation:

$$\frac{\partial n_\alpha}{\partial t} + \nabla \cdot \mathbf{J}_\alpha = S_\alpha, \tag{2.1}$$

$$\mathbf{J}_\alpha = -D_\alpha \nabla n_\alpha - Z_\alpha n_\alpha \mu_\alpha \nabla \phi, \tag{2.2}$$

$$\varepsilon_0 \nabla^2 \phi = -e \sum_\alpha Z_\alpha n_\alpha. \tag{2.3}$$

Here subscript α identifies different species produced in the discharge (positive and negative ions, the electrons, excited states, and radicals); n_α, $\mathbf{J}_\alpha$, D_α, μ_α, S_α, and Z_α are, respectively, number density, density of transport flux, diffusion coefficient, mobility, net volume rate of production, and charge number of species α; ϕ is the electrostatic potential; e is the elementary charge; and ε_0 is the permittivity of free space. The source terms S_α in the equations of conservation for electrons and positive ions include, in addition to terms describing production of these species in collisional processes, the photoionization term S_{ph}. The transport Eqs. (2.2) for the charged particles are written under the so-called drift-diffusion approximation. Henceforth the system of conservation equations with fluxes written as in (2.2), will, for brevity, be referred to as the drift-diffusion equations. This system of equations includes also other relevant equations, such as equations governing the photoionization and the electron and neutral-gas energy equations. If motion of the neutral gas plays a role, then the convective terms have to be added to the lhs of Eqs. (2.1) and the system of equations includes also the Navier-Stokes equations.

The system of equations is supplemented by usual boundary conditions. In particular, boundary conditions for densities of charged particles on the surfaces of the electrodes and dielectric surfaces (in case they border the active zone of the discharge) may be written as described in Appendix A.

Most examples given in this work refer to low-current discharges in high-pressure dry air and have been computed with the use of transport coefficients and a kinetic scheme of plasmachemical processes described in Appendix B. The local-field and quasi-stationary approximations are employed, so all the transport and kinetic coefficients, including those for the electrons, are assumed to depend on the local reduced

electric field E/N and the neutral-gas temperature T. (Here $E = |\nabla\phi|$ is the electric field strength and N is the number density of the neutral gas.) The conditions under which these approximations can be safely employed without voiding their underlying physical assumptions are treated in Appendix D. The kinetic scheme does not consider excited states or radicals and takes into account one species of positive ions, which are designated A^+, the electrons, and three species of negative ions, O_2^-, O^-, and O_3^-, so that $\alpha = A^+$, e, O_2^-, O^-, O_3^- in Eqs. (2.1)-(2.3). The photoionization is evaluated by means of the three-exponential Screened-Poisson model [61]:

$$S_{ph}(\mathbf{r}) = \sum_{j=1}^{3} S_{ph}^{(j)}(\mathbf{r}), \tag{2.4}$$

with each of the terms satisfying the Screened-Poisson partial differential equation,

$$\nabla^2 S_{ph}^{(j)}(\mathbf{r}) - (\lambda_j p_{O_2})^2 S_{ph}^{(j)}(\mathbf{r}) = -A_j p_{O_2}^2 I(\mathbf{r}) \quad (j = 1, 2, 3). \tag{2.5}$$

Here A_j and λ_j are constants (parameters of the three-exponential fit function) given in [61], p_{O_2} is the partial pressure of molecular oxygen, and $I(\mathbf{r})$ is the product of the probability of ionization of a molecule at photon absorption and the local photon production rate. The latter is assumed to be proportional to $S_i(\mathbf{r})$ the rate of ionization of neutral molecules by electron impact and $I(\mathbf{r})$ is written as [62]

$$I(\mathbf{r}) = \left(0.03 + \frac{15.7\,\mathrm{Td}}{E/N}\right) \frac{p_q}{p + p_q} S_i(\mathbf{r}), \tag{2.6}$$

where p is the neutral gas pressure, $p_q/(p + p_q)$ is a quenching factor that accounts for the non-radiative de-excitation of radiating states of nitrogen molecules due to collisions with other molecules. The quenching pressure p_q is set equal to 30 Torr [63, 64]. The examples reported in this work are limited to low discharge currents, where the discharge-induced heating and motion of the neutral gas are negligible, and refer to $T = 300\,\mathrm{K}$.

If dielectric surfaces exist in the studied setup, as will be the case in Chap. 4 and if a time-dependent study is intended, then there is the possibility, that over time, charges accumulate on the surface. The amount of surface-charge, $\varepsilon_0 (\varepsilon_D \mathbf{E}_D - \varepsilon_G \mathbf{E}_G) \cdot \mathbf{n} = \sigma_s$, is a quantity that is therefore now allowed to vary in time,

$$\frac{\partial}{\partial t} \varepsilon_0 (\varepsilon_D \mathbf{E}_D - \varepsilon_G \mathbf{E}_G) \cdot \mathbf{n} = \frac{\partial \sigma_s}{\partial t} \tag{2.7}$$

here and below, subscripts D and G refer, respectively, to the dielectric and the gas; $\mathbf{n}$ is the normal vector pointing from gas to dielectric surface; ε_0 is the vacuum permittivity; ε is the relative permittivity; $\mathbf{E}$ is the electric field.

The boundary conditions for electron and ion densities are those specified at the end of Appendix A. The electron emission flux is related to the flux of incident positive ions by the effective secondary emission coefficient γ, which is assumed to characterize all mechanisms of secondary electron emission (due to ion, photon, and excited species bombardment) [20]. The rate of photoionization is set to zero at all solid surfaces, $S_{ph}^{(j)} = 0$ $(j = 1, 2, 3)$, similarly to [65, 66]. It is assumed that the surface-charge density on the dielectric can change due to the influx of free charges from the gas side, and therefore the boundary condition on the dielectric is

$$\frac{\partial \sigma_s}{\partial t} = j_n, \tag{2.8}$$

where $j_n = \mathbf{j}_G \cdot \mathbf{n}$ is the normal component into the dielectric of the total conduction current density. For stationary calculations, the boundary condition over a dielectric surface will be that associated with the steady-state of the discharge, i.e. zero normal component of current density,

$$j_n = 0. \tag{2.9}$$

The various modelled physical conditions in this work were such that the local-field approximation and the quasi-stationary approximation were well justified. In Appendix D a comment is made on the range of validity of these approximations for atmospheric pressure discharges in air.

The numerical modelling reported in this work was performed with the use of commercial software COMSOL Multiphysics®. The following interfaces were used: Transport of Diluted Species, or TDS (equations of conservation and transport of charged species, Eqs. (2.1) and (2.2)), Electrostatics (the Poisson equation, Eq. (2.3)), and Coefficient Form Partial Differential Equations (the Screened-Poisson equations, Eqs. (2.5)). The streamline (Galerkin-Petrov) and crosswind diffusion stabilizations, which are default options of the TDS interface, were kept activated in all cases except where otherwise indicated. It should be stressed that both stabilizations are consistent, i.e., the corresponding terms vanish when the iterations have converged.

2.3 Computing initiation of self-sustaining gas discharges

2.3.1 The eigenvalue problem

The condition of initiation of a self-sustaining gas discharge, where the discharge voltage is just sufficient for the electron impact ionization to compensate losses of the charged particles, is well known for wide parallel-plate electrodes, where the applied

electric field is uniform and diffusion of the charged particles is of minor importance. The condition reads

$$\alpha d = \ln\left(1/\gamma + 1\right), \tag{2.10}$$

where α is the Townsend ionization coefficient, d is the discharge gap width, and γ is the effective coefficient of secondary electron emission from the cathode. An approximate relation for other discharge configurations is obtained by replacing αd by the so-called ionization integral, which is the line integral of α evaluated along the electric field line that ensures the biggest value of this integral. Such an approach, though theoretically incomplete can, under properly justified assumptions, be extended so as to be applicable in cases of multidimensional volume discharges where the influence of diffusion, photoionization and the presence of dielectric surfaces is minor. It remains the main tool used in industrial applications; e.g., recent work [67] and in the next chapter its derivation for a multidimensional geometry, will be validated against solutions from the eigenvalue problem.

However, the problem of ignition of self-sustaining discharges may be solved by accurate mathematical means and this solution is relatively simple [59]. At the ignition, the charged particle densities are very low and the applied electric field is not perturbed by plasma space-charge, so the rhs of Eq. (2.3) may be dropped and this equation assumes the form of the Laplace equation,

$$\nabla^2 \phi = 0. \tag{2.11}$$

Let us first assume that no dielectric surfaces border the active zone of the discharge, then perturbation of the applied electric field by surface-charges deposited on the dielectric need not be considered as well. (The case of a discharge along a dielectric surface will be considered in Sec. 2.4.2 below.) Therefore, the distribution of the electric field in the gap, for a given gap geometry, is governed solely by the applied voltage U and may be found by means of standard electrostatic simulations disregarding the presence of charged particles in the gap. Of course, the electric field distribution is linear with respect to U and it is sufficient to perform the electrostatic simulation only once and then to scale the computed electric field distribution to each required value of the applied voltage U. For definiteness, it is assumed that the applied voltage is defined as the potential of the anode with respect to the cathode, thus $U > 0$.

At the ignition, there is no need to consider nonlinear processes, such as reactive collisions involving two or more particles produced in the discharge (ions, electrons, excited states, or radicals), which includes the stepwise ionization and the recombination of charged particles. Thus, there is no need to consider excited states and radicals and it is sufficient to consider the equations governing the charged particle distributions in the gap, Eqs. (2.1) and (2.2) with α referring to the charged species.

According to the conventional definition, the ignition-voltage is the value of the applied voltage U such that the applied electric field produces an ionization intensity just sufficient to compensate for the losses of charged particles, so a steady-state balance of the charged particles can be reached. Therefore, the system of equations should be considered in the stationary form, i.e., without derivatives with respect to time in Eqs. (2.1). The resulting equations governing distributions of the ion and electron densities reads

$$\nabla \cdot \mathbf{J}_\alpha = S_\alpha, \tag{2.12}$$

$$\mathbf{J}_\alpha = -D_\alpha \nabla n_\alpha - Z_\alpha n_\alpha \mu_\alpha \nabla \phi, \tag{2.13}$$

where subscript α refers to the charged species (the ions and the electrons).

Since there is no need to consider nonlinear processes at the ignition, the source terms S_α are linear with respect to the charged particle densities. Note that this implies that the dependence of the photoionization rate S_{ph} on the electron density n_e is linear. This is indeed the case as exemplified by Eqs. (2.4)-(2.6): $I(\mathbf{r})$ the rate of ionization of neutral molecules by electron impact is proportional to the local electron density $n_e(\mathbf{r})$, therefore the dependence of $S_{ph}(\mathbf{r})$ on $n_e(\mathbf{r})$, while being non-local, is linear. This is also the case in models where the photoionization rate is computed by evaluation of an integral (e.g., [57, 64, 68, 69]), rather than by solving partial differential equations.

Eqs. (2.12)-(2.13) are supplemented by Eqs. (2.4)-(2.6) or similar and boundary conditions Eq. (A.6) with $\xi_a = \xi_e = 1/2$ or similar. The obtained boundary-value problem, which is considered for a given distribution of the electric field in the gap, governs distributions of the ion and electron densities at inception and is linear (with respect to these densities).

We consider conditions where there is no external ionizing radiation and the ionization mechanisms are direct ionization by impact of electrons, accelerated by the applied electric field, and photoionization by photons produced in the discharge; there is no thermionic, thermo-field, and field electron emission from the cathode, as well as no electron photoemission caused by external radiation. Then the above-described linear boundary-value problem governing distributions of the ion and electron densities in the gap is homogeneous. Since the problem is considered for a given distribution of the electric field in the gap, the applied voltage U is a control parameter of the problem. The aim is to find a value $U = U_0$ such that the problem describes the inception of a self-sustaining discharge, i.e., a low-current steady-state discharge.

From the mathematical perspective, this is a boundary-value problem for a system of partial differential equations (or integro-differential equations, if the photoionization rate is computed by evaluation of an integral) and this problem is linear (with respect

to the charged particle densities) and homogeneous (no external ionization terms). For all values of the applied voltage U, the problem admits a trivial solution: the ion and electron densities are zero at all points in the gap, which corresponds to a situation where no discharge has been ignited. The task is to find a value of U such that the problem admits, in addition to the trivial solution, also a nontrivial one. In mathematical terms, this is an eigenvalue problem and U is the eigenparameter.

Thus, the ignition of a self-sustaining discharge is described by an eigenvalue boundary-value problem for a system of partial differential or integro-differential equations governing distributions of the ion and electron densities. The physical sense of the problem is that the applied voltage should be such that direct ionization by the impact of electrons accelerated by the applied electric field and photoionization by photons generated in the discharge are just sufficient to compensate for the losses of charged particles. In agreement with the above, in the special case of wide parallel-plate electrodes the formulated eigenvalue problem may be reduced to one dimension and will lead to the well-known self-sustainment condition (2.10), provided that similar simplifications are applied: no diffusion, one ion species, no photoionization.

There is one more special case where the applied electric field can be considered uniform and the formulated problem may be reduced to one dimension: the problem of self-sustainment field in the cross section of a plane or cylindrical positive column of a long low-current discharge. The formulated problem takes a form similar to the well-known eigenvalue problem for an ordinary differential equation describing the ambipolar diffusion of charged particles in the cross section of a positive column under the assumption of quasi-neutrality; e.g., [55]. The solution to the latter problem is well known: the cosine for a plane column and the zero-order Bessel function for a cylindrical column; respectively, Eqs. (5.2.26), (5.2.27) and (5.2.35), (5.2.36) from [55]. At the discharge ignition, the transversal electric field is zero, the diffusion is free and not ambipolar, and there is no quasi-neutrality. Therefore, the above-cited solution [55] is valid for the distribution of the electron density n_e at the discharge ignition provided that the ambipolar diffusion coefficient is replaced by the electron diffusion coefficients D_e. The ion density exceeds n_e by the factor D_e/D_i, where D_i is the diffusion coefficient of the ions.

In the general case, the formulated eigenvalue problem for the ignition of a self-sustaining discharge is multidimensional and its numerical solution is not quite trivial. Three methods have been employed for solving this problem and they have been compared with regard to which has a more user-friendly implementation. The first method consists of the direct application of an appropriate eigenvalue solver to the eigenvalue problem as it was formulated, considering U as the eigenparameter. The solver will return a set of eigenvalues (spectrum) and eigenfunctions associated with each of the

eigenvalues. This spectrum has to be analyzed and all but one real eigenvalue for U should exist whose associated vector eigenfunction has all components positive in the domain, where the vector eigenfunctions have components, each describing the number density distribution of one of the ion species or of the electrons. A second method is based on the study of the stability of the 'no-discharge' solution, i.e. a discharge where all density distributions and the total current are zero, while the potential can have any value. It is experimentally known that there is a voltage value above which the 'no-discharge' solution becomes unstable. A method based on stability analysis results, again, in an eigenvalue problem associated with the same equations, but supplemented with a time variation term for the densities, $\partial n_\alpha/\partial t$. The eigenparameter ($\lambda$) is now the coefficient of time in an exponential factor multiplying the densities; $\exp(\lambda t)\, n_\alpha$. Monitoring the spectrum of eigenvalues obtained for ever increasing values of U, will single out an eigenvalue λ that eventually becomes zero, i.e., represents the point of neutral stability characterizing the voltage at which the 'no-discharge' solution loses stability. The voltage at which neutral stability is obtained is the self-sustainment voltage. The third method for solving the stated eigenvalue problem has been called the resonance method and is based on solving a modified eigenvalue problem, in the sense that the associated discharge would be non-self-sustained. Physically it would correspond to the original problem but with an extra production term for the electrons and positive ions. Solving the problem for ever increasing values of voltage will, for a voltage high enough, show a first resonance in the current-voltage characteristic (CVC) of the setup, precisely at the self-sustainment voltage. This method will be explained in detail in the next section.

The three methods are mathematically equivalent as far as computation of the self-sustainment voltage is concerned, so the questions are which method is easier to implement and use, and which method has wider applicability. The method based on the direct numerical solution to the eigenvalue problem requires computing and analyzing the spectrum only once, while the stability method requires doing this several times (for different U values). Thus, the stability method is more laborious. Finding the spectrum by means of an eigenvalue solver, required in the framework of the first and second methods, is a nonlinear task and, as such, requires care in certain cases; in particular, distinguishing between physical and artificial eigenvalues is not always easy. In contrast, the stationary boundary-value problem, describing the non-self-sustained discharge in the framework of the third (resonance) method, is linear and its solution is straightforward. In all geometries to which it was applied, the resonance, and thus the self-sustainment voltage, were readily identifiable and the procedure was straightforward, fast, and reliable.

The resonance method, as the methodologically easier to implement, is preferred

and will be explained in detail in the next section.

2.3.2 The resonance method

The third approach is physics-based and may be described as follows. The stationary boundary-value problem governing distributions of the ion and electron densities at inception, formulated in Sec. 2.3.1, is considered and the equations of conservation of the electrons and one of the positive ion species are supplemented by a term describing an external ionization source. In other words, Eqs. (2.12) for the electrons ($\alpha = e$) and one of the positive ion species ($\alpha = i$) are replaced by the following equations:

$$\nabla \cdot \mathbf{J}_e = S_e + W, \tag{2.14}$$

$$\nabla \cdot \mathbf{J}_i = S_i + W, \tag{2.15}$$

where W is the external ionization term. This term does not depend on the particle densities, in particular, on the electron density, nor on the applied voltage, and is specified more or less arbitrarily. For example, it may be set constant in space in one-dimensional (1D) problems and a Gaussian function with a maximum on the discharge axis is a natural choice in axially symmetric problems.

The obtained stationary boundary-value problem describes the non-self-sustained discharge, generated in the same plasma-producing gas and the same electrode configuration. The problem is solved for different values of the applied voltage U. On physical grounds, one can expect that a kind of resonance will appear when U becomes equal to the self-sustainment voltage.

Note that the problem is linear and the external ionization source W is the only inhomogeneous term. Therefore, the absolute values of W are irrelevant as far as the task is restricted to the calculation of the self-sustainment voltage: the scaling of W affects the scaling of the number densities of the charged particles and does not affect the self-sustainment voltage. On the other hand, some care in the choice of the scaling of W is useful if this method is used as a part of the integrated approach for modelling quasi-stationary low-current discharges in the whole range of their existence starting from the inception; a comment on this point is provided in Sec. 2.4.1.

The stationary boundary-value problem describing the non-self-sustained discharge, being linear (and inhomogeneous), may be routinely solved by means of ready-to-use solvers; hence no need for manual discretization. For example, a linear solver for boundary-value problems for systems of partial differential equations provided by COMSOL Multiphysics® is used in the modelling reported in this work. Note that COMSOL automatically activates the nonlinear solver option in the case where the default streamline and/or crosswind diffusion stabilization is kept activated in the TDS

interface, since the stabilization terms appearing in the species conservation equations are nonlinear. However, the number of iterations required is very small, typically no more than two, so the procedure remains the same whether stabilization is activated or not.

Similarly to the previous one, this method is in essence another way to solve the eigenvalue boundary-value problem for the system of partial differential or integro-differential equations, formulated in Sec. 2.3.1, which finds not the whole spectrum but rather only the self-sustainment voltage. The method was introduced and termed the resonance method in the preceding work [59]. Of course, the very idea of finding a real eigenvalue by varying the eigenparameter and searching for this or that kind of resonance is quite obvious. For example, a change of sign of the determinant of the system of algebraic equations obtained by a finite-difference discretization of a boundary-value problem was used in [70, 71] and [72] as an indication of bifurcation of regimes of current transfer to, respectively, cold cathodes of glow discharges and hot thermionically-emitting cathodes of arc discharges.

The resonance method is, at least for now, the method of choice for calculation of the ignition of self-sustaining discharges. The method has given useful results in a wide range of conditions and complex geometries, e.g., it was used for investigation of discharge ignition in air between concentric-sphere and concentric-cylinder electrodes with microprotrusions of different shapes on the surface of the inner electrode in a wide range of air pressures [73]. Investigation of discharge ignition along a dielectric surface will be considered in Chap. 4. Typical calculations for 2D geometries take about 10 min on a desktop computer.

An important advantage of the resonance method is its physical transparency. In particular, it allows the use of this method not only for simulations of ignition of a self-sustaining discharge, but also as a module of a more general code for the modelling of quasi-stationary (self-sustained) discharges. This is described in the following sections.

2.4 Integrated approach for calculation of low-current quasi-stationary discharges

As discussed in the Introduction, stationary solvers represent an appropriate tool for the modelling of quasi-stationary discharges and offer important advantages over time-dependent solvers. The most time-consuming step when using stationary solvers is usually finding a suitable initial approximation, which requires intelligent guesswork. Fortunately, in simulations of low-current self-sustaining discharges this step can be performed in a routine way using the resonance method. The resonance method pro-

vides a very accurate first approximation for a steady-state solution at a very low current, describing the onset of the self-sustaining discharge. Once this solution has been computed, it can be used as a starting point for the simulations with the discharge current being gradually increased. The solution for each current serves as an initial approximation for simulations with the next current value.

In this way, one obtains an integrated approach for modelling quasi-stationary low-current discharges in the whole range of their existence starting from the inception. This integrated approach is described in this section and examples of its application are given.

2.4.1 Combining the resonance method and stationary solvers

The procedure is illustrated by the flow chart shown in Fig. 2.1 and may be described as follows. At the first step, the non-self-sustained discharge is computed as described in Sec. 2.3.2. We remind that, as discussed in Sec. 2.3.1, the plasma space-charge is neglected at this step, i.e., the rhs of the Poisson equation Eq. (2.3) is dropped or, in other words, the Poisson equation (2.3) is replaced by the Laplace equation (2.11). Nonlinear processes, such as reactive collisions involving two or more particles produced in the discharge, are neglected as well. The discharge voltage U is increased in small increments ΔU until the discharge current becomes negative. Let us designate by U_1 the highest voltage for which the current is still positive and by I_1 the corresponding current.

The second step consists in recalculation of the solution obtained at the first step for $U = U_1$, but with the discharge current being the control parameter instead of the voltage. This amounts to solving the same problem as at the first step, but considering the discharge voltage as an unknown that has to be found from the condition that the discharge current (an integral characteristic of the solution) takes the given value I_1. This problem is nonlinear and, in principle, requires iterations. However, since the initial approximation being used represents the exact solution for $I = I_1$, only one iteration is needed without damping.

At the third step, the solution for $I = I_1$ is recalculated with the external ionization term W in Eqs. (2.14) and (2.15) switched off. The convergence is very fast provided that ΔU is sufficiently small (typically, no more than three iterations are needed without damping if ΔU does not exceed 1% of U). The discharge voltage will slightly increase (by an amount smaller than ΔU) and the obtained value will represent a little more accurate estimate of the self-sustainment voltage.

At the fourth step, the solution for $I = I_1$ is recalculated with account of the space-charge, i.e., with the Laplace equation replaced by the Poisson equation, and

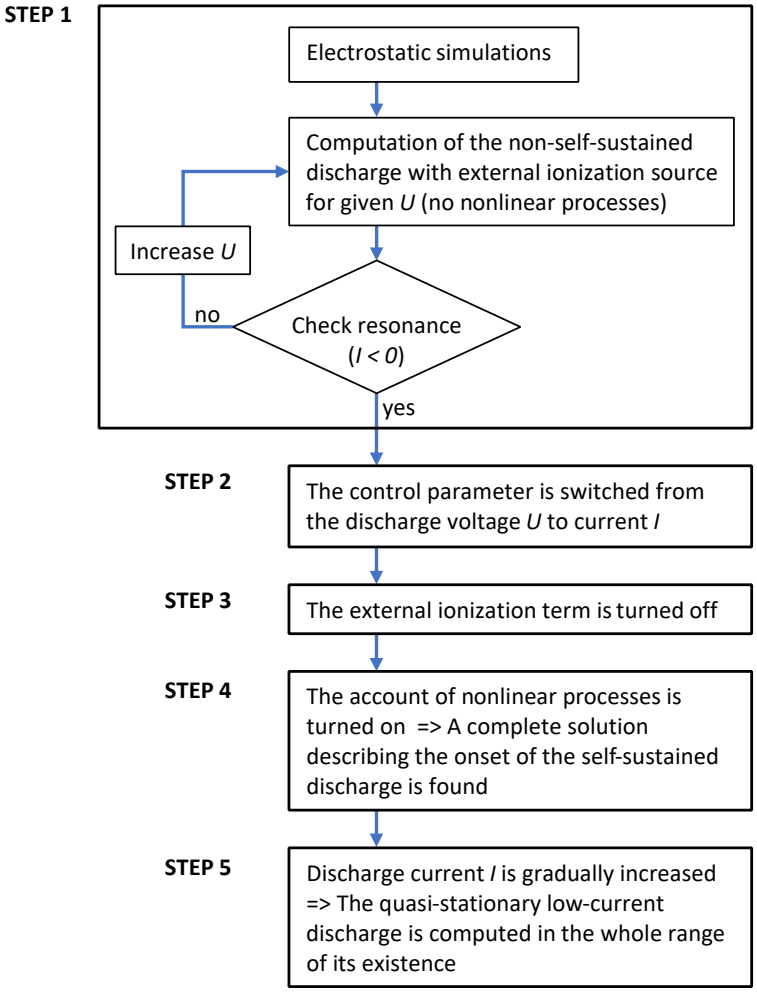

Figure 2.1: Integrated approach for modeling of quasi-stationary low-current discharges.

with account of all relevant nonlinear processes and with the stabilization activated as needed (if it has not been activated right from the first step). The change in U will be very small and only one iteration is needed provided that I_1 is small enough, say, in the order of nanoamps or smaller, which can be ensured by rescaling the external ionization term W, used in the resonance method. As the outcome of this step, one obtains a complete solution describing the onset of the self-sustained discharge.

At the fifth, and final, step, the quasi-stationary low-current discharge is computed in the whole range of its existence. The simulations are performed with the discharge current being gradually increased. The solution describing the onset of the self-sustained discharge, obtained at the previous step, is used as a starting point, and the solution for each current is used as an initial approximation for simulations with for next current value.

We conclude this section with a few practical hints. In gas discharge modelling, the species conservation and transport equations are frequently solved in the logarithmic formulation (e.g., this option is available in the Plasma module of COMSOL Multiphysics®), where the dependent variables are logarithms of the species number densities. The logarithmic formulation ensures that the number density of any of the species is never negative. However, such formulation introduces additional nonlinearity and was found to be less efficient for steady-state modelling than the original formulation (the one with the dependent variables being the species number densities). The modelling reported in this work has been performed in the original formulation and no sizable negative values of species densities have appeared provided that the numerical mesh is not too coarse.

It is essential that the code allows specifying not only the discharge voltage as a control parameter but also the discharge current, with the possibility of an easy and seamless switching between the two. A standard way to specify the discharge current in gas discharge modelling is an implicit one, by means of introducing an external circuit comprising a voltage source and a ballast resistance. In COMSOL Multiphysics®, an alternative is available: one can use the "Global Equation node" option to specify discharge current directly, without introducing an external circuit.

The modelling of the quasi-stationary low-current discharge in the whole range of its existence (the fifth above-described step) starts with the discharge current I being the control parameter. As I gradually increases, it may be helpful to switch the control parameter to U, in order to accelerate convergence. When simulating corona discharges, this can usually be done when the discharge voltage has increased by about 200 V from the ignition-voltage.

It often happens in modelling that iterations converge for a value of the control parameter, but fail to converge for the next value, no matter how small the increment

of the control parameter. Since a solution can turn back or join another solution but cannot just disappear, such a break-off represents a failure of the method. The most frequent reason is that there is a region of fast variation, which is not adequately resolved by the numerical mesh being used (e.g., the corona attachment to the electrode has expanded and is no longer adequately resolved). A refinement of the mesh solves the problem. Adaptive mesh refinement is a powerful tool.

The second most frequent reason is that an extreme point of the CVC or a turning point has been encountered: a code cannot pass through these points if operated with, respectively, U or I as a control parameter. An obvious fix is to switch the control parameter. If the CVC has a complex form, the control parameter has to be switched several times in order to compute the whole range of existence of the steady-state solution.

2.4.2 Discharge along a dielectric surface

Consider now a case where the discharge active zone is in contact with a dielectric surface. The formulation of the eigenvalue problem describing the ignition of a self-sustaining discharge, given in Sec. 2.3.1, needs to be slightly modified in such cases, as well as the procedure of solving it by means of the resonance method.

Continuing to consider low-current quasi-stationary discharges (which implies, in particular, that the time of variation of the applied voltage is much longer than the ion drift time), one can treat surface-charges on a dielectric surface as quasi-stationary. Therefore, the surface is under the floating potential and the boundary condition for the electric field follows from the condition of the normal component of the local current density being equal to zero at each point of the surface. This boundary condition is linear and homogeneous with respect to the ion and electron densities. Therefore, while distributions of the ion and electron densities in low-current quasi-stationary self-sustained discharges vary proportionally to the discharge current I, the electric field distribution is independent from I. This is similar to what happens in the case where no dielectric surfaces border the active zone of the discharge, considered in the preceding sections. It is this independence of the electric field distribution from I that makes the concept of self-sustaining (ignition) voltage applicable in the presence of dielectric surfaces. The difference from the no-dielectric case is that the electric field in the presence of a dielectric is coupled to distributions of the charged particles and cannot be computed independently.

Thus, one needs to consider a stationary boundary-value problem involving partial differential and possibly also integro-differential equations, governing distributions of ions and electrons in the gap, and the Laplace equation governing the electrostatic

potential, with the aim to determine the value $U = U_0$ of applied voltage such that the problem admits a non-trivial solution for the particle densities. Note that this problem becomes ill-posed in the no-discharge situation, where the ion and electron densities are zero and the boundary condition of zero normal component of the current density at the dielectric becomes trivially satisfied and brings no information concerning the electric field. Therefore, it is unclear whether this problem can be solved by means of standard eigenvalue solvers. However, it can be efficiently solved by means of the resonance method.

The procedure is as follows. The first and second steps of the procedure described in Sec. 2.4.1 are performed with the boundary condition of zero normal component of the electric field at the dielectric surfaces (instead of zero normal component of the current density). As in the case where no dielectric is present, the electric field distribution is decoupled from the ion and electron distributions and is linear with respect to U, so it is sufficient to perform the electrostatic simulation only once.

At the next step, the obtained solution for $I = I_1$ is recalculated with the boundary condition of zero normal electric field at the dielectric surfaces being replaced by the condition of zero normal component of the current density. This involves solving the equations governing the distributions of the ions and the electrons in the gap and the Laplace equation for the electrostatic potential, and these equations are now coupled through the boundary condition of zero normal current density. The problem is nonlinear and the distributions computed at the previous steps are used as an initial approximation.

Then the third to fifth steps of the procedure described in Sec. 2.4.1 are performed and thus the discharge is computed in the whole range of its existence. These steps do not need to be modified due to the presence of the dielectric and are performed in the same way as described in Sec. 2.4.1.

In chapter 4 the procedure presented here for the resonance method will be extensively applied for the case of a setup containing a dielectric surface.

2.5 Summary

The work aims at developing an integrated approach for the computation of low-current quasi-stationary discharges, from the inception to a non-stationary transition to another discharge form, such as a transition from the Townsend discharge to a normal glow discharge or the corona-to-streamer transition. This task involves three steps: (i) modelling of the ignition of a self-sustaining discharge, (ii) modelling of the quasi-stationary evolution of the discharge with increasing current, and (iii) the determination of the current range where the quasi-stationary discharge ceases to exist

and the above-mentioned non-stationary transition begins. Each of these three steps is considered in some detail with a number of examples, referring mostly to discharges in atmospheric-pressure air.

The ignition of self-sustained gas discharges is governed by a multidimensional boundary-value eigenvalue problem for a system of stationary partial differential equations (and possibly also integro-differential equations), formulated in Sec. 2.3.1. The physical sense of the problem is that the applied voltage should be such that direct ionization by the impact of electrons accelerated by the applied electric field and photoionization by photons generated in the discharge are just sufficient to compensate for the losses of charged particles. There are two special cases where the applied electric field may be considered as uniform and the formulated problem is reduced to one dimension. The first one is the case of discharge ignition between wide parallel-plate electrodes. The formulated eigenvalue problem leads to the well-known self-sustainment condition (2.10) in this case, provided that similar simplifications are applied. The second special case is the one of self-sustainment field in the cross section of a plane or cylindrical positive column of a long low-current discharge. In this case, the formulated problem takes a form similar to the well-known eigenvalue problem for an ordinary differential equation describing the ambipolar diffusion of charged particles in the cross section of a positive column under the assumption of quasi-neutrality. The difference is that at the discharge ignition the transversal electric field is zero, the diffusion is free and not ambipolar, and there is no quasi-neutrality.

In the general case, the formulated eigenvalue problem for the ignition of a self-sustaining discharge is multidimensional and its numerical solution is not trivial. In Sec. 2.3.2, among other methods to solve the eigenvalue problem for the self-sustainment voltage, the resonance method was recognized as the one easier to implement and use. The method is based on solving linear partial differential equations and can be implemented with the use of standard solvers, including commercial ones. It is robust and fast and has given useful results in a wide range of conditions and complex geometries.

An important advantage of the resonance method is its physical transparency. In particular, it allows one to use this method not only for simulations of ignition of self-sustaining discharges, but also as a module of a more general code for the modelling of quasi-stationary self-sustained discharges. Such an integrated approach, based on a combination of the resonance method and stationary solvers, is described in Sec. 2.4.1 and allows modelling of quasi-stationary low-current discharges in the whole range of their existence starting from the inception. The use of stationary solvers instead of time-dependent ones dramatically reduces the computation time, and this reduction is especially large in discharges with strongly varying length scales, such as

corona discharges, where a variation of the mesh element size by orders of magnitude is indispensable.

The integrated approach to the modelling of quasi-stationary low-current discharges offers the possibility of calculating all existing stationary solutions, or, in other words, all steady-states of the discharge that are theoretically possible, regardless of their stability and whether or not they can be observed in a particular experiment. An example of the usefulness of this feature is the possibility of computation of time-averaged characteristics of pulsed negative coronas by means of a stationary solver, discussed at the end of Sec. IV B of [52]. Note that time-dependent solvers, while being an adequate tool for studies of spatiotemporal evolution of individual pulses, cannot be used for direct calculation of time-averaged characteristics of a pulsed corona.

The stability of the computed steady-states may be studied separately. Stability against small perturbations may be studied by means of solving the eigenvalue problem resulting from the linear stability theory. An alternative approach to the investigation of stability is to employ the same code that was used for calculation of the steady-state solution with the stationary solver replaced by a time-dependent one; a perturbation is applied to the steady-state solution and the development of the perturbation is followed by means of the time-dependent solver. An example of application of a time-dependent solver for investigation of stability of a positive point-to-plane corona discharge against perturbations of various amplitudes is given in Sec. V of [52].

In the following chapters the resonance method will be used to evaluate the self-sustaining state and corresponding voltage for several geometries. In Chap. 4, it will be used to establish a connection between self-sustainment and breakdown voltages.

Chapter 3

Validation of the Townsend criterion for ignition of volume gas discharges

3.1 Introduction

The content of this chapter was adapted from the article [74] published in the journal Plasma Sources Science and Technology (2023).

In accurate mathematical terms, the ignition of self-sustained electrical discharges is governed by an eigenvalue problem for linear partial differential equations describing ion and electron transport in the applied electric field, as explained in Chap. 2. It should be expected that the classical Townsend ignition criterion may be derived from this eigenvalue problem under appropriate assumptions. In the case of parallel-plate geometry, where the electric field distribution is one-dimensional, such derivation should be simple. However, the derivation for multidimensional cases is less obvious.

It is of interest to find this derivation, to identify the relevant assumptions, and to evaluate the error introduced by these assumptions in the computation of the ignition (self-sustainment) voltage. The latter may be performed by means of comparison of the ignition-voltage, computed by means of the Townsend criterion, with values obtained by exact numerical solution of the general eigenvalue problem.

A mathematical validation and evaluation of the accuracy of a classical formula are of considerable scientific interest. In the case of the Townsend criterion, such treatment will also be useful for applications: the ignition-voltage of self-sustained discharges represents an important reference point in the investigation of breakdown in high-voltage electrical equipment in low-frequency, e.g., 50 Hz, electric fields, where the time of variation of the applied voltage is much longer than the ion drift time.

There is a vast literature on different aspects of the Townsend criterion and the (closely related) Paschen law. Without trying to cover this extensive field, we only mention a few examples. Data on cathode processes of importance for discharge initiation in DC uniform electric fields are compiled and analyzed in [75] for argon and in [76] for a number of rare and molecular gases. Equations describing the discharge initiation in RF fields and combined RF and DC fields have been derived in [77] and [78], respectively. A transition from the Townsend discharge to the streamer breakdown was studied in [79]. The effect of electrode shape on Paschen curves was studied in [80] and the conclusion was drawn that for some ranges of conditions the discharge may develop several spatial configurations. While understanding of the initial ionization processes in dense media, including in liquids, remains incomplete (e.g., [12, 81]), it was shown in [82] that in certain cases the discharge inception voltages in liquids can be estimated using the Townsend criterion. An application of the Townsend criterion to the analysis of operation of internal combustion engines is considered in [83]. The determination of molecular parameters relevant to the discharge initiation in high-pressure gases was considered in [84]. A review of the discharge-initiation physics in connection with nanomaterial-based ionization gas sensors is given in [85]. Paschen's law for argon with account of nonuniform DC electric field, the loss of electrons due to radial diffusion, and the applied axial magnetic field has been derived in [86]. Evaluation of inception voltages for quasi-uniform air gaps bounded by dielectric layers is performed in [87]. One can hope that the mathematical validation and evaluation of the accuracy of the classical Townsend criterion, proposed in this chapter, will be a useful addition to these and other works and will contribute to a wider use of their results.

The outline of this chapter is as follows. In section 3.2, the eigenvalue problem for ignition of volume discharges is formulated in the drift approximation and a multidimensional Townsend criterion derived. Verification of the Townsend criterion by comparison with an accurate numerical solution of the general eigenvalue problem is reported in section 3.3. Three examples of discharge ignition in high-pressure air are considered, two of them referring to negative coronas in concentric-cylinder and point-to-plane configurations, and one to an axially symmetric configuration with weakly nonuniform electric field. Conclusions are summarized in section 3.4.

3.2 Eigenvalue problem for ignition of volume discharges and multidimensional Townsend criterion

3.2.1 Drift-approximation eigenvalue problem for discharge ignition

The general eigenvalue problem governing discharge ignition is discussed in detail in Sec. 2.3.1 of the previous chapter. One of the effects taken into account in the model of the last chapter was the diffusion of the charged particles. The diffusion may play a role, for example, in the ignition of discharges along dielectric surfaces. On the other hand, in volume discharges the diffusion is normally a minor effect compared to drift. With the diffusion neglected, the eigenvalue problem is formulated as follows.

The system of conservation equations describing drift of charged particles of various species in an applied electric field reads

$$\nabla \cdot \left(Z_\psi n_\psi \, \mu_\psi \, \mathbf{E} \right) = S_\psi. \tag{3.1}$$

Here $\psi = i_+, \, i_-, \, e$, where the indices i_+, i_-, and e are attributed to different species of positive ions, different species of negative ions, and the electrons, respectively; Z_ψ, n_ψ, and μ_ψ are the charge number, number density, and mobility of species ψ; $\mathbf{E}$ is the applied electric field, and the source terms S_ψ describe volume production and removal of particles of species ψ. Since the charged particle densities at discharge inception are very low, the applied electric field $\mathbf{E}$ is unperturbed by plasma charges and its distribution is considered as known. The source terms S_ψ account for all relevant processes: direct ionization by electron impact, photoionization, attachment, detachment, charge exchange *etc.* Nonlinear processes, including multistep ones (e.g., stepwise ionization) and ion-electron and ion-ion recombination, are insignificant since charged particle densities at discharge inception are very low, hence the source terms S_ψ are linear with respect to the charged particle densities. Heating of the neutral gas is insignificant as well. $|Z_\psi| = 1$ since no multiply charged ions are produced at inception. The mobilities μ_ψ and the kinetic coefficients, which appear when the source terms S_ψ are expanded to describe different processes, are evaluated in the local-field approximation.

According to the conventional definition, the ignition-voltage is a value of the applied voltage such that the applied electric field produces an ionization level just sufficient to compensate losses of the charged particles, so a steady-state balance of the charged particles can be reached. Therefore, Eqs. (3.1) are written in the stationary form, i.e., without derivatives with respect to time.

The system of governing equations includes also equations describing the photoionization rate, which may be computed either by evaluation of an integral (e.g.,

[57, 64, 68, 69]) or by solving partial differential equations (e.g., [61, 88]). It should be stressed that in all the cases the dependence of the photoionization rate on the electron density is linear. Note that the modelling reported in this work has been performed using the three-exponential Screened-Poisson photoionization model [61].

In the general eigenvalue problem for discharge ignition, formulated in Chap. 2, the particle conservation equations are written with account of diffusion and represent second-order partial differential equations of elliptic type, therefore the equation for each species requires a boundary condition at each boundary of the computation domain, including both electrodes. In contrast, Eqs. (3.1), where diffusion is neglected, are partial differential equations of the first order and the equation for each species requires a boundary condition at one of the electrodes. There are no fluxes of positive ions from the anode and the boundary conditions at the anode may be written as

$$n_{\psi a} = 0 \quad (\psi = i_+)\,. \tag{3.2}$$

The indices a and c here and further denote values at the anode and cathode, respectively.

Fluxes of negative ions, if any, from the cathode are absent and the electron density at the cathode is governed by the ion-electron emission,

$$n_{\psi c} = 0 \quad (\psi = i_-)\,, \tag{3.3}$$

$$\mu_{ec} n_{ec} E_c = \gamma \sum_{\psi=i+} \mu_{\psi c} n_{\psi c} E_c - \frac{1}{2} n_{ec} \bar{C}_{ec}. \tag{3.4}$$

Here γ is an effective coefficient of secondary electron emission from the cathode, which is assumed to be the same for different species of positive ions, and $\bar{C}_{ec} = \sqrt{8kT_{ec}/\pi m_e}$ is the mean speed of chaotic motion of the electrons evaluated at the cathode. The second term on the rhs of Eq. (3.4) describes flux of the electrons backscattered to the cathode after suffering one or more collisions with neutral particles; e.g., Appendix A and Appendix A of [75]. Note that the emission of electrons from the cathode can take place also due to photoeffect. Photoeffect can be important for discharge ignition by short voltage pulses, with duration smaller than the time of ion drift. In quasi-stationary conditions, the role of photoeffect is typically small, but in any case it can be taken into account in terms of parameter γ, as is done frequently (e.g., section 4.7.2 of book [20]).

The above-described boundary-value problem, describing drift of the ions and the electrons in an applied electric field, is linear with respect to the ion and electron densities. Moreover, the problem does not contain external ionization terms, which means that from a mathematical point of view it is homogeneous. For all values of the applied voltage, the problem admits a trivial solution: the ion and electron

densities are zero at all points in the gap. This solution describes a situation where the voltage is applied, but no discharge has been ignited. One needs to find the value of the discharge voltage for which the problem admits also a nontrivial solution. This nontrivial solution will describe the particle densities at discharge inception and the corresponding discharge voltage value will represent the inception voltage. In mathematical terms, this is an eigenvalue problem for a system of linear homogeneous partial differential equations (e.g., [89]) and the discharge voltage is eigenparameter. Further details are discussed in Sec. 2.3.1 of Chap. 2.

It should be emphasized that the above-described eigenvalue problem takes into account all processes that may affect the discharge inception. (We remind that nonlinear processes and neutral gas heating are insignificant since the charged particle densities are very low at discharge inception.) Volume processes are accounted for in the source terms S_ψ in Eqs. (3.1) and include direct ionization by electron impact, photoionization, attachment, detachment, charge exchange *etc.* Processes at the cathode surface are described in terms of the effective ion-electron emission coefficient γ in the boundary condition (3.4); note that this is the only additional approximation, beyond the drift local-field approximation, employed in the above-described eigenvalue problem. If only the processes of direct ionization, photoionization, and attachment are taken into account while all the other processes are neglected, then the above-described eigenvalue problem is reduced to the model proposed in the recent paper [90] to study the inception of positive coronas.

3.2.2 Transforming the eigenvalue problem

Since the applied electric field, being unperturbed, satisfies Gauss's law with zero volume charge density, $\nabla \cdot \mathbf{E} = 0$, Eqs. (3.1) may be rewritten in the form

$$Z_\psi \mathbf{E} \cdot \nabla \left(n_\psi \, \mu_\psi \right) = S_\psi. \tag{3.5}$$

Let us designate by z a coordinate measured along a field line, say, from the cathode to the anode. Then $\mathbf{E} = -E\mathbf{e}_z$, where $\mathbf{e}_z$ is a unit vector directed along the field line (needless to say, this vector varies from one point of a line to another), and Eqs. (3.5) may be written as

$$Z_\psi E \frac{\partial}{\partial z} \left(n_\psi \, \mu_\psi \right) = -S_\psi. \tag{3.6}$$

This is an equivalent form of Eqs. (3.1), describing drift of charged particles of various species.

Boundary condition (3.4) may be rewritten in a more compact form:

$$n_{ec}\mu_{ec} = \gamma' \sum_{\psi=i+} \mu_{\psi c} n_{\psi c}, \tag{3.7}$$

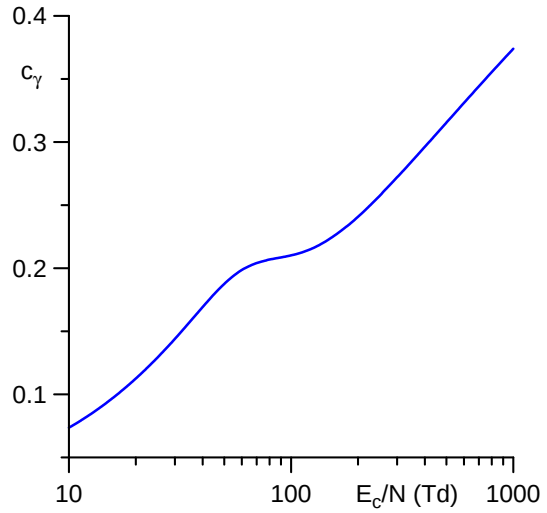

Figure 3.1: Coefficient c_γ, characterizing the effect of backscattering of emitted electrons to the cathode.

where

$$\gamma' = c_\gamma \gamma, \qquad c_\gamma = \left(1 + \frac{1}{2}\frac{\bar{C}_{ec}}{v_{ec}}\right)^{-1}, \tag{3.8}$$

and $v_{ec} = \mu_{ec} E_c$ is the electron drift speed evaluated at the cathode. For convenience, graph of the quantity c_γ for dry air is shown in Fig. 3.1. The electron drift speed and temperature were evaluated as described in Appendix B. N is the total number density of neutral particles, so E_c/N is the reduced electric field at the cathode.

Equations describing the photoionization rate involve the electron density, but not densities of the ions. Since, additionally, ion-electron and ion-ion recombination and similar nonlinear processes are insignificant at discharge ignition, the net production rates S_ψ of the electrons and negative ions at discharge ignition do not depend on the densities of positive ions. It follows that the equations of conservation of the electrons and negative ions, Eqs. (2.12) [or, equivalently, (3.6)] for $\psi = e, i_-$, do not involve the densities of positive ions. The same is true for the boundary conditions for the negative ions, Eqs. (3.3). On the other hand, the boundary condition for the electrons, Eq. (3.4), does involve the positive ion densities. Hence, the evaluation of the negative-particle densities and the photoionization rate cannot be decoupled from the evaluation of the density of positive ions and the eigenvalue problem (3.1)-(3.4) needs to be solved as a whole.

However, one can transform the boundary condition for the electrons, Eq. (3.4) [or, equivalently, (3.7)], to an equivalent form which would not involve densities of positive ions. Multiplying Eqs. (3.6) by Z_ψ, summing over ψ, and taking into account that the rhs of the obtained equation vanishes due to charge conservation in reactions, one

obtains

$$\frac{\partial}{\partial z}\left(\sum_{\psi}\mu_{\psi}n_{\psi}\right)=0. \tag{3.9}$$

The meaning of this equation is clear: electrical conductivity of the ionized gas is constant along each field line; a feature of media which are subject to Ohm's law in cases where the electric field distribution is Laplacian.

Equating the electrical conductivities at the anode and the cathode and making use of the boundary conditions (3.2), (3.3), and (3.7), one can write

$$\mu_{ea}n_{ea}+\sum_{\psi=i-}\mu_{\psi a}n_{\psi a}=\mu_{ec}n_{ec}\left(1+\frac{1}{\gamma'}\right). \tag{3.10}$$

This relation applies to points of the same field line positioned on the cathode and the anode and is valid for each field line. It may be viewed as an equivalent form of Eq. (3.4), i.e., as a boundary condition for the electron density specifying the ion-electron emission at the cathode surface. As desired, this boundary condition does not involve densities of positive ions.

Thus, the eigenvalue problem (3.1)-(3.4), supplemented with equations describing the photoionization rate, which governs the ignition of a self-sustaining drift-dominated discharge and describes drift of charged particles in an applied electric field, may be split: in order to find the ignition-voltage, it is sufficient to solve the eigenvalue problem comprising Eqs. (3.1) [or (3.6)] for $\psi=e,i_-$, boundary conditions (3.3) and (3.10), and equations for the photoionization rate, which describes drift of only negative particles.

3.2.3 Multidimensional Townsend criterion

Since the photoionization rate depends on the electron density values in the whole discharge region, the equations of conservation of the electrons and negative ions, Eqs. (3.6) for $\psi=e,i_-$, in the general case cannot be solved for a single field line without regard of the electron and negative ion densities in the rest of the discharge region. Therefore, analytical solution of the eigenvalue problem formulated in the preceding section with account of photoionization is hardly possible.

Let us assume that photoionization is insignificant and may be discarded. Then Eqs. (3.6) for $\psi=e,i_-$ represent a system of linear ordinary differential equations, which may be solved separately for each field line without regard of the densities along other field lines. If the electric field is uniform in space, coefficients of these differential equations are constant and the equations may be solved analytically; e.g., equation (16) on p. 709 of [91].

In the general case, coefficients of the linear ordinary differential Eqs. (3.6) for $\psi=e,i_-$, being functions of E, vary with z, therefore an analytic solution is still

hardly possible. However, there are cases where a partial integration is possible: these are cases of electropositive gases and electronegative gases provided that the detachment is insignificant. The electron source term S_e in these cases may be written as $S_e = \mu_e E(\alpha - \eta) n_e$, where α is the Townsend ionization coefficient and η is the Townsend integral attachment coefficient, which takes into account all relevant attachment reactions ($\eta = 0$ for electropositive gases). Equation (3.6) for $\psi = e$ becomes independent of the densities of negative ions and may be readily integrated to give

$$\mu_e n_e = \mu_{ec} n_{ec} e^K, \tag{3.11}$$

where

$$K = K(z) = \int_0^z (\alpha - \eta)\, dz \tag{3.12}$$

is the so-called ionization integral.

Let us sum Eqs. (3.6) for the negative ions. Taking into account that $\sum_{\psi=i-} S_\psi = \mu_e E \eta n_e$, one obtains

$$\frac{\partial}{\partial z}\left(\sum_{\psi=i-} n_\psi \mu_\psi\right) = \eta \mu_e n_e. \tag{3.13}$$

Substituting Eq. (3.11), integrating over z from 0 to z_a (along the whole field line from the cathode to the anode), and making use of boundary condition (3.2), one obtains

$$\sum_{\psi=i-} \mu_{\psi a} n_{\psi a} = \mu_{ec} n_{ec} \int_0^{z_a} \eta e^K dz. \tag{3.14}$$

It follows from Eq. (3.11) that $\mu_{ea} n_{ea} = \mu_{ec} n_{ec} e^{K_a}$. [Here $K_a = K(z_a)$ is the ionization integral evaluated along the whole field line.] Substituting this relation and Eq. (3.14) into, respectively, the first and second terms on the lhs of the boundary condition (3.10), one may transform this boundary condition to

$$n_{ec}(W_1 - W_2) = 0, \tag{3.15}$$

where

$$W_1 = e^{K_a} + \int_0^{z_a} \eta e^K dz, \quad W_2 = 1 + \frac{1}{\gamma'}. \tag{3.16}$$

Equation (3.15) must be satisfied for each field line. Hence, there are two possibilities for each field line: either $n_{ec} = 0$, or $W_1 = W_2$. If n_{ec} the electron density at the cathode is zero for a given field line, then the electrical conductivity is zero at all points of the line [cf. Eqs. (3.9) and (3.10)] and therefore the charged particle densities equal zero as well. Therefore, the equality $W_1 = W_2$ should hold for at least one field line, otherwise the charged particle densities will be zero in the whole calculation domain or, in other words, only the trivial solution will exist.

Equation (3.15) was obtained by partial integration, under certain assumptions, of the eigenvalue problem (3.1)-(3.4), governing the ignition of self-sustained drift-dominated discharges and describing ion and electron transport in the applied electric field. However, Eq. (3.15) only requires knowledge of the input parameters of the problem: the Townsend ionization and attachment coefficients α and η and the secondary electron emission coefficient γ', specified as functions of the reduced electric field, and the spatial distribution of the applied electric field. Thus, Eq. (3.15) represents a necessary condition for the problem (3.1)-(3.4) to be solvable, i.e., to admit a nontrivial solution for distributions of the ion and electron densities. In mathematical terms, (3.15) is an equation for the eigenvalue parameter. From the point of view of gas discharge physics, Eq. (3.15) represents the multidimensional Townsend ignition criterion.

Note that the terms on the rhs of the first Eq. (3.16) describe contributions of, respectively, electrons and negative ions to the electrical conductivity of the ionized gas at the anode. Substituting into the second term the expression $\eta = \alpha - dK/dz$, which follows from Eq. (3.12), one can obtain for $W_1 - W_2$ a compact formula

$$W_1 - W_2 = \int_0^{z_a} \alpha e^K dz - \frac{1}{\gamma'}. \tag{3.17}$$

Note also that in the particular case $\eta = 0$, where no attachment takes place and hence no negative ions are present, the second term on the rhs of the first Eq. (3.16) vanishes and one can write

$$W_1 = \exp \int_0^{z_a} \alpha \, dz, \quad W_2 = 1 + \frac{1}{\gamma'}. \tag{3.18}$$

Expressions for the Townsend criterion available in the literature refer to a single field line. For brevity, let us call this case one-dimensional (1D). The Townsend criterion (3.15) is reduced to

$$W_1 - W_2 = 0 \tag{3.19}$$

in this case. This 1D version of the Townsend criterion must be consistent with accurate expressions for the Townsend criterion available in the literature. Indeed, Eq. (3.19), supplemented with Eq. (3.18), represents the well-known Townsend criterion in electropositive gases, except that the conventional effective ion-electron emission coefficient γ is replaced with the coefficient γ', accounting for the return of a fraction of emitted electrons to the cathode after suffering one or more collisions with neutral molecules. On the other hand, Eq. (3.19), supplemented with Eq. (3.17), coincides with the Townsend criterion obtained by noting that the integral on the rhs of Eq. (3.17) represents the total number of ionizations along the field line per one electron emitted from the cathode (e.g., [92]).

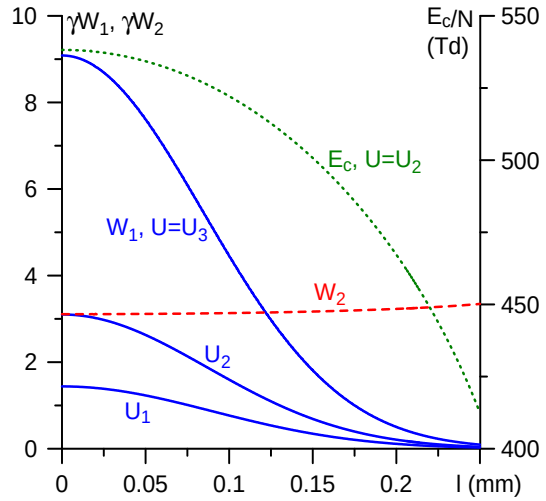

Figure 3.2: Example of application of the multidimensional Townsend criterion (3.15), (3.16) to a point-to-plane negative corona. l: distance from the axis of symmetry measured along the cathode surface. Solid: W_1 for different field lines and for three values of the applied voltage. Dashed: W_2. Dotted: reduced electric field at the cathode surface.

To see how the multidimensional version of the Townsend criterion should be applied, let us consider as a simple example a point-to-plane negative corona. Typical values of quantities γW_1 and γW_2 are plotted in Fig. 3.2 for different field lines, which are identified by l the distance from the axis of symmetry measured along the cathode surface, and for three values of the applied voltage $U_1 < U_2 < U_3$. Also plotted is a typical distribution of the reduced electric field at the cathode surface. With the use of the data exemplified by Fig. 3.1, the quantity W_2 may be evaluated in terms of E_c; its values for all three values of the applied voltage are very close to each other and are represented by the same line.

If the applied voltage is low, then the inequality $W_1 < W_2$ will hold for all field lines as illustrated by the curve $U = U_1$ in Fig. 3.2. It was shown above that $n_{ec} = 0$ for all field lines and, consequently, the charged particle densities are zero at all points of all field lines, meaning zero current density. Hence, no discharge is possible for this voltage. As the applied voltage is increased, a voltage value is reached at which Eq. (3.19) is satisfied for a field line coinciding with the axis; the curve $U = U_2$ in Fig. 3.2. The current can flow along this line. $n_{ec} = 0$ for all the other field lines, meaning that no current can flow along any off-axis field line. Hence, there is a self-sustaining discharge localized at the axis (and in its vicinity, because of the diffusion of the electrons and the ions in the radial direction).

As the applied voltage is increased further, $U = U_3$, Eq. (3.19) is satisfied for an off-

axis field line or, more precisely, for a set of field lines forming an axially symmetric cylinder-like surface. One could think of a stationary solution with current flowing along this surface and no current both inside and outside the surface, although this solution is likely to be unstable since perturbations inside the surface will be amplified.

The ignition-voltage, by definition, is the minimum voltage for which a self-sustaining discharge is possible, and this is $U = U_2$. Thus, the eigenvalue problem governing the ignition-voltage in multidimensional configurations leads to the requirement that the applied voltage be just high enough for the Eq. (3.19) to be satisfied for at least one field line; an intuitively clear result.

3.2.4 Discussion

Equation (3.15), which is a corollary of the eigenvalue problem (3.1)-(3.4), governing the ignition of a self-sustaining drift-dominated discharge, represents the Townsend ignition criterion as expected, and may be viewed as a natural extension of the classical criterion to multidimensional configurations.

The validity of the Eq. (3.15) is limited by the neglect of the diffusion of the charged particles, of the photoionization, and, in the case of electronegative gases, also of the detachment. It is well known that the photoionization is a major effect in positive corona-like configurations. Therefore, the Townsend criterion may be useful only for negative corona-like configurations and configurations with weakly nonuniform electric field.

Neglecting detachment prevents straightforward application of Eq. (3.15) to electronegative gases. However, it still provides useful information: the Townsend criterion in the form (3.15), (3.16), which accounts for the attachment but neglects the detachment, gives an upper estimate of the inception voltage, while the Townsend criterion in the form (3.15), (3.18) neglects the attachment (and thus the presence of negative ions altogether) and therefore gives a lower estimate of the inception voltage. Moreover, one can try to obtain an accurate estimate for the inception voltage by means of the Townsend criterion in the form (3.15), (3.16) if the Townsend attachment coefficient η is replaced with an effective attachment coefficient, which would take into account, in an approximate way, also the detachment.

3.3 Verification of the Townsend criterion by results of numerical simulations

In this section, the Townsend criterion is applied to three examples of discharge ignition in high-pressure room-temperature air, two of them referring to negative corona-like

configurations and one to a configuration with weakly nonuniform electric field. The results are compared with those obtained by an accurate numerical solution of the general eigenvalue problem that governs discharge ignition, as in Chap. 2, and takes into account diffusion, photoionization, and the presence of multiple ion species with various reactions. The numerical solution of the eigenvalue problem was obtained by means of the resonance method, introduced in the previous chapter, for a reasonably detailed plasmachemical model of high-pressure dry air summarized in Appendix B. The photoionization rate was evaluated by means of the three-exponential Screened-Poisson model [61].

The data from Tab. B.1 of Appendix B were used for the evaluation of ionization and integral attachment coefficients α and η in the Townsend criterion. η was evaluated as

$$\eta = \eta_2 + \eta_3, \tag{3.20}$$

where η_2 and η_3 are Townsend coefficients of production of ions O^- via two-body (dissociative) attachment and of ions O_2^- via three-body attachment. The electron mobility, needed for the evaluation of γ', was estimated as given in Appendix A.

As mentioned in the preceding section, one can try to improve the Townsend criterion (3.15), (3.16) by replacing the Townsend integral attachment coefficient with an effective attachment coefficient, which would take into account, in an approximate way, also the detachment. In the case of air, one can try using the effective attachment coefficient proposed in [62]:

$$\eta = \eta_2 \frac{k_8 n_{O_2} N}{k_6 n_{N_2} + k_7 n_{O_2} + k_8 n_{O_2} N}. \tag{3.21}$$

Here k_6 is the rate constant of associative detachment from O^-, k_7 is the rate constant of charge transfer from O^- to O_2; k_8 is the rate constant of conversion of O^- to O_3^-; n_{N_2} and n_{O_2} are the number densities of, respectively, nitrogen and oxygen molecules; and the total number density of neutral molecules is expressed as $N = n_{N_2} + n_{O_2}$. The above rate constants were evaluated using formulas from Tab. B.1 of Appendix B.

The negative corona experiment [93] is considered as the first example. The configuration is that of coaxial cylinders, the diameter of the inner cylinder was either 0.239 cm or 0.0178 cm, the diameter of the outer cylinder was 9.75 cm.

It should be emphasized that the methodologically correct way to assess the accuracy of an approximate relation is to compare it with the exact solution of the full theoretical model wherever available, since a direct comparison of an approximate relation with experiment would characterize not only the quality of the approximations, but in the first place the suitability of the theoretical model used. On the other hand, a comparison of results given by the full theoretical model with experimental results

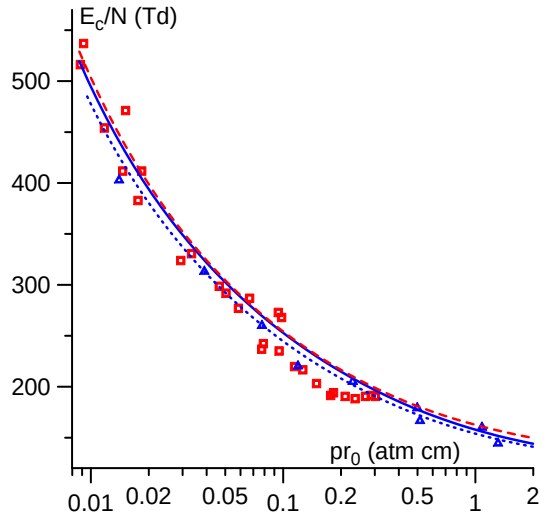

Figure 3.3: Reduced ignition field at the surface of negative corona electrode. Conditions of the experiment [93]: concentric-cylinder corona in air, two values of the diameter of the inner electrode, $2r_0$, diameter of the outer electrode 9.75 cm, pressure varying over the range $0.1 - 35$ atm. Lines: numerical solution of the eigenvalue problem. Scatters: experimental data [93]. Solid, triangles: $2r_0 = 0.239$ cm. Dashed, squares: $2r_0 = 0.0178$ cm. Dotted: $c_\gamma = 1$, $2r_0 = 0.239$ cm.

illustrates the accuracy that the theory can claim. In Fig. 3.3, the computed ignition field is compared with the experimental data obtained in a wide pressure range. The dotted line was computed without account of backscattering of emitted electrons to the surface of the cathode and coincides with the corresponding line in figure 8 of [62].

The calculated values depend on the choice of the effective ion-electron emission coefficient γ. The exact value of γ in a particular experiment is not known, and in the modelling γ was taken equal to 10^{-4} and no attempt was made to adjust it to best fit the experimental results. Therefore, the agreement between the calculated and measured data within about 10% (15% for a few points) seems to be quite satisfactory, especially for illustrative purposes as in this work.

The data in Tabs. 3.1 and 3.2 illustrate the effect of longitudinal diffusion over the accuracy of the 1D Townsend criterion under conditions of the negative corona experiment [93]. Here U and U_T are values of the ignition-voltage evaluated by means of, respectively, numerical solution of the eigenvalue problem, obtained without account of photoionization, and the 1D Townsend criterion (3.19). Thus, the deviation of the ratio U_T/U from unity represents a natural measure of the accuracy of the Townsend criterion. Another natural measure is a residual appearing in the Townsend criterion if it is evaluated at the applied voltage equal to the numerical value (U). Following tradition, we write the 1D Townsend criterion (3.19) in logarithmic form, $\ln W_1 = \ln W_2$

γ	U (kV)	K_a	Δ_T (%)	U_T (kV)	$\frac{U_T}{U}-1$ (%)
10^{-6}	25.14	15.00	−0.46	25.21	0.32
10^{-4}	22.90	10.49	−0.34	22.94	0.17
10^{-3}	21.56	8.24	−0.27	21.59	0.13
10^{-2}	19.96	5.98	−0.19	19.98	0.09

Table 3.1: Effect of longitudinal diffusion over the accuracy of the Townsend criterion in air without account of attachment. Coaxial-cylinder negative corona under conditions of experiment [93], $2r_0 = 0.239\,\text{cm}$, $pr_0 = 0.1\,\text{atm cm}$, different values of secondary electron emission coefficient.

pr_0 (atm cm)	U (kV)	K_a	Δ_T (%)	U_T (kV)	$\frac{U_T}{U}-1$ (%)
0.01	4.59	9.66	−1.51	4.64	1.11
0.1	23.37	−11.04	−0.35	23.41	0.17
1	152.04	−3281	−0.07	152.07	0.02

Table 3.2: Effect of longitudinal diffusion over the accuracy of the Townsend criterion in air without account of detachment. Coaxial-cylinder negative corona under conditions of experiment [93], $2r_0 = 0.239\,\text{cm}$, different values of pressure.

[in the case without negative ions, this form is reduced to the conventional condition of the ionization integral being equal to $\ln(1+1/\gamma')$], and define the normalized residual as

$$\Delta_T = \frac{\ln W_1 - \ln W_2}{\ln W_1 + \ln W_2}, \tag{3.22}$$

where W_1 and W_2 are evaluated at the applied voltage equal to the numerical value (U). Also shown in the tables is the ionization integral K_a evaluated at the applied voltage equal to the numerical value. Note that all the data in the tables, as well in the subsequent Tabs. 3.3-3.5, are independent of the numerical mesh (they did not change when each mesh element in the computation domain was split in half).

U in Tab. 3.1 was evaluated numerically disregarding the presence of negative ions and photoionization and U_T was evaluated by means of the 1D Townsend criterion (3.19), (3.18). Thus, Tab. 3.1 corresponds to conditions in electropositive gases. The only source of error in the Townsend criterion compared to the exact numerical solution in this table is the longitudinal diffusion, which is taken into account in the numerical solution but not in Eqs. (3.19), (3.18). One can see that the error is quite small for all values of γ, below about 0.3% for the ignition-voltage values and 0.5% as far as the residual is concerned. Note that there is a difference of about 1.2 to 1.4 between K_a and the value of $\ln\left(1+\gamma^{-1}\right)$, which is due to γ' being different from γ.

The data in Tab. 3.2 were evaluated with account of the presence of negative ions, which are produced via attachment, but without account of detachment. More

pr_0	Eigenvalue problem				Townsend criterion (3.19)				Exp.
(atm cm)	a)	b)	c)	d)	(3.16), (3.20)	(3.18)	(3.16), (3.21)	(3.23)	[93]
0.014	5.60	5.70	5.72	5.68	5.77	5.73	5.73	5.81	5.1
0.119	26.16	26.23	26.69	26.10	26.73	26.14	26.16	27.10	24
1.083	153.21	153.24	163.12	148.39	163.15	148.42	152.77	166.58	157

Table 3.3: Ignition voltages for the negative corona in the concentric-cylinder configuration under conditions of experiment [93], in kV. $2r_0 = 0.239\,\text{cm}$, different values of pressure. a)Full model. b)No photoionization. c)No photoionization and no detachment. d)No photoionization and no attachment.

precisely, U was evaluated numerically disregarding detachment and photoionization and U_T was evaluated by means of the 1D Townsend criterion (3.19), (3.16). The secondary electron emission coefficient γ was taken equal to 10^{-4}, as well as when calculating the data in Tabs. 3.3 and 3.4 below. Again, the longitudinal diffusion is the only source of error in the Townsend criterion compared to the exact numerical solution. The maximum error is somewhat bigger than that in Tab. 3.1, however still quite small, of the order of 1% as the inception voltage is concerned, including for the higher values of pr_0, when the ionization integral K_a is strongly negative.

The effect of diffusion, the photoionization, and the detachment over the self-sustainment voltage and over the accuracy of the Townsend criterion is illustrated by Tabs. 3.3-3.5 for different discharge configurations. The tables show the ignition-voltage values obtained by numerically solving the eigenvalue problem in various approximations and from various forms of the Townsend criterion. Although the most important aspect for the purposes of this work is the accuracy of various forms of the Townsend criterion compared to the numerical solution of the eigenvalue problem subject to appropriate approximations, it is nonetheless interesting to illustrate the accuracy of the results given by the full eigenvalue problem compared to experiment. Therefore, experimental values of the inception voltage are included in Tabs. 3.3-3.5.

Table 3.3 refers to a negative concentric-cylinder corona. Results of the numerical solution of the eigenvalue problem have a transparent physical meaning. Comparison of the data in columns a) and b) shows that the disregard of the photoionization results in a weak increase of the ignition-voltage. The disregard of detachment results in a further increase of the ignition-voltage (columns b) and c)), which is weak for lower pressures but becomes more appreciable for higher values. The disregard of attachment results in a decrease of the ignition-voltage (columns b) and d)), which is weak for low pressures but becomes stronger for higher pressures. One can see that the models c) and d), which disregard, in addition to the photoionization, also detachment or attachment, provide upper and lower estimates for the inception voltage given by the model b), which accounts for the full kinetics involving negative ions (but still neglecting

the photoionization). Of course, this result should have been expected. Moreover, since the effect of photoionization is weak, the models [c)] and [d)] provide reasonably accurate upper and lower estimates also for the full model[a)].

The ignition-voltages given by the 1D Townsend criterion in the form (3.19), (3.16), (3.20) are very close to the values given by numerical solution of the eigenvalue problem without account of photoionization and detachment (column [c)]). The voltages given by the 1D Townsend criterion in the form (3.19), (3.18) and the values given by numerical solution of the eigenvalue problem without account of photoionization and attachment (column [d)]) are close as well. (This is another indication that the effect of longitudinal diffusion is within approximately 1%.) It is unsurprising therefore that the two versions of the Townsend criterion, Eqs. (3.19), (3.16), (3.20) and Eqs. (3.19), (3.18), provide reasonably accurate upper and lower estimates for the inception voltage given by the numerical solution of the full model[a)].

For lower pressures, the upper and lower estimates provided by Eqs. (3.19), (3.16), (3.20) and by Eqs. (3.19), (3.18) are close to each other, indicating that the effect of the presence of negative ions on the ignition-voltage is weak in these conditions. With increase of pressure, however, the gap between the lower and upper estimates widens and reaches approximately 15 kV for $pr_0 = 1.083\,\mathrm{atm\,cm}$, thus significantly exceeding the difference between the full model and the experiment (approximately 4 kV). Therefore, it is worth trying to obtain a more accurate theoretical estimate for the inception voltage. One can see that the 1D Townsend criterion (3.19), (3.16) with the effective attachment coefficient given by Eq. (3.21), which was proposed in [62], provides high accuracy for all pressures.

A popular approximate form of the 1D Townsend criterion in electronegative gases is

$$\int_{\alpha\geq\eta} (\alpha - \eta)\, dz = \ln\left(1 + \frac{1}{\gamma'}\right), \tag{3.23}$$

where the integral on the lhs is evaluated over the ionization zone, i.e., the section of the field line where $\alpha \geq \eta$; e.g., equation (12.14) on p. 346 of the book [20] (note that the latter equation involves γ, rather than γ'). For comparison, values of ignition-voltage given by this formula are shown in Tab. 3.3 as well. One can see that these values for high pressures are significantly less accurate than those given by the Townsend criterion (3.19), (3.16), (3.21).

Table 3.4 refers to a point-to-plane negative corona under conditions of experiment [94]. This is a 2D configuration, so the multidimensional Townsend criterion (3.15) should be used. Its application is illustrated by Fig. 3.2, which actually refers to the experimental conditions [94] with point-to-plane distance $d = 5\,\mathrm{mm}$, the Townsend

d	Eigenvalue problem				Townsend criterion (3.15)			Exp.
(mm)	a)	b)	c)	d)	(3.16), (3.20)	(3.18)	(3.16), (3.21)	[94]
5	4.28	4.28	4.29	4.27	4.33	4.31	4.31	4.5
8	4.82	4.83	4.84	4.82	4.88	4.86	4.86	4.7
10	4.95	4.95	4.96	4.94	5.01	4.98	4.98	5.0
14	5.31	5.32	5.33	5.31	5.38	5.35	5.35	6.1

Table 3.4: Ignition voltages for the negative corona in the point-to-plane configuration under conditions of experiment [94], in kV. 1 atm, tip curvature 0.2 mm, variable point-to-plane distance d. $^{a)-d)}$: same as in table 3.

criterion in the form (3.15), (3.16), (3.20), $U_1 = 4.2\,\mathrm{kV}$, $U_2 = 4.33\,\mathrm{kV}$, $U_3 = 4.5\,\mathrm{kV}$, and E_c/N corresponding to $U = 4.33\,\mathrm{kV}$. As should have been expected, the maximum value of W_1 in this case is reached for the field line coinciding with axis of symmetry.

The mesh elements in the modelling were triangles, and the data in Tab. 3.4 did not change when each mesh element in the computation domain was split in half. (The same applies to the Tab. 3.5.)

The data shown in Tab. 3.4 follow the same pattern as those in Tab. 3.3, except that the values of the ignition-voltage, estimated using different approximations for a given point-to-plane distance, are all very close to each other. This means that the effect of the presence of negative ions over the ignition-voltage is insignificant for all values of the point-to-plane distance. This is a consequence of the small tip curvature (0.2 mm): the electric field in the bulk of the ionization zone significantly exceeds the critical field and hence the attachment is insignificant. The only source of error in the Townsend criterion in the form (3.15), (3.16), (3.20) or in the form (3.15), (3.18) compared to the exact numerical solution in the column$^{c)}$ or $^{d)}$ is diffusion, which is both longitudinal and transversal in this geometry. One can see that the effect of diffusion again is around 1%.

In Fig. 3.4, a setup with a weakly non-uniform electric field studied in the experiment [25] is shown: an axially symmetric configuration consisting of a cylindrical dielectric spacer stacked between two disk electrodes. Also shown is an example of distribution of the electron density at discharge inception, obtained from the numerical solution of the eigenvalue problem. Note that the computed charged particle density distributions at inception are proportional to the discharge current due to the linearity of the eigenvalue problem; the absolute values shown in the figure correspond to the discharge current of 100 μA. (This seems to be a reasonable value for the inception current given the relatively large area of the discharge attachments, which are rings with a radius of approximately 7.5 mm.) Note also that the secondary electron emission coefficient was set equal to 0.03 in the modelling performed for this setup.

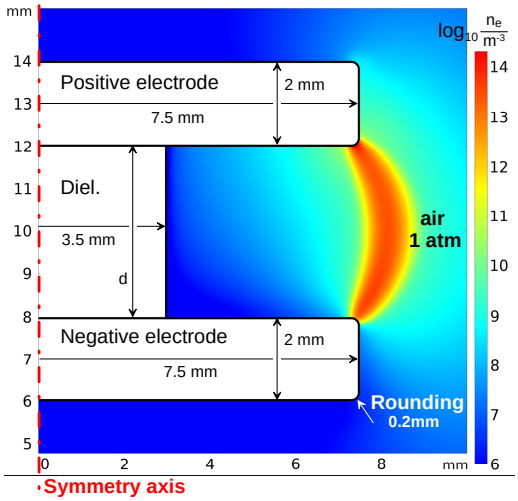

Figure 3.4: Setup of the experiment [25]. The computed distribution of the electron density at discharge inception corresponds to $d = 4\,\mathrm{mm}$ and the discharge current of $100\,\mu\mathrm{A}$.

The application of the multidimensional Townsend criterion (3.15) to this setup is illustrated by Fig. 3.5. The quantities W_2 for all three values of the applied voltage (6.3, 6.46, and 6.6 kV) are very close to each other and are represented by the same line. As should have been expected, the maximum value of W_1 is reached for the field line that begins and ends at the roundings of the electrodes (and not for the field line coinciding with the axis of symmetry, in contrast to the point-to-plane configuration to which Fig. 3.2 and Tab. 3.4 refer). However, the points where the maximum-W_1 field line begins and ends do not coincide with the points of maximum of the surface electric field E_c, again in contrast to the point-to-plane configuration to which Fig. 3.2 and Tab. 3.4 refer.

Computed data referring to the setup shown in Fig. 3.4 are given in Tab. 3.5. The data in the last column of the table were obtained by averaging the experimental mean DC breakdown fields for cases where the dielectric spacer material is Teflon, Plexiglas (for $d = 4\,\mathrm{mm}$), Pyrex glass, and Macor glass ceramic, given in table III of [25]. Note that while the experimental values refer to the DC breakdown (flashover), the breakdown voltage in configurations with weakly non-uniform electric field usually is close to the ignition-voltage.

One can see that the accuracy of the Townsend criterion in this more complex 2D geometry with a weakly non-uniform field is comparable to the accuracy in the two previous geometries. The effect of diffusion again is around 1%.

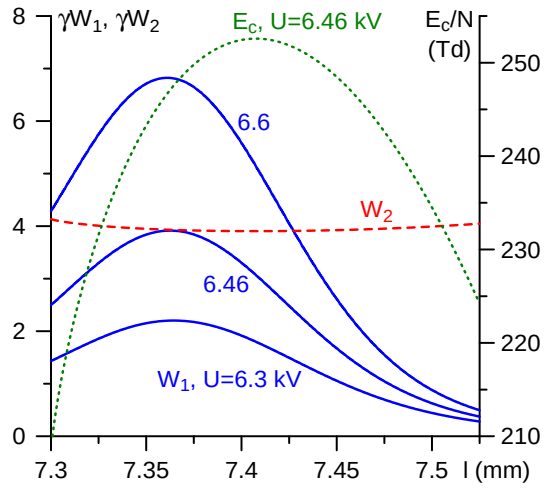

Figure 3.5: Application of the of the multidimensional Townsend criterion (3.15) to the device shown in figure 3.4. $d = 2\,\mathrm{mm}$. l: distance from the symmetry axis measured along the cathode surface. Solid: quantity W_1, evaluated by means of equations (3.16), (3.20), for different field lines and three values of the applied voltage. Dashed: W_2. Dotted: reduced electric field at the cathode surface for $U = 6.46\,\mathrm{kV}$.

d	Eigenvalue problem				Townsend criterion (3.15)			Exp.
(mm)	*a)*	*b)*	*c)*	*d)*	(3.16), (3.20)	(3.18)	(3.16), (3.21)	[25]
2	6.24	6.24	6.52	6.16	6.46	6.10	6.16	6.0
4	9.92	9.92	10.45	9.62	10.35	9.52	9.79	9.6

Table 3.5: Ignition voltages under conditions of experiment [25], in kV. 1 atm, variable gap length d. *a)–d)*: same as in Tab. 3.3.

3.4 Conclusions

An eigenvalue problem governing ignition of volume discharges is formulated in the drift approximation. Diffusion of the charged particles is neglected, while other potentially relevant effects, in particular, photoionization and the presence of multiple ion species with various reactions, are taken into account. By means of partial integration the problem may be split: in order to find the ignition-voltage, it is sufficient to solve equations describing drift of electrons and negative ions coupled with equations for the photoionization rate, without expressly considering positive ions, also in cases where the ion-electron emission from the cathode plays a role.

By performing further partial integrations under certain assumptions, the Townsend ignition (self-sustainment) criterion is derived. The assumptions limiting the validity of the derived criterion are the neglect of the diffusion of the charged particles, of the photoionization, and, in the case of electronegative gases, of the detachment.

The effect of diffusion is presumably insignificant for volume discharges. The neglect of photoionization limits the applicability of the criterion to negative corona-like configurations and configurations with weakly non-uniform electric field.

Neglecting detachment prevents straightforward application of the Townsend criterion to electronegative gases. However, it still provides useful information: the Townsend criterion in the form (3.15), (3.16), which accounts for the attachment but neglects the detachment, gives an upper estimate of the inception voltage, while the Townsend criterion in the form (3.15), (3.18), which neglects the attachment, gives a lower estimate. Moreover, one can try to obtain an accurate estimate for the inception voltage by means of replacing the integral attachment coefficient in the Townsend criterion in the form (3.15), (3.16) with an effective coefficient, which would take into account, in an approximate way, also the detachment.

The Townsend criterion is applied to three examples of discharge ignition in high-pressure air, two of them referring to negative coronas in concentric-cylinder and point-to-plane configurations and one to an axially symmetric configuration with weakly nonuniform electric field. In all the cases, the ignition-voltage was computed also by an accurate numerical solution of the general eigenvalue problem governing discharge ignition. The results of the numerical solution show that the effect of photoionization in these cases is weak as expected. The comparison of the results obtained from different forms of the Townsend criterion with those obtained by the numerical solution of the eigenvalue problem shows that the neglect of diffusion produces an error in the ignition-voltage of the order of 1% or less in all the cases.

The lower and upper estimates of the ignition-voltage, obtained from the Townsend criterion without account of attachment or with account of attachment but not de-

tachment, are close to each other in most, but not all, cases considered. This indicates that the effect of negative ions over the inception voltage is weak in these cases; a conclusion confirmed by the numerical results. In other cases, the gap between the lower and upper estimates is significant. The Townsend criterion in the form (3.15), (3.16), (3.21), which employs the effective attachment coefficient in air taking into account, in an approximate way, also the detachment, gives a virtually exact ignition-voltage in all the cases considered and is in this sense a safe bet.

The above results provide validation and extension of the Townsend self-sustainment criterion, which remains widely used as an engineering tool for evaluation of the ignition-voltage in conditions of industrial interest, e.g., for estimation of the hold-off capabilities of high-voltage switchgear operating in low-frequency fields.

Let us try to formulate practical recommendations on when the use of the Townsend self-sustainment criterion is justified, and when one should instead resort to a numerical solution of the general eigenvalue problem governing discharge inception. Both approaches require previous knowledge of the spatial distribution of the applied electric field, which may be found by means of standard electrostatic simulations disregarding the presence of charged particles in the gap. The ionization and integral attachment coefficients, α and η, and the reduced electron mobility $\mu_e N$ should be specified as functions of the reduced electric field in order to use the Townsend criterion. A large amount of data and numerical tools for evaluation of these quantities are publicly available; e.g., databases [53, 54]. The general eigenvalue problem, in principle, takes into account all processes that may affect the discharge inception, including diffusion of the charged particles, direct ionization by electron impact, photoionization, attachment, detachment, charge exchange *etc*, and therefore requires information on relevant plasmachemical processes, photoionization, and transport coefficients. For example, the model summarized in Appendix A may be used for high-pressure dry air.

From the computational point of view, the evaluation of the Townsend criterion is straightforward, except for cases where the position of the electric field line that maximizes the quantity W_1 is not known in advance, as is the case for the setup shown in Fig. 3.4. The general eigenvalue problem may be readily solved by means of the resonance method introduced in Chap. 2. The method is physics-based, robust, and may routinely be implemented with the use of ready-to-use solvers for linear partial differential equations, including commercial solvers such as those provided by the computational platform COMSOL Multiphysics®. Still, implementation of the solution of the general eigenvalue problem is a more complex task than the evaluation of the Townsend criterion.

Therefore, the Townsend self-sustainment criterion is the method of choice for volume discharges in negative corona-like configurations and configurations with weakly

non-uniform electric field. The numerical solution of the general eigenvalue problem is required in cases where the Townsend criterion is not applicable, e.g., for positive corona-like configurations. If the goal is to develop a tool which can be used for a wide variety of conditions, the numerical solution of the general eigenvalue problem is the method of choice.

Chapter 4

Calculation of self-sustainment voltages in the presence of a dielectric surface

4.1 Introduction

Let us assume that, for a certain setup, the applied voltage coincides with the self-sustainment voltage (SSV). Then, over the course of time a steady-state discharge will develop across the setup with current limited to low values. The characteristic time-scale of the development of the steady-state discharge is the time-scale of accumulation of surface-charges on the dielectric, which is slower than the processes occurring in the bulk of the discharge.

A given setup can also be characterized by a certain breakdown voltage (BDV). At this voltage it will undergo a transient and fairly rapid transition from a low residual current discharge regime, to one of high current discharge. This will be our working definition for breakdown, as also commonly used in the electrical engineering community, and the BDV will be the minimum voltage bringing about the setup's breakdown in a circuit with no current limitation. Elsewhere, e.g. [55] p. 544, the term breakdown is used for what we call the setup's SSV. When the setup includes a dielectric along the discharge path between the electrodes, breakdown is also called flashover, indicating that a conduction channel gets created over the dielectric surface accompanied by the emission of a flash of light. The corresponding voltage is also called the surface flashover voltage, but we will keep with the term BDV.

The physical mechanism involved in breakdown, whether in air or in vacuum, is still mainly characterized as streamer formation and propagation until the gap is bridged. In the case of a setup with a strongly non-uniform field, and likewise no restriction on

current increase, there may be partial discharges with audible crackling sounds and stable corona discharges at voltages above the SSV and up to the BDV.

It has been more than a century of incremental understanding into the physics of flashover phenomena since the paper by Peek [95] on the flashover of different types of insulators for overhead high-voltage transmission lines in 1912. Breakdown phenomena are of widespread practical interest in high-voltage switchgear, where they are considered to be the technical bottleneck in the development of advanced power transmission and distribution equipment. In this field, breakdown is considered an unwanted destructive process and much of the research is on how to prevent it, or at least how to design devices that better withstand breakdown.

In general the precise relation between a setup's SSV and BDV is not known, except in a few simple cases of parallel-plates [10] and coaxial cylinders [22] where they coincide. In [20] Section 7.3.3, Raizer argues that for the DC case an overvoltage of 10% will trigger breakdown. It is a common engineering practice to evaluate the BDV resorting to the Townsend criterion, e.g. [83], which only requires the specification of the ionization coefficient, the cathode emission coefficient and evaluating path integrals in the electrostatic field distribution. However this criterion actually gives what we have called the SSV of the discharge. Though in some cases this criterion can be extended as was done in Chap. 3, it isn't generally applicable, namely when diffusion, or photoemission are important. Furthermore, in cases with a more complicated geometry, setting it up can be quite laborious and unjustified since there is a more general method for calculating the SSV, called the resonance method, of which the theoretical and numerical aspects have been detailed in Chap. 2.

Though there are plenty of numerical studies on the effect of dielectric surfaces at breakdown voltages (BDVs) [28, 46, 96], there seem to be no published measurements of the effect of dielectric surfaces on self-sustainment voltages (SSVs). It is of considerable interest to be able to estimate the minimum voltage that causes breakdown for any given setup. In a general setup that may contain a dielectric and may have a complex configuration, the standard way to check whether breakdown occurs at high pressures, would be to employ a fluid model of the gaseous medium which includes a kinetic scheme, and then perform time-dependent simulations starting from initial low particle density distributions at a given DC voltage, to see if the discharge evolves to breakdown, or to extinction. Through a somewhat time-consuming trial and error procedure, the voltage range containing the BDV can be narrowed down. In this chapter a more efficient way to calculate the BDV is proposed for setups with weakly non-uniform fields. Specifically, in this work and referring to Fig. 4.1 below, a simplified setup to model a vacuum interrupter of industrial interest is used, where breakdown is observed along the insulator's outer surface.

When a setup, like the one that is studied containing a dielectric surface, is being tested for the first time with regard to its breakdown voltage, it is natural to assume no surface-charges are present on the dielectric surface prior to the test. Naturally the initial number density of charged particles will also be low. In this case the outcome of the test will be called the first-breakdown voltage. On performing the same test with the setup stressed beforehand, possibly through previous breakdowns, if no specific action is taken to remove accumulated surface-charges on the dielectric, then it is natural to assume that surface-charges are present on the dielectric surface prior to the test. In this latter case the outcome of the test will be called the repetitive-breakdown voltage. It is clear that in these two cases, different breakdown voltages are expected. In this chapter boundary conditions are proposed for the resonance method to estimate voltages for first and repetitive-breakdowns. A numerical study is performed on the dependence of the SSV and BDV on the proximity of a dielectric surface to the active discharge path.

The outline of this chapter is as follows. In Sec. 4.2 the simulated setup's geometry, the used boundary conditions and the initial conditions are detailed. For the SSV calculations, we resort to the resonance method of Chap. 2, and for BDV non-stationary simulations solve the same model, but with time-dependent terms. Time-dependent simulations of the formation of the self-sustaining steady-state discharge are performed in Sec. 4.3. In 4.4, boundary conditions (BCs) are tentatively proposed for the resonance method to estimate voltages for first and repetitive-breakdowns. In Sec. 4.5.1 initial conditions (ICs) for time-dependent modelling of first-breakdown and repetitive-breakdowns are given, results for the first-BDV and the repetitive-BDV, computed by the resonance method and by the time-dependent simulations, are compared and discussed. Having established that the SSV calculated by the resonance method is close to the BDV, Sec. 4.5.2 goes on to characterize in more detail the SSV and how it varies in the selected setup when various characteristic parameters are changed. Some aspects of breakdown that are not captured by a characterization just in terms of the BDV value, are mentioned in passing in Sec. 4.5.3. In Sec. 4.6 a brief conclusion is made.

4.2 The modelled setup

The device of industrial interest in Fig. 4.1a is a medium voltage vacuum interrupter and calculations are performed in a simplified setup for modelling breakdown that occurs over the housing of this type of interrupters. The calculation domain is axially-symmetric as shown in Fig. 4.1b and comprises two disc-shaped electrodes separated by a cylindrical dielectric surrounded by dry air at atmospheric pressure. The electrodes

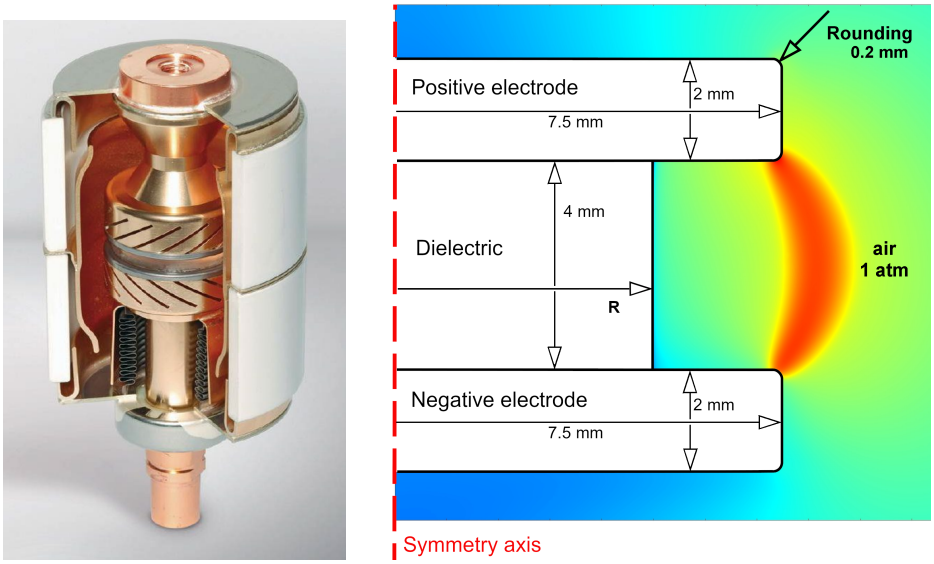

a) b)

Figure 4.1: (a) Industrial low and medium-voltage vacuum interrupter. Taken from Siemens AG catalog. (b) Schematic representation of the axially-symmetric calculation domain, which corresponds to a discharge between two disk electrodes separated by a cylindrical dielectric of radius R. Calculations are done for different R. Shown is the case $R = 5\,\mathrm{mm}$.

have a radius of 7.5 mm and a thickness of 2 mm. The height of the dielectric in the selected setup is 4 mm, unless stated otherwise. The radius, R, of the dielectric is varied in the range from 3 mm to 8.2 mm. The angular aperture into the air at the triple junctions, i.e. the electrode-dielectric-air contacts, was in all cases 90 °. A curvature of 0.2 mm was applied on the edges of the dielectric and electrodes. The domain's numerical boundary for the case of the dielectric height of 4 mm, is at the radius of 20 mm and at a distance 10 mm below and above the dielectric's center.

The model and boundary conditions have been introduced in Chap. 2, but for clarity the boundary conditions for the normal fluxes of charged particles into the dielectric surface, are here written out in full

$$\begin{aligned} (\mathbf{J}_\alpha)_n &= \frac{n_\alpha}{2}\bar{C}_\alpha, \text{ for all species } \alpha, \text{ except electrons.} \\ (\mathbf{J}_e)_n &= \frac{n_e}{2}\bar{C}_e - \gamma\,(\mathbf{J}_+)_n, \text{ for electrons.} \end{aligned} \tag{4.1}$$

here $(\mathbf{J}_+)_n$ is the flux of positive ions into the dielectric and γ is the secondary electron emission (SEE) coefficient of dielectric due to A^+ impact, $\bar{C}_\alpha = \sqrt{8kT_\alpha/(m_\alpha\pi)}$ is the thermal velocity of species α. In Sec. 4.4 below, two specific BCs are put forward for the floating potential on the dielectric when doing stationary calculations.

The initial conditions (ICs) for the time-dependent modelling are considered 'no

discharge' conditions, where (i) the densities for the species is low, (ii) the electric field Laplacian and (iii) photoionization terms vanish. Unless stated otherwise, results of the time-dependent simulations start from uniform initial number densities of $10^{10}\,\mathrm{m}^{-3}$ for the positive ions and one fourth of this value for all remaining species, this order of magnitude is warranted on the basis of ambient radiation [97].

In all calculations the effective SEE coefficient is assumed to characterize all mechanisms of SEE (due to ion, photon, and excited species bombardment) [20]. This coefficient is set to 3 %, on both dielectric and cathode surfaces, except when studying the effect of SEE from the dielectric surface, where it will be varied from 0 % to 100 %.

4.3 Deposition of charge on dielectric surfaces

Reviews that have been written, e.g. [24, 40], recognize the importance of the accumulation of surface-charges, specially in DC powered setups. Surface-charges have the effect of changing the electric field over dielectrics, this was seen to have an effect on the setups' operation. The effect has been studied by pre-treating the dielectric surface, depositing charges of a certain polarity onto the dielectric surface and applying different polarities to one of the electrodes. In [98, 99] various surface-charge measurements were made on different spacers for gas insulated lines. A dielectric spacer was proposed with zero normal component of the electric field on its surface so that the charging process would be minimal [99]. In [100] and [24] it is recognized that surface charging can actually be used to increase the breakdown voltage, it is reported that the shape of the spacer between electrodes can be used to induce a certain surface-charge distribution that reduces the electric field from highly stressed parts of the device, resulting in a higher breakdown voltage. Surface-charges on dielectric surfaces however are known to have a long decay time, between 30 and 200 hours are mentioned in experiments done by Fujinami [99]. It is well known that at the triple junctions the electric field can spike. In an initial stage prior to breakdown, micro and partial discharges, where streamers don't fully bridge the gap, are believed to be the major source of charges for the surface charging process and these streamers originate from highly stressed parts. Partial streamers can take place where the electric field strength exceeds the critical value for gas ionization.

In the present modelling, in order to study the evolution from a 'no-discharge' state towards the self-sustained steady-state, the setup is connected in series to an external circuit with a ballast of $R_{ext} = 295\mathrm{M}\Omega$ in series with a voltage source of $U_{ext} = 9.74\,\mathrm{kV}$. In the numerical simulations, Kirchhoff's second law for the circuit is solved with respect to the voltage applied at the anode. The time-dependent simulations start from ICs of no surface-charge on the dielectric.

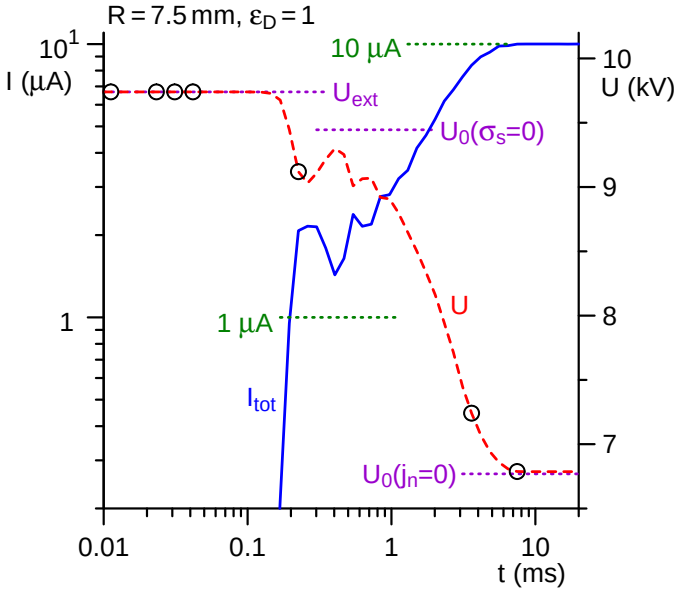

Figure 4.2: Time evolution from the 'no discharge' state to the steady-state. Solid line: I_{tot} the total current evaluated at the cathode; dashed line: U the discharge voltage; dotted horizontal line: U_{ext} the voltage source of external circuit; dotted horizontal lines: $(1\ \mu\text{A}; U_0(\sigma_s = 0))$ is (current;voltage) in external circuit; dotted horizontal lines:$(10\ \mu\text{A}; U_0(j_n = 0))$ is (current;voltage) in external circuit; circles: time-instants of Figs. 4.3b–4.3h. Considered case is $R = 7.5\,\text{mm}$ and $\varepsilon_D = 1$.

In Fig. 4.2 the time evolution of the potential U and the total current at the cathode I_{tot}, are shown. The dash-dotted horizontal lines in Fig. 4.2 correspond to SSVs calculated by the resonance method; SSV$(\sigma_s = 0)$ is obtained with the BC of local zero surface-charge on the dielectric, while horizontal line SSV$(j_n = 0)$ is obtained using the BC of zero local current density on the dielectric surface. The values for R_{ext} and U_{ext} were chosen so that the load line of the external circuit would intersect the current-voltage characteristics of self-sustaining discharges for BCs $\sigma_s = 0$ and $j_n = 0$, at the currents of $1\,\mu$A and $10\,\mu$A respectively.

In Fig. 4.2, one can see that the total current is constant until about $\sim 0.1\,\text{ms}$ when it steeply increases several orders of magnitude. At about $\sim 0.2\,\text{ms}$, oscillations are seen that cease at about $\sim 0.7\,\text{ms}$, after which the current monotonically increases again but at a slower rate. After approximately 8 ms, I_{tot} finally becomes constant. The physical interpretation is clear. For $t \lesssim 0.1\,\text{ms}$, the discharge current is low, the voltage drop over the ballast in the power supply circuit is low and the discharge voltage coincides with the voltage generated by the power supply, which is shown by the dotted horizontal line in Fig. 4.2. The discharge current becomes appreciable and the discharge voltage starts decreasing at approximately 0.1 ms. The discharge current

increase follows upon successive electron avalanches, each separated by the ion drift time of about 10 μs, as seen in Figs. 4.3a–4.3e. At 0.2 ms, when the total current starts showing some oscillations, a fully developed volume discharge is formed as confirmed by Fig. 4.3f. The horizontal dash-dotted line SSV($\sigma_s = 0$) gives a reasonable idea of the discharge voltage in the range of fractions of ms when the amount of surface-charge on the dielectric is small. It was verified that starting from an IC of $n_{A^+} = 10^9\,\mathrm{m}^{-3}$, apart from the expected higher initial currents due to the higher initial densities, the time evolution was very similar to that of Fig. 4.2.

The buildup of surface-charge starts taking effect for times somewhat below 1 ms. At $t \approx 8$ ms the buildup of surface-charge is completed and the discharge on the whole attains a steady-state.

It is therefore established that there are two time-scales: one for the volume discharge formation, which is of the order of fractions of millisecond, and one for the surface-charge deposition, which is of the order of a few milliseconds in these conditions.

The positive ion density distribution for eight time-instants, associated with the above-described time-evolution towards the steady-state, are given in Figs. 4.3a–4.3h.

In Fig. 4.3a the clearly distinguishable higher positive ion density front is a result of the initial uniform density of electrons having previously drifted to the anode and having ionized neutrals mainly in the high field region close to the anode triple junction. The resulting well-defined high density front is at 1 μs seen propagating towards the cathode under drift. This same front has a peculiar stretched out form at 11.2 μs as it reaches the cathode, see Fig. 4.3b. Its form is a result of the setup's electrostatic field lines. Those ions travelling along the innermost field lines have higher drift velocity than those in the outermost field lines, particularly when close to the electrodes. The gradual decrease of velocities for field lines in the radial outward direction, combined with the longer distances travelled by ions on the outermost field lines, yields the elongated form of the positive ion density front at 11.2 μs. Results not given here, show that the production of positive ions is maximum close to the anode where the field magnitude, and therefore ionization, are high. Subsequently the continuously produced ions, drift along the field lines in the direction of the cathode, giving rise to the trail behind the density front seen in Fig. 4.3a. The initial high density areas close to the anode in Figs. 4.3b–4.3d, created through ionization by successive avalanches of secondary electrons emitted from the cathode, are seen in the next time-instant, Figs. 4.3c–4.3e, to arrive at the cathode. The reason why it is only the first positive ion density front that has a well defined and elongated front, is because the drift of the initial uniform electron density towards the anode, created this well defined positive ion density front over the anode surface through ionization. At 226 μs, see Fig. 4.3f,

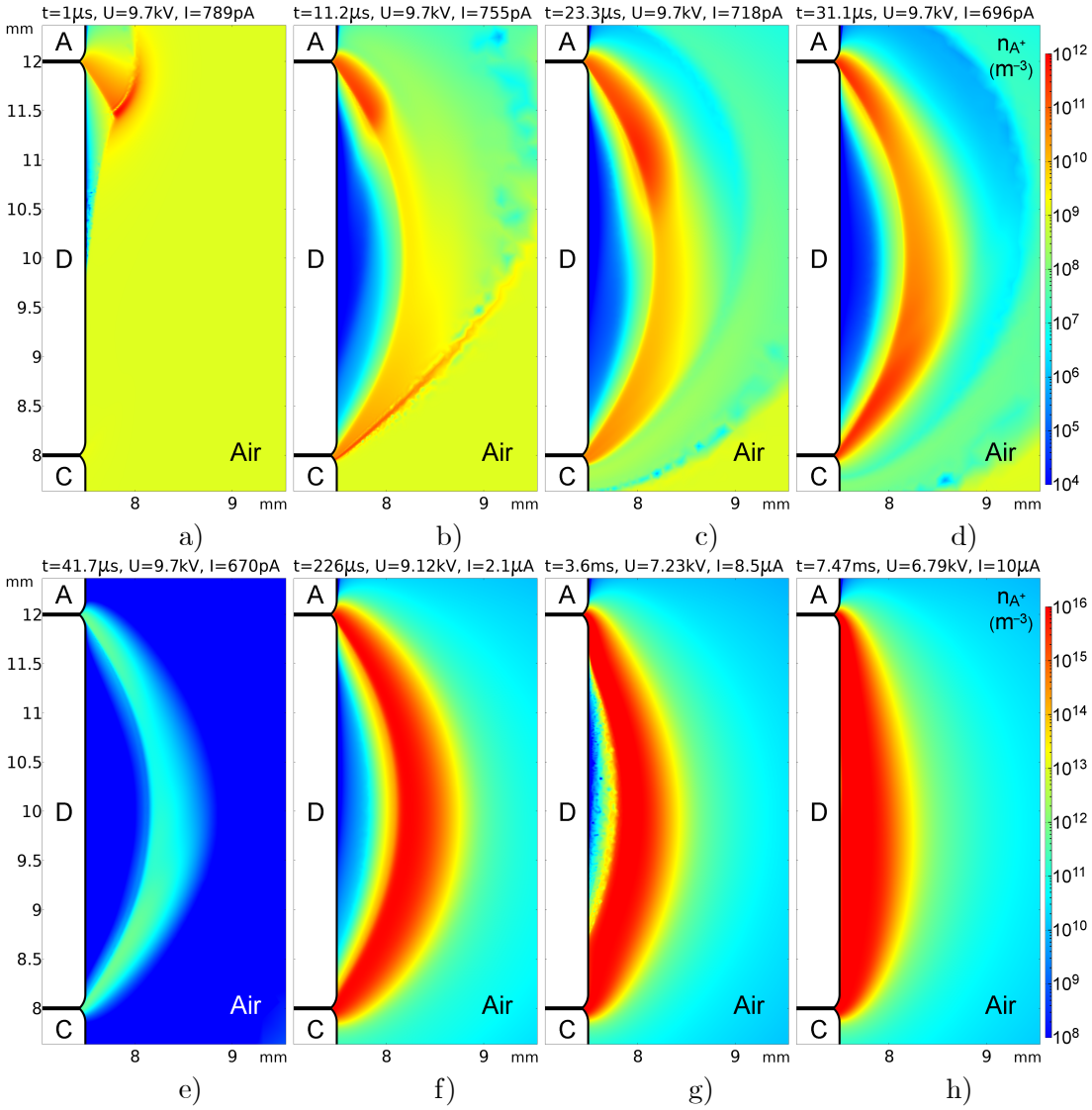

Figure 4.3: Time-evolution from the 'no discharge' state to the steady-state. Positive ion density distribution for eight time-instants marked as circles in Fig. 4.2. Color legend of an image is at the far rhs. Details of each picture are in their headers. A,D and C are respectively the anode, dielectric and cathode. Considered case is $R = 7.5\,\mathrm{mm}$, $\varepsilon_D = 1$ and IC $n_{\mathrm{A}^+} = 10^9\,\mathrm{m}^{-3}$.

after tens of successive avalanches have buildup the charge density along the discharge path, the formation of the volume discharge is complete. The two subsequent instants of 3.6 ms and 7.47 ms in Figs. 4.3g–4.3h illustrate two time-instants of the density distribution evolution as surface-charge is deposited on the dielectric surface. The last time-instant corresponds to the steady-state discharge and no more surface-charge is deposited.

4.4 Resonance method in the presence of dielectrics

It has been noted that for first-breakdown no surface-charge is expected to be on the dielectric and that for repetitive-breakdowns there is surface-charge on the dielectric. Furthermore, results from the previous section suggest that the SSV($\sigma_s = 0$) is connected with the zero surface-charge quasi-stationary discharge state, while the SSV($j_n = 0$) is connected with the steady-state discharge which has a non-zero surface-charge density. These observations are now systematized into tentative BCs on the dielectric for the resonance method to estimate the voltages of first-breakdown and repetitive-breakdowns.

To estimate the voltage of the first-breakdown it is natural to assume as BC, that the surface-charge density is zero at each point of the dielectric

$$\varepsilon_0 \left(\varepsilon_D \mathbf{E}_D - \varepsilon_G \mathbf{E}_G\right) \cdot \mathbf{n} = \sigma_s = 0 \tag{4.2}$$

here, and below, subscripts D and G refer, respectively, to the dielectric and the gas; $\mathbf{n}$ is the normal vector pointing from gas to dielectric surface; ε_0 is the vacuum permittivity; ε is the relative permittivity; $\mathbf{E}$ is the electric field; σ_s the surface-charge density. This BC on the dielectric corresponds to a non-prestressed setup, the associated SSV will be compared with the first-BDV. It implies that the electric field has to be known inside the dielectric and therefore the Laplace equation has to be solved in the dielectric. Note that results for the SSV will depend on the dielectric permittivity.

To estimate the voltage of repetitive-breakdowns it is assumed that the presence of surface-charge on the dielectric prevents any further buildup of charge, in other words, the BC assumes that the net current density at each point of the dielectric surface is zero as given by Eq. (2.9) of Chap. 2. This BC on the dielectric corresponds to a prestressed setup, the associated SSV will be compared with the repetitive-BDV. To satisfy this BC only the particle fluxes and the electric field on the gas side need to be known, i.e. in this case the Laplace equation doesn't need to be solved inside the dielectric and therefore results won't depend on the dielectric permittivity.

Both BCs $\sigma_s = 0$ and $j_n = 0$ imply the existence of a certain floating potential at all points of the dielectric surface able to satisfy these conditions, i.e. they are electrostatic BCs locally constraining the potential for a stationary problem. As was shown in Fig. 4.2, BCs $\sigma_s = 0$ and $j_n = 0$ are associated with self-sustained states that are realized, at different time-scales, during the time-evolution from the 'no discharge' condition to the steady-state using an external circuit. It should be noted that the self-sustained state with BC $\sigma_s = 0$ is associated with an initial discharge stage and can be considered a quasi-stationary state for time-scales much smaller than the characteristic charge accumulation time. Discharges with BC $\sigma_s = 0$ are quasi-stationary states in the sense that there is no strict conservation of the current entering and exiting the electrodes. This is because a small amount of charge is being deposited on the dielectric.

4.5 Results

4.5.1 Comparing self-sustainment and breakdown voltages

In this section, results for first and repetitive BDVs obtained by the resonance method in the presence of dielectrics, will be validated. Validation will be performed against time-dependent simulations of the same model as used for the resonance method.

When using time-dependent simulations for the study of breakdown, a new variable is introduced, namely the surface-charge density on the dielectric, governed by the partial differential equation for charge accumulation (2.7). The new surface-charge variable, required the introduction of BC (2.8) given in Chap. 2, and its initial condition has to be specified on the dielectric when performing time-dependent simulations.

To simulate the development towards a first-breakdown, i.e., of a non-prestressed setup, it is clear that the IC must be that of a zero surface-charge density on the dielectric. While for the simulation towards repetitive-breakdowns, i.e., of a prestressed setup, the IC must prescribe a non-zero surface-charge density distribution on the dielectric. The initial surface-charge for the latter case is taken to be the surface-charge distribution obtained from the self-sustained discharge with BC $j_n = 0$.

Hereafter $\sigma_s = 0$ will refer to a non-prestressed setup and $j_n = 0$ to a prestressed setup, with corresponding conditions. Meaning that the conditions are BC when $\sigma_s = 0$ and $j_n = 0$ refer to the resonance method, and IC when they refer to time-dependent modelling method.

A comparison is made between the SSV obtained by the resonance method and the BDV obtained by the time-dependent simulations of the discharge. The SSV was computed by means of the procedure laid out in Sec. 2.4.1 (excluding the fourth and

R (mm)	ε_D	Self-sustainment $\sigma_s = 0$	First-breakdown $\sigma_s = 0$	Self-sustainment $j_n = 0$	Repetitive-breakdowns $j_n = 0$
3	1	9.9 kV	10.0 kV	9.9 kV	10.0 kV
	12				
7.5	1	9.4 kV	9.5 kV	6.8 kV	6.9 kV (+2%)
	12	11.9 kV	12.0 kV		
8.2	1	14.0 kV	14.2 kV	11.5 kV	11.6 kV
	12	8.3 kV	8.7 kV (+5%)		

Table 4.1: Calculated values for the SSV and the BDV. R is the dielectric radius; ε_D the dielectric constant; $\sigma_s = 0$ for non-prestressed setups; $j_n = 0$ for prestressed setups. When time-dependent simulations need an overvoltage of more than 1% above the SSV, the percentage is indicated between brackets.

fifth steps) and in Sec. 2.4.2. In Tab. 4.1, SSVs and BDVs of the studied setup are obtained for cases where the dielectric was recessed ($R = 3$ mm), aligned ($R = 7.5$ mm) and protruding ($R = 8.2$ mm) relative to the electrodes. Results in Tab. 4.1 are for dry air at 1 atm, with dielectrics of 4 mm height and either a dielectric constant of $\varepsilon_D = 1$ or $\varepsilon_D = 12$. For the resonance method a given low current of 1 p A was used. Columns further distinguish whether the setup is pre-stressed ($:j_n = 0$) or not ($:\sigma_s = 0$), i.e., respectively, whether there is an initial surface-charge density on the dielectric or not.

The first two columns of Tab. 4.1 identify, respectively, the three dielectric radii of 3 mm, 7.5 mm, and 8.2 mm, and the two values of the dielectric relative permittivity, 1 and 12, that were used. The next two columns correspond, respectively, to the SSV as calculated by the resonance method and to the BDV as calculated by the non-stationary method, both when $\sigma_s = 0$. The next to last column corresponds to the SSV as calculated by the resonance method and the last column shows the BDV as calculated by the time-dependent simulation, both when $j_n = 0$. At the SSV, the time-dependent simulation leads to discharge extinction. If the discharge extinguishes, the applied voltage is increased in 1% of the SSV. This successive 1% increase is repeated until the time-dependent simulation produced breakdown. The last applied voltage is tabulated as the BDV. It is observed from Tab. 4.1 that the SSV is close to the BDV.

For the retracted dielectric radius of 3 mm and $\sigma_s = 0$, the SSV and BDV are not affected by the permittivity of the dielectric. This is understandable, as the discharge channel will be in the gap volume between the inner edge of the electrodes and therefore away from the dielectric surface, like in Fig. 4.1.

For the aligned dielectric with $\varepsilon_D = 1$, Figs. 4.4 show two sequences in time of the positive ion densities during the development, starting from the 'no-discharge' state and IC $\sigma_s = 0$. The top row, 4.4a, is a sequence obtained during first-breakdown calculations at a given voltage 1% above the SSV. The bottom row, 4.4b, is a sequence

obtained during the development at a given current of 100 nA, but where no charge was allowed to accumulate on the dielectric.

For the sequence towards breakdown in row a), similarly to Figs. 4.3a–4.3b, the first two time-instants refer to the first positive ion front leaving the anode just before 1 μs and subsequently arriving at the cathode at 11 μs. At this instant, the secondary electrons emitted from the cathode due to impact of the positive ion front, originate an electron avalanche responsible for the high positive ion density seen at the anode. At around 200 μs, there is a well formed volume discharge, but at this timescale no surface-charge has accumulated on the dielectric. In the last image of Fig. 4.4a, at around 600 μs, while there is still not much accumulated surface-charge, first-breakdown occurs. This breakdown follows upon a gradual increase in the space-charge in the region in front of the cathode to a degree that it significantly distorts the background electric field. As a result a streamer-like ionization wave develops in this region and starts propagating toward the cathode. For the sequence in row b), the first three time-instants are similar to the sequence of row a). From 200 μs onwards, the density grows until becoming constant at around 84 ms. From the comparison of the two developments in Figs. 4.4, it is concluded that during the development of first-breakdown, a density distribution is attained very similar to the self-sustaining state with BC $\sigma_s = 0$.

In both sequences of Fig. 4.4, i.e., of first-breakdown and of the formation of a self-sustained state, the physical process towards the development of the volume discharge at 218 μs, is the same and has already been described in Sec. 4.3. It is just because there is no current limitation during the evolution in Fig. 4.4a, that it evolves to breakdown. This observation strengthens the association of non-stationary modelling of first-breakdown, i.e. IC $\sigma_s = 0$, with the stationary resonance method with BC $\sigma_s = 0$.

Figs. 4.5 show a sequence similar to Fig. 4.4, for the same aligned dielectric, with the same permittivity and the same initial 'no-discharge' state, but now starting from IC $j_n = 0$. The top row, 4.5a, is a sequence obtained during repetitive-breakdown calculations at a given voltage 2% above the SSV. The bottom row, 4.5b, is a sequence of the evolution towards the steady-state discharge at a given current of 100 nA.

For the repetitive-breakdown sequence in row a) of Fig. 4.5, a fully developed discharge appears at around 200 μs 'embracing' the dielectric surface. In the last image of Fig. 4.5a, at around 828 μs, the current grows several orders of magnitude and repetitive-breakdown occurs. Similarly to first-breakdown, also for repetitive-breakdown a near-cathode, streamer-like, ionization wave develops and starts propagating toward the cathode. For the sequence in row b) of Fig. 4.5, the first three time-instants are similar to the sequence of row a). From 200 μs onwards, the den-

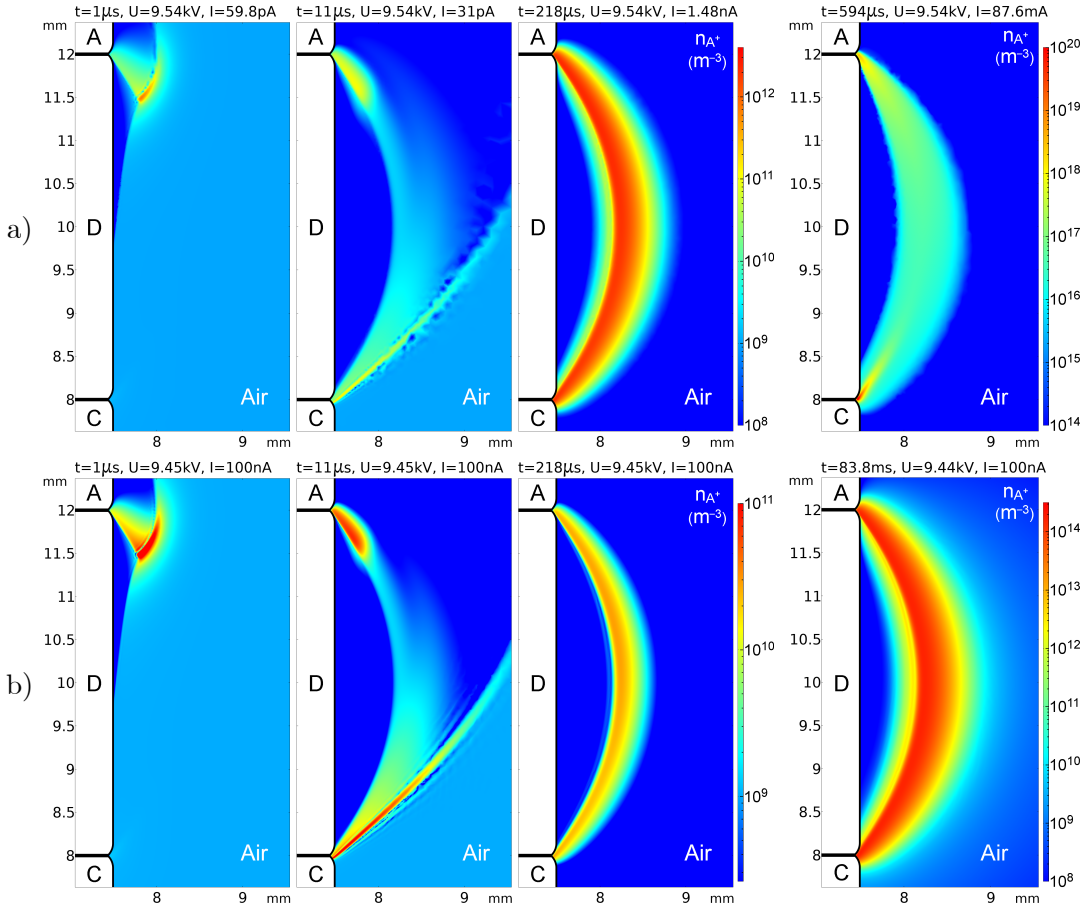

Figure 4.4: Positive ion density evolution towards breakdown and towards the self-sustained discharge for $\sigma_s = 0$. Row a): 4 time-instants in the first-breakdown development, $U = 101\% \times SSV$. Row b): 4 time-instants in steady-state development, $I = 100\,\mathrm{nA}$. A,D and C are respectively the anode, dielectric and cathode. Considered case is $R = 7.5\,\mathrm{mm}$, $\varepsilon_D = 1$ and IC $n_{\mathrm{A}^+} = 10^9\,\mathrm{m}^{-3}$. Color legend of a picture is the first on its rhs.

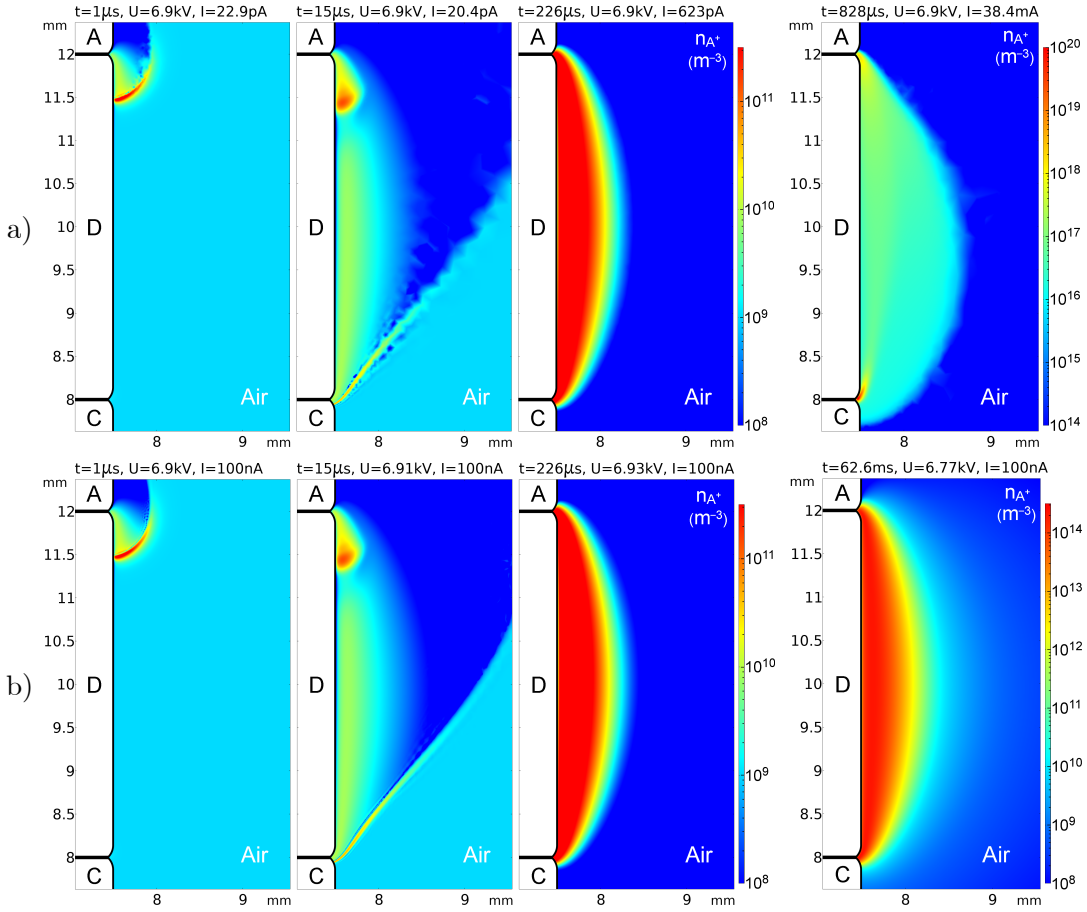

Figure 4.5: Positive ion density evolution towards breakdown and towards the steady-state discharge for $j_n = 0$. Row a): 4 time-instants in the repetitive-breakdown development, $U = 102\% \times SSV$. Row b): 4 time-instants in steady-state development, $I = 100\,\mathrm{nA}$. A,D and C are respectively the anode, dielectric and cathode. Considered case is $R = 7.5\,\mathrm{mm}$, $\varepsilon_D = 1$ and IC $n_{\mathrm{A}^+} = 10^9\,\mathrm{m}^{-3}$. Color legend of a picture is the first on its rhs.

sity grows until becoming constant at around 63 ms. From the comparison of the two developments in Figs. 4.5, it is concluded that during the development of repetitive-breakdown, a density distribution is attained very similar to the self-sustaining state with BC $j_n = 0$.

In both sequences of Fig. 4.5, i.e. of repetitive-breakdown and of the steady-state formation, the physical process towards the development of the volume discharge at 218 μs, is similar to that described in Sec. 4.3. It is just because there is no current limitation during the evolution in Fig. 4.5a, that it evolves to breakdown. This observation strengthens the association of time-dependent simulations of repetitive-breakdown, i.e. IC $j_n = 0$, with the stationary resonance method with BC $j_n = 0$.

Note that the densities of the last time-instant in row b) of Fig. 4.4 agree with the corresponding densities of the self-sustained state obtained by the resonance method shown in Fig. 4.7a. Likewise, the densities of the last time-instant in row b) of Fig. 4.5 agree with the corresponding densities of the self-sustained state obtained by the resonance method shown in Fig. 4.7c. The fact that during both the first and repetitive breakdown sequences, a volume discharge attains that is very similar to the corresponding self-sustained discharge, makes it physically understandable why corresponding BDVs and the SSVs are so close in Tab. 4.1.

Like for $R = 7.5\,\mathrm{mm}$, also for the protruding dielectric radius of 8.2 mm, agreement between the BDV and SSV for both $\sigma_s = 0$ and $j_n = 0$, match similarities in the development sequences under given voltage and given current. The noticeable difference when comparing $R = 8.2\,\mathrm{mm}$ with 7.5 mm, is that for $\sigma_s = 0$ the voltages decrease with increasing permittivity. This is related with a geometric feature and the electrostatic field line distribution for the two permittivities, as will be seen in more detail in the next section.

4.5.2 Characterization of the self-sustained discharge

From the foregoing it can be claimed that the SSVs in setups with weakly non-uniform fields, give some insight into the study of first-breakdown and repetitive-breakdown in low overvoltages, namely into to the BDV and the 2D distributions that are realized. In this section some geometric aspects of the setup are varied and their effect on the self-sustaining discharge analyzed.

For Fig. 4.6 calculations were performed for 17 dielectric radii R in the range from 3 to 8.2 mm. The figure shows, for various dielectric radii, self-sustaining discharge voltages for both the initial discharge stage ($\sigma_s = 0$), and for the steady-state discharge ($j_n = 0$). The solid line is the SSV associated with $j_n = 0$. The dashed line corresponds to the initial discharge stage with a dielectric constant of 1 and the dashed-dotted line with a dielectric constant of 12. Also shown is a dotted line that represents the length (L) of the field line that maximizes the path-integral of the effective ionization coefficient as given in Sec. 3.3 of Chap. 3, i.e. the ionization integral for the steady-state. The curve for L represents the geometrical effect of the dielectric on the electric field line distribution, since longer field lines connecting the electrodes, imply higher SSVs.

For $R \lesssim 5\,\mathrm{mm}$, when the dielectric is away from the edges of the electrode disks, the SSV is virtually constant and equals approximately 10 kV, irrespective of the BC on the dielectric. This value is in good agreement with the experimental BDV for $R = 3.5\,\mathrm{mm}$ reported in [25], which is represented in Fig. 4.6 by a filled diamond.

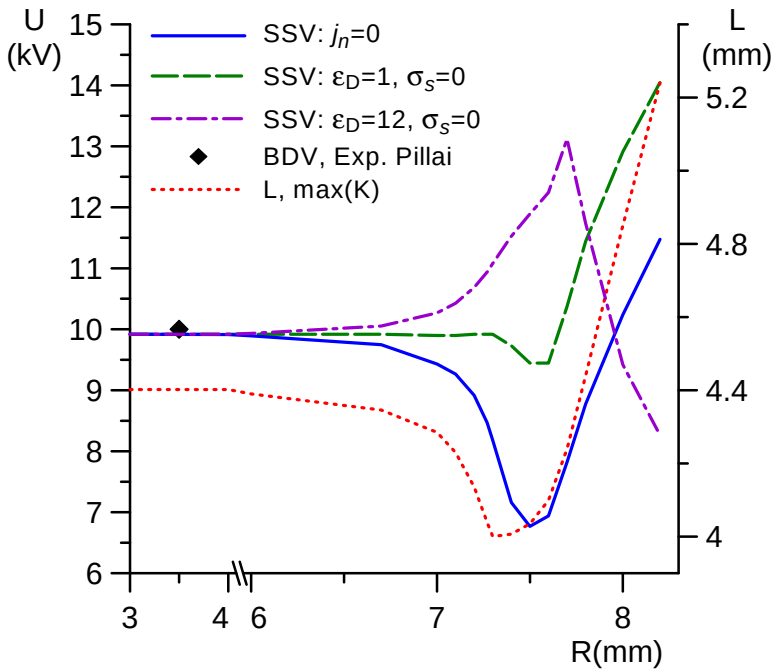

Figure 4.6: Self-sustainment voltages as a function of dielectric radius R, for the two studied BCs. Lines calculated with the resonance method; solid: $j_n = 0$; dashed: $\varepsilon_D = 1$ and $\sigma_s = 0$; dashed-dotted: $\varepsilon_D = 12$ and $\sigma_s = 0$. Dotted line: electric field line length L, from the steady-state discharge, that maximizes the ionization integral. Filled diamond: experimental BDV from [25].

Note that the calculated value is lower than the corresponding value taken from the Paschen curve (approximately 11 kV), which is consistent with the discharge being not plane-parallel but having a weak field non-uniformity. As R increases, i.e., as the dielectric approaches the active zone of the discharge, the SSV behaves differently depending on the BC on the dielectric. For $\sigma_s = 0$ the SSV also depends on the dielectric permittivity.

For $\sigma_s = 0$ and the smaller permittivity of $\varepsilon_D = 1$, the SSV is a non-monotonous function of R, being practically constant for retracted dielectrics, having a slight minimum for the aligned dielectric and increasing sharply as the dielectric starts to protrude. This decrease in the SSV for the aligned dielectric, stems from an increase of the ionization rate along the field line that maximizes the ionization integral, a field line that passes in regions where the electric field is greatly enhanced owing to the proximity of the triple junctions. As the dielectric starts to protrude, the SSV starts increasing since the field line that maximizes the ionization integral starts further away from the high electric field region.

For $\sigma_s = 0$ and the higher permittivity of $\varepsilon_D = 12$, the SSV is a non-monotonous function of R. It is practically constant for deeply retracted dielectrics, increasing monotonically until it reaches a maximum at $R = 7.7\,\text{mm}$ (protruding dielectric), after which it sharply decreases. The reason for this decrease lies in the electrostatics and will be clarified below.

For $j_n = 0$, the SSV is a non-monotonous function of R, with a qualitatively similar behavior as for the smaller permittivity of $\varepsilon_D = 1$, except it has a more pronounced minimum and the SSVs are lower. A similar analysis as for case $\varepsilon_D = 1$ can be given, with the note that the overall lower SSVs are mainly due to having shorter field lines connecting the electrodes. For $j_n = 0$, surface-charge is screening the gas from the effect of the dielectric and therefore the SSV does not depend on the dielectric permittivity. The field line that maximizes the ionization integral, runs roughly along the center of the active discharge path for the retracted dielectrics, and shifts towards the inner edge of the active discharge path as the dielectric becomes aligned and starts protruding. This is why in Fig. 4.6 the SSV dependence on R is similar to that of L.

Our results for $j_n = 0$ agree qualitatively with the behavior of the BDV reported in the experiment of Fig. 10 in [27] under AC voltage (60 Hz), with a dielectric disk spacer tightly stacked between disk electrodes. A comparison of the SSV with the BDV in these conditions is well justified since all characteristic plasma frequencies are much higher than 60 Hz and the discharge can be considered to be in a quasi-stationary state at each voltage value. Further, the experimental BDV should be compared with the SSV for $j_n = 0$ as it is clearly a repetitive-breakdown case, where charge of previous breakdowns is still on the dielectric. In this experimental setup, similar to ours, the

presence of the dielectric lowers the BDV when compared to having no dielectric at all for nitrogen at pressures higher than 1 atm. In experiments by Timatkov [101] and by Lazaridis [102] with pulsed voltage in a point-to-plane geometry, the effect of a dielectric in the gap was studied with regard to the measured BDV. Though in the latter case the electric field non-uniformity may be significantly higher than in the here studied geometry, their experimental results are in line with our results that indicate a lower breakdown voltage when a pre-stressed dielectric is close to the discharge area.

Figs. 4.7a–4.7c show 2D distributions for the positive ions in the three self-sustaining states of Fig. 4.6 for $R = 7.5\,\text{mm}$, namely in a) for $\sigma_s = 0$ and $\varepsilon_D = 1$, in b) for $\sigma_s = 0$ and $\varepsilon_D = 12$, and in c) for $j_n = 0$. In Figs. 4.7d–4.7f the corresponding 2D distributions for the production rates of the positive ions are given. The calculated SSV U_0, is shown at the top of each of the figures Fig. 4.7. The distribution of positive ions clearly identifies the curved conduction channel produced in the discharge which can be understood as a consequence of the charged particles following the electric field lines. Net production of positive ions occurs mainly close to the anode, see Figs. 4.7d–4.7f, and it is their drift in the electric field towards the cathode that renders a high density along the discharge channel.

Figs. 4.8a–4.8f will serve to better understand the form of the discharges for $R = 7.5\,\text{mm}$ and $8.2\,\text{mm}$. In particular, the figures better explain why the dielectric doesn't affect the SSV for $j_n = 0$ and why for $R > 7.7\,\text{mm}$, $\sigma_s = 0$ and $\varepsilon_D = 12$, the SSV suddenly decreases as was observed in Fig. 4.6. These figures show, in the vicinity of the cathode triple junction, the normalized electric field $\widetilde{E}$, i.e. the electric field corresponding to a normalized potential $\widetilde{\phi} = \phi/U_0$, where U_0 is the SSV. Results are shown for $R = 7.5\,\text{mm}$ and $8.2\,\text{mm}$, for $\sigma_s = 0$ and $j_n = 0$ and for $\varepsilon_D = 1$ and 12. When $\varepsilon_D = 1$ the field lines undergo no deviation when passing from the dielectric to the air as seen in Figs. 4.8a and 4.8d. In Figs. 4.8b and 4.8e for $\varepsilon_D = 12$, the electric field lines undergo a significant deviation when passing from the dielectric to the air. For this higher permittivity, the continuity of the normal component of the electric displacement field across the dielectric surface accounts for the deviation of the field lines on crossing from air to dielectric, associated with a twelvefold reduction of the normal component of the electric field. One of the consequences is that the field lines exiting the dielectric into the air tend to deviate towards the surface normal, making the field lines more arced and therefore those connecting the electrodes are longer, as inferred from comparing Figs. 4.7a and 4.7b. This explains why for $\sigma_s = 0$ the SSV for $\varepsilon_D = 1$ is overall lower than for $\varepsilon_D = 12$, excluding the abnormal behavior for $\varepsilon_D = 12$ and $R > 7.7\,\text{mm}$ that will now be addressed.

As we know from Chap. 3, the field line that maximizes the ionization integral is a good gauge to locate the active discharge path in a setup. There is an abrupt

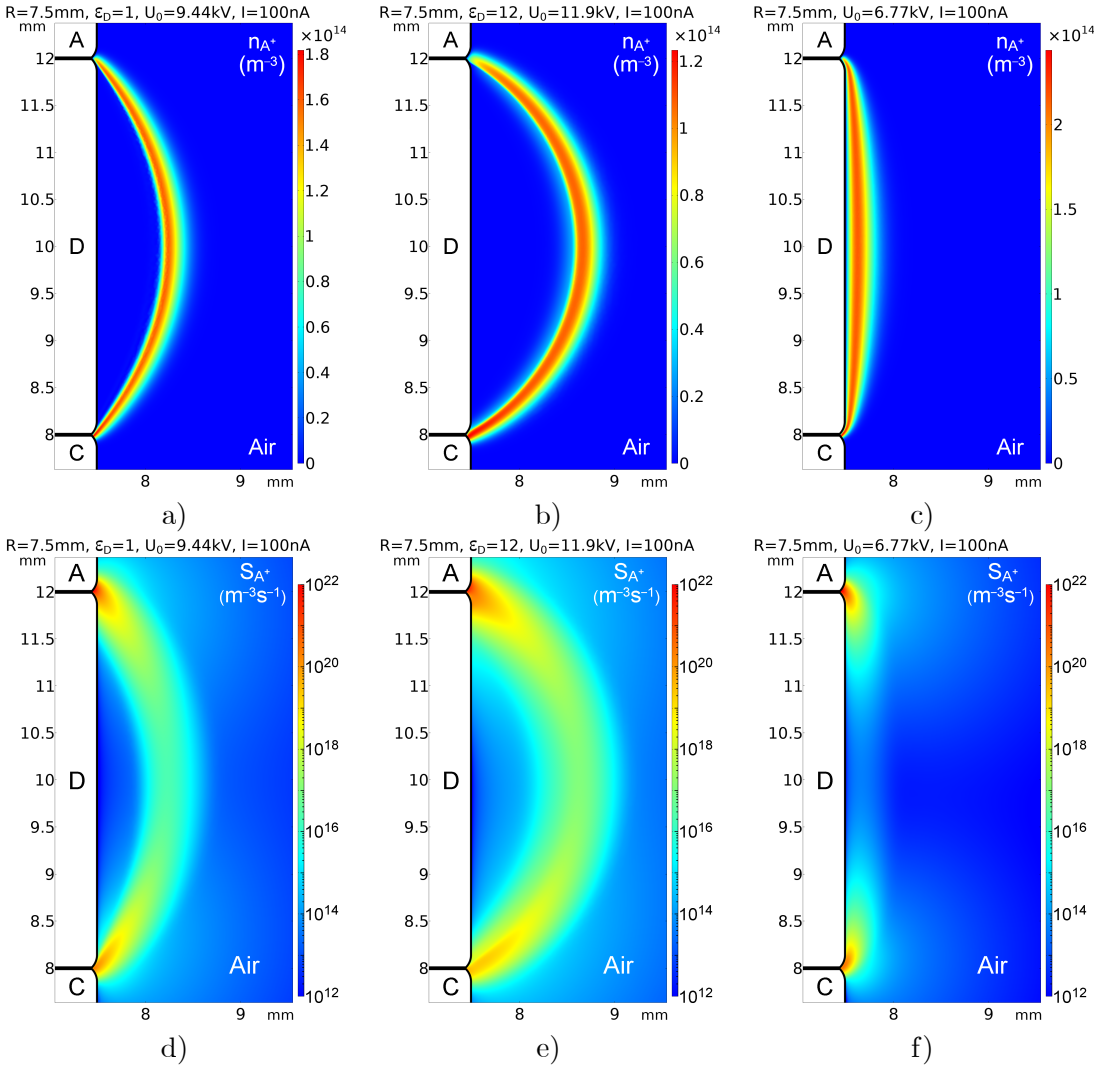

Figure 4.7: Density of positive ions in a)–c) and production rate of positive ions in d)–f), for self-sustaining discharges with a current of 100 nA. a) and d): $\varepsilon_D = 1$ and $\sigma_s = 0$. b) and e): $\varepsilon_D = 12$ and $\sigma_s = 0$. c) and f): $j_n = 0$. A,D and C are respectively the anode, dielectric and cathode. Considered case is $R = 7.5$ mm. Note that color legend is linear for a)–c), and is in orders of magnitude for d)–e).

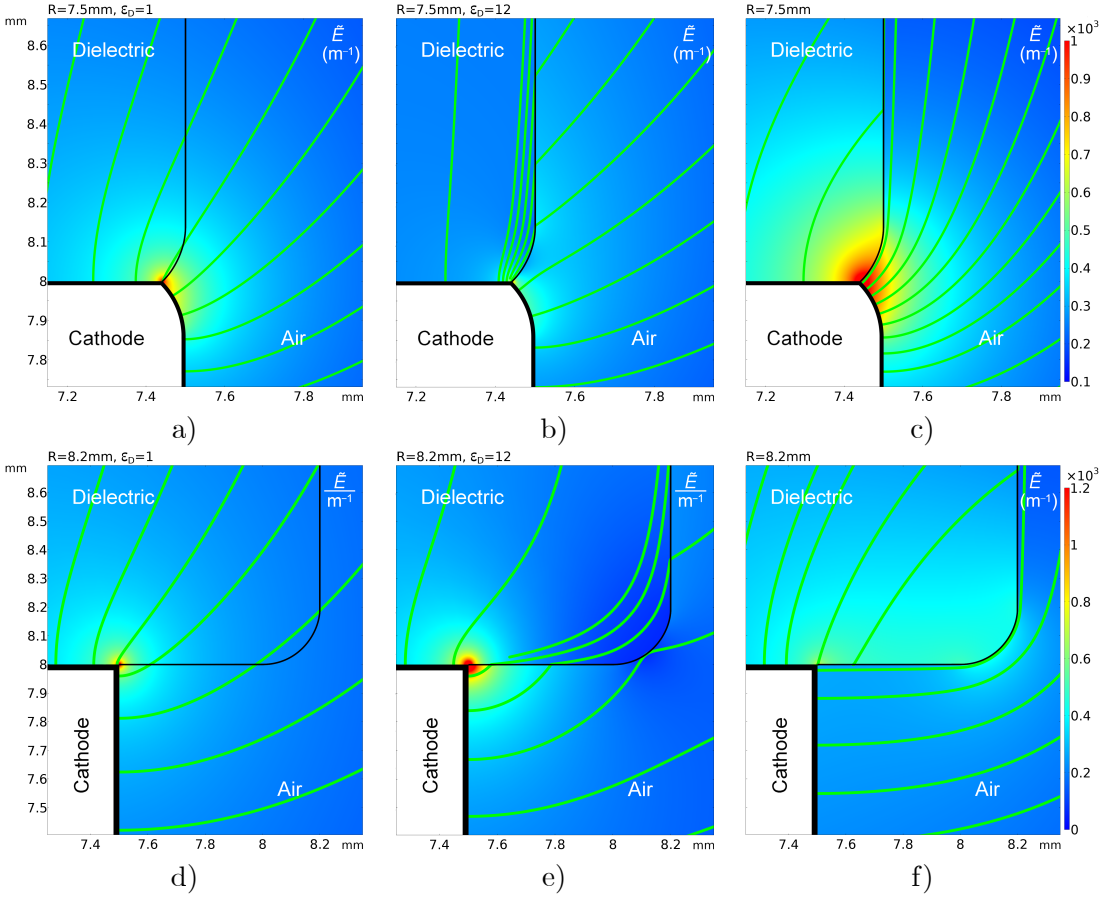

Figure 4.8: Normalized electric field strength and field lines close to the cathode triple junction. Row a) – c): $R = 7.5\,\mathrm{mm}$. Row d) – f): $R = 8.2\,\mathrm{mm}$. Column a), d): $\varepsilon_D = 1$ and $\sigma_s = 0$. Column b), e): $\varepsilon_D = 12$ and $\sigma_s = 0$. Column c), f): $j_n = 0$. The color legend for the rows is at the rhs.

decrease observed in the self-sustainment voltage for $\sigma_s = 0$ and $\varepsilon_D = 12$ (dashed-dotted in Fig. 4.6) and dielectric radii above 7.7 mm. In results not shown here, this reduction happens because the discharge path that maximizes the ionization integral, ceases to be associated with a field line connecting cathode to anode through the air. Instead, for $R > 7.7$ mm, the field lines that maximize the ionization integral, start at the cathode, close to the triple junction, and travel a short distance in the air before entering the dielectric, see Fig. 4.8e. The short field line length and associated high field strength, explain the decrease in self-sustainment voltages for these cases.

The application of BC $j_n = 0$, results in very small normal components for the electric field on the dielectric surface. As a consequence there will be an electric field line on the gas side that closely follows the dielectric surface contour, this is apparent in Figs. 4.8c and 4.8f. Since discharge paths follow electric field lines, it is clear why for $j_n = 0$ the SSV is strongly correlated with geometry and therefore the variation of the length of the field lines connecting the electrodes, dotted line in Fig. 4.6, explain the variation obtained for the SSVs, solid line in Fig. 4.6. Note that in Fig. 4.6 the shortest field line that maximizes the ionization integral occurs for $R = 7.3$ mm, while the lowest SSV occurs for $R = 7.5$ mm. This small discrepancy is due to the ionization integral being based on an approximation that uses an effective ionization coefficient and just the electric field distribution, lacking in particular information about the particle densities.

In order to understand to what extent the value of the effective secondary electron emission coefficient (γ_D) of the dielectric surface affects the present results, γ_D was varied from 0 to 100%. This variation was seen to affect the densities of charged particles at the dielectric surface, mainly that of electrons. The density of electrons at the dielectric surface could change as much as 50%, however this difference faded away after just a few micrometers into the gas; it had no impact on the discharge channel and therefore no significant impact on the SSV. It was seen to affect the SSV by less than 0.1% for the case $R = 8.2$ mm with $j_n = 0$, where the variation of γ_D was expected to have the largest effect.

Just for the case of dielectric radius 7.5 mm, the SSV is shown in Tab. 4.2 for dielectric heights of 2 mm, 4 mm and 6 mm. As expected, the obtained SSVs follow the general understanding in terms of higher values for longer field lines connecting the electrodes.

There seem to be no quantitative experimental data published on the effect of dielectric surfaces on SSVs. It is known from experiment that the presence of a dielectric facilitates the breakdown (e.g., review [103]), and it is indeed seen in the solid line of Fig. 4.6 that the SSV decreases as the radius of the dielectric approaches that of the electrodes. It would be very interesting to check experimentally the rapid increase of

Gap	ε_D	SSV ($\sigma_s = 0$)	SSV ($j_n = 0$)
2 mm	1	6.1 kV	5.0 kV
	12	7.1 kV	
4 mm	1	9.4 kV	6.8 kV
	12	11.9 kV	
6 mm	1	11.8 kV	7.9 kV
	12	15.7 kV	

Table 4.2: Self-sustainment voltages as a function of dielectric height (Gap) and dielectric constant (ε_D). Results for $\sigma_s = 0$ and $j_n = 0$. Considered case is $R = 7.5$ mm.

the SSV and/or repetitive-BDV when the dielectric is protruding, predicted by the modelling and seen in Fig. 4.6 in the range $R \geq 7.5$ mm.

4.5.3 Characterization of breakdown for low overvoltages.

Differently from many other simulations, e.g. [46, 96], where a particle density seed is used to facilitate breakdown, in the present simulations, we have considered as ICs the 'no discharge' condition and $j_n = 0$. These are the conditions of this section to further investigate repetitive-breakdown in the setup with dielectric radius 7.5 mm. The current oscillograms for this case and for permittivities $\varepsilon_D = 1$ and $\varepsilon_D = 12$ are given in Fig. 4.9. The applied DC voltage is 6.9 kV, i.e. a low overvoltage, 2% above the setup's SSV. What is seen in these oscillograms is that the current decreases in a first stage of the discharge ($0 < t \lesssim 30\,\mu$s). This decrease of the current is due to the fact that the electrons are being depleted from the gap mainly due to (i) their conversion into the less mobile O_2^- ions in three-body attachment reactions and due to (ii) their drift motion to the anode. These mechanisms cause a decrease in the electron density, with a consequent decrease in the current. Another contributing factor to the initially decreasing current is that the applied voltage is close to the SSV; this current decrease is not seen for significantly higher overvoltages. The initial front of positive ions, after the ion drift time ($\sim 15\,\mu$s), has traversed the gap, see Fig. 4.5, and gives rise to the first electron avalanche. This avalanche is initiated by the seed electrons ejected from the cathode by secondary electron emission due to the impact of the positive ions. Through a positive feedback loop, these electrons ionize neutrals close to the anode, increasing there the density of positive ions. The peaks in current provoked by the avalanches are however hardly visible in the current oscillograms of Fig. 4.9 due to the logarithmic scale. The successive avalanches raise the overall charge density in the gap and consequently, at about 200 μs, the current goes up.

Breakdown happens at around 0.5 ms and is a consequence of the buildup of space-charge in the gas volume not far from the cathode. This space-charge grows and

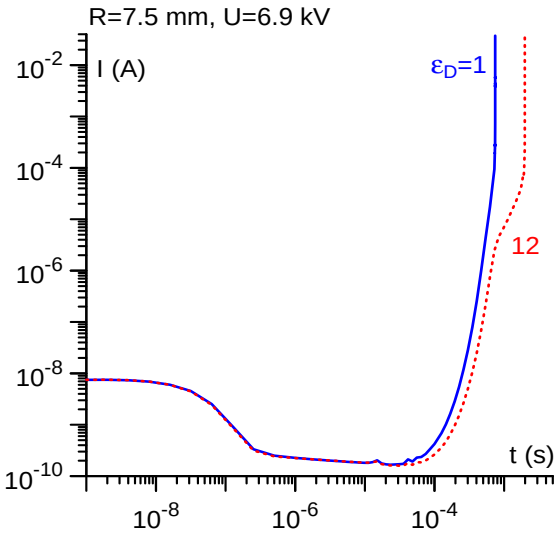

Figure 4.9: Current-time oscillograms for a discharge development towards breakdown. Solid line: $\varepsilon_D = 1$; dotted line: $\varepsilon_D = 12$. Considered case is $R = 7.5\,\text{mm}$ and $j_n = 0$.

contracts in space, with its maximum moving towards the cathode. When densities reach about $10^{19}\,\text{m}^{-3}$, the background electric field of the electrode setup becomes significantly distorted and as a result an ionization wave develops in this region that starts propagating to the cathode. In fractions of a millisecond the current grows more than 6 orders of magnitude, fulfilling our definition of breakdown.

The current oscillograms of Fig. 4.9 do show that over time, setups with different dielectric permittivities will exhibit different characteristics. For instance, it takes more than 2 times longer for breakdown to occur for the higher permittivity as compared to the smaller permittivity. Differences are expected between the two setups, since the evolution from an initial condition of 'no-discharge', which is quite different from the densities in the self-sustained state of each setup, will affect differently the dynamics of the different charge-distributions on the dielectric.

For a general comparison between the case of low overvoltages with one of high overvoltages, Figs. 4.10 show distributions of the reduced electric field at instants just prior to breakdown for $R = 3\,\text{mm}$. Fig. 4.10a is for a 1% overvoltage, and Fig. 4.10b for 30% overvoltage. In Fig. 4.10a, close to the cathode, a severe distortion of the background field is seen, where a very short low field region trails behind a high field front. In Fig. 4.10b, a similar situation is found, however there is now also an elongated low electric field region in the upper half of the gap trailing behind a high field front in the middle of the gap. The space-charge is high in regions where the electric field is high, due to the high production rates there, and is also high in the neighboring low field (high conductivity) channels where charges drift to. In results not shown here,

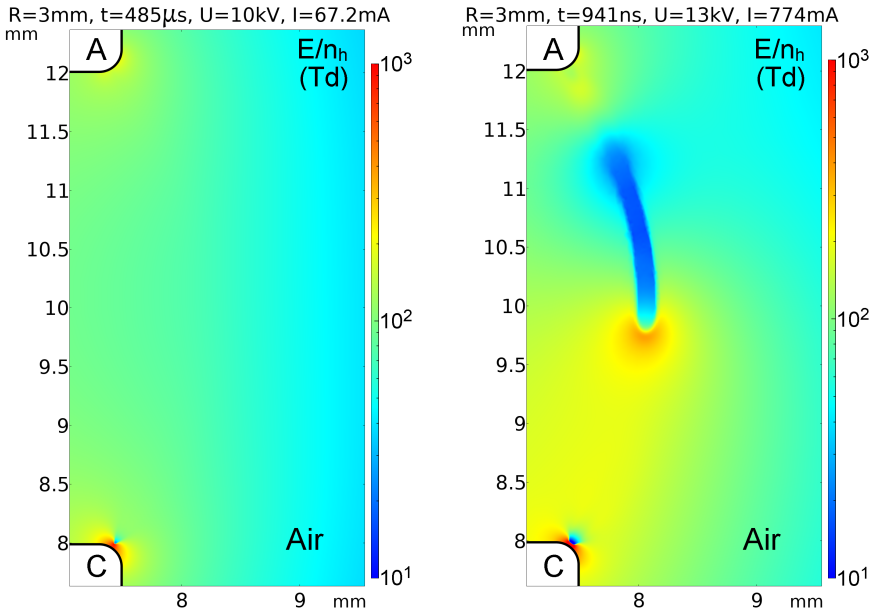

Figure 4.10: Reduced electric field at a time-instant close to breakdown. a) 1% overvoltage; b) 30% overvoltage. Further details are at the header of each figure. A and C are respectively the anode and cathode. Considered case is $R = 3\,\mathrm{mm}$.

the high electric field fronts are fronts of cathode-directed ionization waves. In Fig. 4.10b the mid gap ionization wave originated at the anode and is therefore also called a positive streamer.

In Fig. 4.10a we have again the situation encountered for low overvoltages in $R = 7.5\,\mathrm{mm}$, see last instants of Fig. 4.4a and last instant of Fig. 4.5a, where a near-cathode ionization wave has formed close to the cathode and is propagating towards the cathode. It should be stressed that at this low overvoltage, there is no streamer propagating across the totality of the gap. In Fig. 4.10b, for an overvoltage of 30%, a positive streamer has traversed about half the gap length, when densities in the region in front of the cathode grew to a point where a near-cathode ionization wave formed and is now also propagating towards the cathode. As shown in the header of Figs. 4.10, breakdown happens in about 0.5 ms for the SSV, much longer than for the higher overvoltage, where it takes about $1\,\mu\mathrm{s}$. Also, the average power consumption at the instants in Figs. 4.10, was about 1 W for the low overvoltage, and 34 W for the high overvoltage.

4.6 Conclusion

A simplified setup for modelling a device of industrial interest, made up of a dielectric disk tightly stacked between two disk electrodes, was selected as a case study. The resonance method, developed in Chap. 2, was used to calculate the first-breakdown voltage and repetitive-breakdown voltage in this setup. The calculated voltages were compared with those obtained from time-dependent modelling of breakdown. The mutual agreement was to within 5% and therefore validates the use of the resonance method to setups with a weakly non-uniform distribution of the electric field. This is a finding of some importance, since unlike time-dependent modelling, where the breakdown voltage has to be obtained by a very computationally intensive and time-consuming trial and error procedure, the resonance method, based on stationary modelling, provides a systematic procedure to calculate the self-sustainment voltage. It is unclear exactly how much time would be needed to calculate the breakdown voltage to within 1% exclusively using non-stationary calculations, i.e. without using the self-sustainment voltage provided by the resonance method. In the considered setup and without efforts of optimization, typical computation time of one self-sustainment voltage was about 2 h, while typical computation time for a certain breakdown voltage, was about 48 h.

It was recognized that during the temporal evolution towards breakdown, a density distribution is attained that very much resembles that of the corresponding quasi-stationary state with no surface-charge on the dielectric. The time-scale of formation of this quasi-stationary volume discharge, is much shorter than the time-scale for the formation of the steady-state, where all the surface-charge has accumulated on the dielectric. This analysis led to the formulation of two boundary conditions for the resonance method. The first boundary condition of a non-prestressed setup, prescribed no surface-charge on the dielectric, and produced a quasi-stationary state that was associated with a first-breakdown discharge. The second boundary condition of a prestressed setup, prescribed zero current density on the dielectric, and produced a steady-state that was associated with a repetitive-breakdown discharge.

Results for the first-breakdown voltage and the repetitive-breakdown voltage were obtained for various radii of the dielectric disk and for two dielectric permittivities. It was found that with the non-prestressed condition, the self-sustainment voltage is generally higher than with the prestressed condition. A notable exception occurs when the dielectric constant is 12 and the dielectric protrudes the electrodes, where an abrupt voltage decrease with R was seen to be connected to the most favorable discharge path becoming one that connects directly cathode to dielectric surface, instead of anode. For the radius of 3 mm the obtained result could be compared to the available experiment

with good agreement. Results for the recessed dielectrics also agreed qualitatively with experiment. It would be interesting to see if experiments will confirm the calculated self-sustainment voltages for protruding dielectrics.

From the obtained results, the best configuration to withstand breakdown, both first and repetitive-breakdown, for the studied setup with dielectric height of 4 mm, is to use the dielectric with low permittivity and a radius of 8.2 mm. Though for lower permittivity it was seen that breakdown happens faster than for higher permittivity.

It was verified that the dynamics of breakdown in low overvoltages was similar in all cases, though this was not the main focus of this work. During a first breakdown development, a volume discharge formed similar to the self-sustaining discharge without surface-charge on the dielectric surface. During a repetitive breakdown development, a volume discharge formed similar to the self-sustaining discharge with surface-charge on the dielectric. In the last stage of both types of breakdown, no streamer was seen bridging the gap, instead close to the cathode, electron and positive ions densities would increase to values of order $10^{19}\,\mathrm{m}^{-3}$ whereupon a streamer-like ionization wave would move towards the cathode, dramatically raising the conduction and displacement currents locally across the gap. At significantly higher overvoltages, positive streamers were seen to propagate from the anode to the cathode.

The axi-symmetric calculations here presented are not expected to be experimentally observed because the presence of 3D perturbations, which are not allowed in axi-symmetric calculation domains, would break the axial symmetry. Nevertheless we still consider that the present work provides valuable qualitative and quantitative information on the evaluation of self-sustainment and breakdown voltages, since the main processes of formation and propagation are captured by an axi-symmetric domain.

In the selected setup the electric field has a weak non-uniformity, i.e. $E_{\max}/\langle E\rangle \leq 7.4$, where $\langle E\rangle = SSV/Gap$, and it was possible to establish that the self-sustainment voltage (SSV) and breakdown voltage (BDV) are close. It should be stressed that for the purpose of calculating the field non-uniformity, $E_{\max}$ was gauged in the whole domain excluding the triple junctions and their immediate vicinity ($10\,\mu$m), where it is known to diverge. It is not expected that the agreement between the SSV and BDV will hold in cases where the field non-uniformity is several orders of magnitude. Future work could study the degree of field non-uniformity above which the resonance method significantly deviates from standard time-dependent simulations of breakdown.

Chapter 5

Conclusions and future work

The present work has revisited the mathematical formulation of low-current discharges. The system of equations governing the ignition of quasi-stationary, high-pressure and low-current self-sustained gas discharges, includes the conventional system of equations for the conservation of particles, the Laplace equation for the potential and partial differential equations for the photoionization terms. At ignition space-charge and recombination are negligible and there are steady distributions for the calculated quantities. A careful analysis showed that the system of equations is best understood as a multidimensional boundary-value eigenvalue problem for a system of stationary partial differential equations. The applied voltage is the eigenparameter that determines whether charged particles production processes, like ionization by electron or photon impact, generated in the discharge, are sufficient to compensate for the loss of charged particles drifting to the electrodes and walls or disappearing through attachment. Only in very special cases can this system be solved analytically, for complicated geometries a numerical solution is the only viable option. For this purpose several methods were investigated to ascertain which was the fastest and most efficient to solve this eigenvalue problem, i.e., to obtain the value for the applied voltage (eigenvalue) and the associated distributions of densities, potential and photoionization (eigenfunctions). Three different methods were investigated, namely direct solution of the eigenvalue problem for the self-sustainment voltage, investigation of stability of the no-discharge solution, and the resonance method. Given that all methods produced the same results, the latter resonance method was chosen as the method of choice, because it was the easier to implement.

The self-sustaining discharge obtained by the resonance method can be used as the starting point in the construction of the current-voltage characteristic (CVC) of any setup, where points of the CVC for ever increasing values of current are obtained in an iterative process. It is well known that convergence of a stationary non-linear problem,

like in the construction of the CVC, is difficult, unless a good initial approximation is used. Therefore the resonance method greatly facilitates the task of obtaining the CVC. The stationary solution to a given problem can of course also be obtained by means of temporal relaxation using non-stationary modelling, as was done on several occasions in Chap. 4. However, since time-dependent modelling is generally much more time consuming, obtaining the solution through stationary modelling is to be preferred. The complete procedure for the application of the resonance method has been summarized in a simple five step flowchart.

The resonance method was seen to be capable of calculating the self-sustained discharge of a variety of setups, in fact to date, in no setup has it failed to produce the low-current self-sustained discharge state. The research group of IPFN at UMa has successfully applied the resonance method to the following geometries: plane-to-plane, coaxial cylinders, point-to-plane, rod-to-plane, (plane with protrusion)-to-plane, dielectric disk tightly stacked between disk electrodes and there is no reason why it should not work for an arbitrary geometry. When the studied physical phenomena display oscillatory behavior, like in pulsed corona, using a stationary solver allows to capture time-averaged characteristics of the discharge.

Returning to the starting point of calculating the voltage of a low-current self-sustained discharge, the Townsend criterion as still a very widely used tool, is revisited. This tool is attractive since it needs only as input parameters the ionization and attachment coefficients and the secondary electron emission coefficient, specified as functions of the reduced electric field. In a complex setup, seasoned engineers would, with educated guesswork, select the probable field line along which they expect the discharge to happen. They would be able to equate the ionization integral to a tabulated value at which self-sustainment or breakdown is known to occur and adjust the voltage value to produce the needed electric field. A rigorous mathematical foundation for this type of heuristic procedure, is what was sought. Having recognized self-sustainment phenomena in low-current discharges as being described by an eigenvalue problem, an attempt to derive the classical Townsend criterion from the corresponding equations has enabled to obtain a more general expression. The derived expression is applicable to multidimensional setups with non-uniform electric fields and reduces to the classical Townsend expression in the case of a plane-to-plane geometry. The general outline for the derivation, involves neglecting diffusion and parametrizing the conservation equations of the charged particles along the electric field lines. The effect of diffusion is assumed insignificant for volume discharges. It is subsequently possible to set up a closed set of equations involving just electrons and negative ions. For an analytical solution of these equations, some simplifying assumptions had to be made, namely photoionization and detachment were neglected. On neglecting photoionization, the

applicability of the criterion is restricted to electronegative gases in configurations with weakly non-uniform electric field, however the neglect of detachment may degrade the criterion's results for electronegative gases. The latter shortcoming can be remedied by using an effective attachment coefficient which, in an approximate way, takes into account the detachment. The validity of the various simplifying assumptions were checked by comparison with similarly simplified versions of the resonance method. Comparisons were done for air in three geometries, namely negative coronas in concentric-cylinder, in point-to-plane configurations and in an axially symmetric configuration with weakly nonuniform electric field. In the studied cases it was found that neglect of diffusion produces an error in the self-sustainment voltage of the order of 1% and that photoionization was negligible. In all studied geometries and conditions, the most accurate version of the extended criterion, i.e., using the effective attachment coefficient, produced a self-sustainment voltage virtually equal to the one calculated by the resonance method. The largest deviation was of 2% for the coaxial cylinder geometry at 0.1 atm.

In brief, to evaluate the self-sustainment voltage of a setup where the electric field non-uniformity is not too strong and the gas is electronegative, the Townsend criterion is the most economic option requiring just the publicly available (e.g. LoKI [54]) field-dependent coefficients for ionization, attachment, electron mobility and electron temperature. If however the aim is to have a tool capable of calculating the self-sustainment voltage in a general setup, then the more elaborate option of the resonance method is to be preferred.

As the next logical step in the research, a unique opportunity presented itself, i.e., to investigate the difference between the self-sustainment voltage and the breakdown voltage in a given setup. Note that experimentally, in certain conditions the two voltages coincide; e.g. [22] for a setup of coaxial cylinders. For calculating the self-sustainment voltage, the developed resonance method is well suited, while for the breakdown voltage the same hydrodynamic framework was used, but complemented with the non-stationary terms in the particle density conservation equations and a new boundary condition at the dielectric surface allowing for charge accumulation.

This research focused mainly on a simplified setup of a disk dielectric, tightly stacked between two disk electrodes, intended to model breakdown observed in a medium DC-voltage circuit-breaker. In this setup the electric field non-uniformity was not very high. When powered by a DC-voltage source and a ballast resistor, this setup was seen to first evolve to a volume discharge at a voltage corresponding to a self–sustained state without surface-charge on the dielectric. This state was attained within fractions of a millisecond. After about 10 milliseconds the steady-state discharge was obtained, with a voltage equal to the self-sustainment voltage of the steady-state. In

this state, the necessary surface-charge has been deposited on the dielectric to satisfy the steady state's boundary condition of zero current density across the dielectric surface. Based on these findings, the following two initial conditions were introduced for non-stationary simulations of two types of breakdown. First-breakdown implies an initial condition where there are no surface-charges on the dielectric. Repetitive-breakdown implies an initial condition where there is a surface-charge distribution on the dielectric. This latter distribution is taken from the self-sustained steady-state calculated by the resonance method using as boundary condition zero current density across the dielectric. Apart from the initial condition for the surface-charge, low 'no-discharge' densities were ascribed to all the charged particle densities. In other terms, the initial conditions distinguish a setup that has been pre-stressed, i.e., has accumulated surface-charge, from a 'fresh' non-prestressed setup with no surface-charge on it. Calculations of the breakdown voltages using time-dependent modelling relied on a previous calculation of the self-sustainment voltage by the resonance method, insofar as the initially tried breakdown voltage was precisely the self-sustainment voltage.

For the studied setup in each of its initial conditions, time-dependent modelling was seen to lead to discharge extinction at an applied voltage equal to the self-sustainment voltage of the setup. The applied voltage was then increased by 1%. Time-dependent modelling was performed at the new voltage value and it was checked whether breakdown occurred. If the discharge extinguished, the applied voltage would be increased a further 1% and so successively until the time-dependent modelling evolved to breakdown. Several conclusions were made regarding these calculated voltages. First, the breakdown voltages calculated using the non-stationary description were seen to be no more than 2% above the self-sustainment voltage, the one exception being with the protruding dielectric of higher permittivity that needed an overvoltage of 5%. Secondly, the first-breakdown voltage, i.e., when starting from the non-prestressed setup, was systematically higher than the repetitive-breakdown voltage, i.e., when starting from a pre-stressed setup, except for the protruding dielectric. Thirdly, for repetitive-breakdown, when the boundary condition of the resonance method is that of zero current density across the dielectric surface, or equivalently in the non-stationary description, when the setup is pre-stressed, results confirm that breakdown is facilitated when there is a dielectric close to the active discharge path. The repetitive-breakdown voltages don't depend on the dielectric constant nor on details of the secondary electron emission from the dielectric. Results for the modelled circuit-breaker indicate that the setup that best withstands both first and repetitive-breakdown, is one where the dielectric has low permittivity and protrudes the electrodes.

The dynamics of repetitive-breakdown in the studied setup was observed for low overvoltages to be qualitatively similar, whether the dielectric surface was close to the

active discharge area or not. In brief the dynamics unfolds as follows, upon successive avalanches, the charge density increased along field lines connecting cathode to anode, but does so at a higher rate in front of the cathode. Eventually the space-charge in front of the cathode increases to a point where it locally distorts the electric field of the electrodes. The created conditions give rise to the self-propagating structure of an ionization wave travelling towards the cathode. This wave originates in the volume not far from the cathode, and has characteristics similar to a positive streamer. The time-scale for repetitive-breakdown was of the order of milliseconds and happened earlier for the dielectric of lower permittivity.

In future work the degree of field non-uniformity above which the resonance method significantly deviates from standard time-dependent simulations of breakdown could be studied. A more systematic study is expected of the streamer dynamics in low and high overvoltages, with and without a dielectric surface along the discharge path. The study of the effect of other quantities, like the secondary electron emission coefficient on streamer velocity would be of interest. Also, the development and implementation of photoemission from dielectric surfaces is desirable, especially for simulations where the streamer propagates close to dielectric surfaces. Further developments of the present model could be its implementation as a 3D model, which would bring the results closer to the physically realized situation, but it is however not expected to substantially affect the presented results, namely the values of the calculated self-sustainment and breakdown voltages. A proper extension of the working model could be to include the plasma-surface interaction at the cathode. This would allow to prolong the modelling when the ionization wave, or streamer, hits the cathode and possibly allow to model the transition to a spark discharge. It would however require taking into account the substantial heat flux towards the cathode, estimating the Murphy and Good field emission, Nottingham effect, heat propagation inside the cathode and more, and is therefore a challenging task.

Appendix A

Boundary conditions for drift-diffusion equations

The hydrodynamic (drift-diffusion) equations (2.2) are justified provided that the local macroscopic length scale L is much larger than the relevant microscopic scale λ_α. When α refers to an ion species, λ_α is represented by the ion mean free path. When $\alpha = e$, λ_e is represented by the electron energy relaxation or maxwellization length. On distances of the order of λ_α or smaller from solid surfaces, the hydrodynamic equations lose their validity. Therefore, a kinetic analysis is indispensable in order to formulate boundary conditions on solid surfaces for hydrodynamic equations in a rigorous way: a kinetic equation for the velocity distribution function on distances of the order of λ_α must be solved in the first approximation in the small parameter λ_α/L and the obtained solution must be asymptotically matched with a solution of the hydrodynamic equations on the scale L; the procedure of the asymptotic matching will provide the boundary condition being sought.

Let us denote by the index n the projections of the corresponding vectors onto the local normal directed from the solid into the plasma. Let us first consider the case where (i) E_n, the local normal electric field at the surface, is weak enough so that its work over the charged particles of species α over the distance λ_α is much smaller than the characteristic translational energy of the particles, $e\,|E_n|\,\lambda_\alpha \ll kT_\alpha$; (ii) all particles of species α coming to the surface from the plasma are absorbed and none are reflected; and (iii) the surface does not emit the particles of species α. (Here T_α is the species effective temperature and k is Boltzmann's constant.) In this case, the distribution function on distances of the order of λ_α is of the order of λ_α/L, i.e., asymptotically small, compared to values of the distribution function on distances of the order L. Therefore, the above-described asymptotic matching procedure requires that n_α the particle number density governed by the hydrodynamic equations vanishes

at the surface, thus giving the trivial boundary condition $n_\alpha = 0$ for the hydrodynamic equations. Note that this boundary condition has exactly the same physical meaning as the standard no-slip boundary condition on solid surfaces for the Navier-Stokes equations.

If the local electric field is moderate or strong, $e\,|E_n|\,\lambda_\alpha \gtrsim kT_\alpha$, then the asymptotic structure of the solution on the distances of the order λ_α is rather complex for both the electrons [104–106] and the ions [107]; no simple exact solution is possible and therefore there is no unique way to formulate simple boundary conditions. This explains why the number of different existing variants of boundary conditions is so large; e.g., [108, 109] and references therein. On the other hand, the effect of the boundary conditions over the distribution of particles attracted to the surface (the positive ions in the case $E_n < 0$ and the negative ions and the electrons in the case $E_n > 0$) is localized on the length scale $kT_\alpha/e\,|E_n|$ in the case of moderate or strong electric fields. This scale is comparable to, or smaller than, λ_α and the hydrodynamic (drift-diffusion) equations are anyway inapplicable on this scale. The effect of the boundary conditions on the distribution of the repelled particles will be qualitatively correct if the flux of particles emitted by the surface is described correctly. Hence, the exact form of the boundary conditions is not very important in the case of moderate or strong electric fields, and this is consistent with what is found in the modelling practice. Therefore, the use of simple approximations is advisable.

The simplest variants may be summarized as follows. The hydrodynamic transport flux of particles of species α in the direction from a solid surface into the plasma may be represented as

$$J_{\alpha n} = r_\alpha J_{\alpha-} + J_{em}^{(\alpha)} - J_{\alpha-}, \tag{A.1}$$

where $J_{\alpha-}$ is the density of the flux of the particles coming from the plasma to the surface, r_α is the reflection coefficient, and $J_{em}^{(\alpha)}$ is the density of the flux of the particles emitted by the surface. Considering r_α and $J_{em}^{(\alpha)}$ as known, one needs to express the kinetic quantity $J_{\alpha-}$ in terms of hydrodynamic parameters in order to obtain an explicit boundary condition for hydrodynamic equations.

The simplest approximation is to assume that $J_{\alpha-}$ is proportional to n_α the local number density and the mean speed of chaotic motion, $\bar{C}_\alpha = \sqrt{8kT_\alpha/\pi m_\alpha}$: $J_{\alpha-} = \xi_\alpha n_\alpha \bar{C}_\alpha$, where ξ_α is a numerical coefficient and m_α is the species particle mass. Eq. (A.1) assumes the form

$$J_{\alpha n} = J_{em}^{(\alpha)} - \xi_\alpha\,(1 - r_\alpha)\,n_\alpha \bar{C}_\alpha. \tag{A.2}$$

It is well known that if the velocity distribution of particles of species α is isotropic and Maxwellian, then the density of particle flux in any direction, in particular, in

the direction to the surface, equals $n_\alpha \bar{C}_\alpha/4$, so ξ_α in Eq. (A.2) may be set equal to 1/4. The condition obtained in this way is equivalent to the so-called Thomson-Loeb formula, which has been widely used in fluid modelling of gas discharges; e.g., [75] and references therein.

If the number of particles moving from the surface is low, then the velocity distribution near the surface is strongly anisotropic. Approximating this distribution by a half-Maxwellian function, one obtains $\xi_\alpha = 1/2$. Note that the obtained boundary condition in the case of the electrons and $r_e = 0$ coincides with the corresponding boundary condition employed in Plasma module of COMSOL Multiphysics®.

Another variant of boundary condition may be obtained by representing the velocity distribution near the surface as a superposition of two distributions, describing the particles moving to and from the surface. Assuming that each of these distributions is half-Maxwellian, one can write

$$r_\alpha J_{\alpha-} + J_{em}^{(\alpha)} = \frac{n_{\alpha+}\bar{C}_\alpha}{2}, \quad J_- = \frac{n_{\alpha-}\bar{C}_\alpha}{2}, \tag{A.3}$$

where $n_{\alpha+}$ and $n_{\alpha-}$ are the number densities of the particles moving into the plasma and to the surface, respectively. Solving these equations for $n_{\alpha+}$ and $n_{\alpha-}$ and substituting into the expression for the net particle number density, $n_\alpha = n_{\alpha+} + n_{\alpha-}$, one finds

$$n_\alpha = \left(r_\alpha J_{\alpha-} + J_{em}^{(\alpha)}\right)\frac{2}{\bar{C}_\alpha} + J_{\alpha-}\frac{2}{\bar{C}_\alpha}. \tag{A.4}$$

Solving this equation for $J_{\alpha-}$ and substituting into Eq. (A.1), one obtains the boundary condition

$$J_{\alpha n} = \frac{2J_{em}^{(\alpha)}}{1+r_\alpha} - \frac{1-r_\alpha}{1+r_\alpha}\frac{n_\alpha \bar{C}_\alpha}{2}. \tag{A.5}$$

This condition has been known for a long time, e.g., in the particular case $r_\alpha = 0$ it coincides with Eq. (38) of [110]; see also recent work [109]. The second term on the rhs of Eq. (A.5) is consistent with the second term on the rhs of Eq. (A.2) if one sets $\xi_\alpha = 1/2\,(1 + r_\alpha)$. However, the first term on the rhs of Eq. (A.5) involves the coefficient $2/\,(1 + r_a)$, which is absent in Eq. (A.2) and which exceeds unity except for $r_a = 1$.

From now on, let us restrict the consideration to the usual situation where the reflection of the charged particles is insignificant, i.e., $r_\alpha = 0$ for all charged-particle species. Let us apply each of the above boundary conditions to three limiting cases. The first one is the case of local equilibrium, where most of the emitted particles return to the surface: $|J_{\alpha n}| \ll J_{em}^{(a)}$. Eq. (A.2) with $\xi_\alpha = 1/4$ and Eq. (A.5) give the correct result $n_\alpha = 4J_{em}^{(\alpha)}/\bar{C}_\alpha$. Eq. (A.2) with $\xi_\alpha = 1/2$ assumes a somewhat different form $n_\alpha = 2J_{em}^{(\alpha)}/\bar{C}_\alpha$.

The second limiting case is the one where most of the emitted particles are swept away by the electric field into the bulk of the plasma and only a small number return to the surface. The drift velocity of the particles in the vicinity of the surface is directed into the plasma and is much greater than $\bar{C}_\alpha$, so the second term on the rhs of Eqs. (A.2) and (A.5) is small. Eq. (A.2) assumes the form $J_{\alpha n} = J_{em}^{(\alpha)}$ as it should. On the other hand, Eq. (A.5) gives $J_{\alpha n} = 2J_{em}^{(a)}$; a physically unrealistic result.

The third limiting case is the one where the emission flux is much smaller than the flux of the particles coming from the plasma, i.e., the first term on the rhs of Eqs. (A.2) and (A.5) is small. Eq. (A.2) with $\xi_\alpha = 1/4$ assumes the form $J_{\alpha n} = -n_\alpha \bar{C}_\alpha/4$, while Eq. (A.2) with $\xi_\alpha = 1/2$ and Eq. (A.5) give $J_{\alpha n} = -n_\alpha \bar{C}_\alpha/2$. The former expression would be adequate for an isotropic velocity distribution function. However, the distribution near an absorbing non-emitting surface is strongly anisotropic, and the latter expression appears to be more appropriate in such cases.

Thus, each of the boundary conditions correctly reproduces two of the limiting cases, but not the third one. Since the boundary condition (A.5) gives an unrealistic result in the important limiting case where most of the emitted particles are swept away by the electric field into the plasma, this condition can be hardly recommended. Eq. (A.2) with ξ_a equal to 1/4 or 1/2 appears to be more physical.

In many cases the ion emission is neglected, i.e., $J_{em}^{(\alpha)}$ for all ion species may be set equal to zero. Then Eq. (A.2) assumes the form

$$J_{\alpha n} = -\xi_\alpha n_\alpha \bar{C}_\alpha, \quad J_{en} = J_{em}^{(e)} - \xi_e n_e \bar{C}_e \tag{A.6}$$

for the ions and the electrons, respectively. The electron emission flux $J_{em}^{(e)}$ must be evaluated with account of all relevant mechanisms, including the electron emission under the effect of charged and excited particles and photons produced in the discharge (secondary electron emission), photoemission caused by external radiation, thermionic emission, thermo-field and field electron emission from the cathode surface. It should be stressed that in the case of weak electric field, where $e\,|E_n|\,\lambda_\alpha \ll kT_\alpha$ or, equivalently, the drift speed is much smaller than $\bar{C}_\alpha$, the first boundary condition in Eq. (A.6) is equivalent to the trivial boundary condition $n_\alpha = 0$ as it should.

The natural choice is to set $\xi_a = 1/2$ in the first equation Eq. (A.6). ξ_e in the second equation may also be set equal to 1/2 except at hot surfaces in high-pressure (arc) plasmas, where the dominating electron emission mechanism is thermionic emission and a significant part of the emitted electrons return to the surface, hence the value $\xi_e = 1/4$ may be more appropriate. The boundary conditions (A.6) with $\xi_a = \xi_e = 1/2$ were used in most of the simulations described in this work.

For computational reasons, it may be convenient to replace the boundary condition Eq. (A.6) for the positive ions at the cathode and negative ions and the electrons at the

anode by the condition of zero normal derivative of n_α, which amounts to neglecting the diffusion flux of the attracted particles to the electrode in comparison with the drift flux. This eliminates difficulties with the computation of the distribution of the attracted particles on the length scale $kT_\alpha/e\,|E_n|$, where the solution given by the hydrodynamic equations is non-physical anyway. This simplification was employed in most of the simulations described in this work.

As mentioned above, the effect of the precise form of boundary conditions in the modelling is not strong. As an example, one can refer to the parallel-plate discharge, considered in Sec. III E of [52]: the discharge initiation voltage, computed numerically using the boundary conditions Eq. (A.6) with $\xi_i = \xi_e = 1/2$, differs from the value obtained using the boundary conditions $J_{en} = -\gamma J_{in}$ at the cathode and $n_i = 0$ at the anode, by mere 1.2%. (The index i here refers to the positive ions.) As another example, one can mention that the change of the boundary conditions for the negative ions at the cathode and for the positive ions at the anode from the condition (A.6) with $\xi_\alpha = 1/2$ to $n_\alpha = 0$ produced little effect in the modelling of corona discharges reported in [94].

Appendix B

Plasmachemical processes and transport coefficients for modelling of low-current discharges in high-pressure air

The model of plasmachemical processes and transport coefficients of low-current discharges in dry air at pressures of the order of atmospheric and higher, used in this work, was obtained by modifying, as described in this section, the 'minimal' model [62]. Note that the 'minimal' model was validated in [62] by comparing the computed inception voltage of corona discharges with several sets of experimental data on positive and negative glow coronas between concentric cylinders, over a wide range of pressures and diameters of the cylinders, and on positive coronas in the rod-to-plane configuration. It should be stressed that modifications described in this section do not affect the inception voltage, which was the parameter computed in [62]. The modified model was validated in [94] by comparing the computed steady-state corona parameters with time-averaged measurements in DC corona discharges in point-plane gaps in ambient air over a wide range of currents of both polarities and various gap lengths.

The modified model takes into account the following charged species: the electrons, an effective species of positive ions, which will be designated A^+ in this work instead of M^+ as in [62], and the negative ions O_2^-, O^-, and O_3^-. The ions generated in air by the electron impact ionization are N_2^+ and O_2^+. Ions O_2^+ are generated also by the photoionization, which is produced by UV radiation emitted by N_2 molecules excited by electron impact. The N_2^+ ions in air at pressures of about 1 atm and higher are rapidly converted into O_2^+. One channel of such conversion is the fast charge transfer

reaction $N_2^+ + O_2 \rightarrow O_2^+ + N_2$. Another channel comprises a three-body conversion process of N_2^+ and N_2 molecules into the N_4^+ ions, followed by the charge transfer from N_4^+ to O_2. Therefore, the positive ions in the ionization zone are represented mostly by O_2^+.

If the reduced electric field E/N is sufficiently low and the effective ion temperature is not appreciably higher than the neutral gas temperature T (which is typically of the order of 300 K), then the O_2^+ ions may be converted into complex ions; e.g., [111]. In the case of humid air, the formation of cluster ions containing several H_2O molecules is also possible.

Consider, as a characteristic example, complex ions O_4^+, which are created mostly in the reaction $O_2^+ + 2O_2 \rightarrow O_4^+ + O_2$ and destroyed in the reverse reaction. Using the rate constants [112], one obtains

$$z = 1.78 \times 10^{-5} \frac{n_{O_2}}{N_0} \left(\frac{T_{O_4^+}}{300\,\mathrm{K}} \right)^4 \left(\frac{300\,\mathrm{K}}{T_{O_2^+}} \right)^{3.2} \exp \frac{5030\,\mathrm{K}}{T_{O_4^+}}, \tag{B.1}$$

where $z = n_{O_4^+}/n_{O_2^+}$, n_α and T_α are the number density and the effective temperature of species α, and $N_0 = 2.45 \times 10^{25}\ \mathrm{m}^{-3}$ is the standard gas number density (the number density corresponding to the pressure of 1 atm and the gas temperature of 300 K).

Assuming the value of $2.3 \times 10^{-4}\,\mathrm{m^2\,V^{-1}\,s^{-1}}$ for the reduced mobility (the mobility scaled to the standard number density) of ions O_4^+ in air [111], one obtains the following estimate from the Wannier formula (C.1): $T_{O_4^+} = T + 0.037(E/N)^2\,\mathrm{Td}^{-2}$ K. Assuming for the reduced mobility of the O_2^+ ions in air the value of $2.8 \times 10^{-4}\,\mathrm{m^2\,V^{-1}\,s^{-1}}$, which corresponds to the reduced mobility given in Table IIb (p. 68) of compilation [113] for the reduced field of 100 Td, one obtains $T_{O_2^+} = T + 0.054(E/N)^2\,\mathrm{Td}^{-2}$ K.

It follows from Eq. (B.1) that, for atmospheric pressure and $T = 300\,\mathrm{K}$, $z > 1$ for $E/N \lesssim 51\,\mathrm{Td}$ and $z < 1$ for higher reduced fields; in particular, $z \approx 0.0063$ for $E/N = 100\,\mathrm{Td}$, which is an approximate value of the critical reduced field in air. This example confirms that the main positive ion species in the active zone of corona and corona-like discharges in air are the O_2^+ ions, with a typical value of the reduced mobility of $2.8 \times 10^{-4}\,\mathrm{m^2\,V^{-1}\,s^{-1}}$. In the drift zone complex positive ions dominate, while in the case of humid air, it are cluster ions that dominate (except in the region adjacent to the active zone where E/N approaches 100 Td). Typical reduced mobilities of the positive ions are in the range $(2.0 - 2.5) \times 10^{-4}\,\mathrm{m^2\,V^{-1}\,s^{-1}}$ [111].

The dominating process in the active zone is electron multiplication, which is not directly affected by the presence of positive ions. Hence, values of the mobility of positive ions in the drift zone are the relevant ones. In this model, the reduced mobility of an effective positive ion species is set equal to $2.2 \times 10^{-4}\,\mathrm{m^2\,V^{-1}\,s^{-1}}$. Similarly, the

reduced mobility of the ions O_2^- is also set equal to 2.2 $\times 10^{-4}\,m^2\,V^{-1}\,s^{-1}$, reflecting the possible formation in the drift zone of complex and, in the case of humid air, cluster ions [111, 114].

The O^- ions are present mostly in the active zone, at high reduced electric fields, since in the drift zone most of them are destroyed by detachment, charge transfer to the oxygen molecules, and conversion into ozone ions. According to [113], the reduced mobility of O^- varies between approximately $3.7 \times 10^{-4}\,m^2\,V^{-1}\,s^{-1}$ and $5.2 \times 10^{-4}\,m^2\,V^{-1}\,s^{-1}$ over the reduced field range up to 100 Td (there are no data for higher fields). According to [115], the reduced mobility of O^- varies between approximately $3.3 \times 10^{-4}\,m^2\,V^{-1}\,s^{-1}$ and $4.9 \times 10^{-4}\,m^2\,V^{-1}\,s^{-1}$ over the reduced field range up to 120 Td. In principle, variations of reduced mobilities with the reduced field can be readily introduced into numerical models. Since, however, a constant value is used for the mobility of O_2^- (and complex/cluster ions), and given that the above variations are not huge, a constant value of $5.2\,cm^2\,V^{-1}\,s^{-1}$ is chosen for the reduced mobility of O^- in order to be consistent. Note that this value corresponds to the value given in Table IIf (p. 81) of [113] for the reduced field of 100 Td.

The O_3^- ions are present mostly in the drift zone, at low reduced fields. According to [113], the reduced mobility of O_3^- varies between approximately $2.7 \times 10^{-4}\,m^2\,V^{-1}\,s^{-1}$ and $3.4 \times 10^{-4}\,m^2\,V^{-1}\,s^{-1}$ over the reduced field range up to 100 Td, and between approximately $3.5 \times 10^{-4}\,m^2\,V^{-1}\,s^{-1}$ and $3.3 \times 10^{-4}\,m^2\,V^{-1}\,s^{-1}$ over the reduced field range between 100 Td and 200 Td. According to [115], the reduced mobility of O_3^- varies between $2.5 \times 10^{-4}\,m^2\,V^{-1}\,s^{-1}$ and $3.1 \times 10^{-4}\,m^2\,V^{-1}\,s^{-1}$ over the reduced field range up to 100 Td, and between $3.1 \times 10^{-4}\,m^2\,V^{-1}\,s^{-1}$ and $2.9 \times 10^{-4}\,m^2\,V^{-1}\,s^{-1}$ over the reduced field range between 100 Td and 240 Td. In order to be consistent, we have chosen for the reduced mobility of O_3^- ions a constant value of $2.7 \times 10^{-4}\,m^2\,V^{-1}\,s^{-1}$, which corresponds to the value shown in figure 2 of [115] for the reduced field of 60 Td.

The diffusion coefficients of all ion species are related to the mobilities through Einstein's relation with the corresponding effective ion temperatures evaluated by means of the Wannier formula, Eq. (C.1) of Appendix C. We remind that both Einstein's relation and the Wannier formula are accurate in the case of ions with a constant mobility. The mobility of the electrons was taken from [116] and the longitudinal and transversal diffusion coefficients of the electrons were evaluated with the use of the online version of the Bolsig+ solver [117] and the cross sections [118].

The kinetic scheme and relevant kinetic data used in this model are summarized in Tab. B.1. Reactions 1-4 and 6-8 are the same that were considered in [62]. In [62], collisional detachment from O_2^-, reaction 5, was written, following [119], in the form $O_2^- + M \rightarrow e + O_2 + M$, where M is any of the molecules N_2 and O_2. However, the contribution of the process $O_2^- + N_2$ is small, therefore the collisional detachment

No.	Reaction	Evaluation of reaction rate	Ref.
1	$e + M \rightarrow 2e + A^+$	Same as in [62]	[62]
2	$e + O_2 \rightarrow O^- + O$	Same as in [62]	[62]
3	$e + O_2 + M \rightarrow O_2^- + M$	[a] $\frac{\eta_3}{N^2} = 1.6 \times 10^{-47} \, (E/N)^{-1.1}$ m^5	[116]
4	$M + h\nu \rightarrow e + A^+$	[b] Eqs. (2.4)-(2.6)	[61]
5	$O_2^- + O_2 \rightarrow e + 2O_2$	[c] $6.1 \times 10^{-17} \exp\left[-\frac{9050}{T+0.305(E/N)^2}\right] \frac{\text{m}^3}{\text{s}}$	see text
6	$O^- + N_2 \rightarrow e + N_2O$	[c] $1.16 \times 10^{-18} \exp\left[-\frac{882}{T+0.436(E/N)^2}\right] \frac{\text{m}^3}{\text{s}}$	[119]
7	$O^- + O_2 \rightarrow O + O_2^-$	[c] $6.9 \times 10^{-17} \exp\left[-\frac{16200}{T+0.436(E/N)^2}\right] \frac{\text{m}^3}{\text{s}}$	[119]
8	$O^- + O_2 + M \rightarrow O_3^- + M$	[c] $1.3 \times 10^{-42} \exp\left[-\frac{T+0.436(E/N)^2}{1860}\right] \frac{\text{m}^6}{\text{s}}$	[119]
9	$A^+ + B^- \rightarrow$ products	[d] Eq. (B.2)	
10	$A^+ + e \rightarrow$ products	[d] Eq. (B.3)	

Table B.1: Kinetic scheme and relevant kinetic data. [a]Townsend coefficient. [b] reaction rate. [c]reaction rate constant. T in K, E/N in Td. [d]recombination coefficient. A^+: the effective positive ion species. B^-: any of the negative ions O^-, O_2^-, O_3^-. M: any of the molecules N_2 and O_2.

from O_2^- is written in this model with account of collisions only with O_2. The approximations of rate constants of reactions 5-8 were taken from Table 2 of [119]. (The rate constant of the collisional detachment from O_2^- was multiplied by the factor of 5, in agreement with the above.) It should be stressed that these approximations are valid for variable gas temperature T, in contrast to the approximations given in Appendix of [119] and used in [62], which are valid only for $T = 300\,\text{K}$.

Note that, although numerical results reported in this work refer to the constant gas temperature $T = 300\,\text{K}$, the applicability of the modified model for variable T is an improvement that will be exploited in subsequent work. It is expected that the modified model is applicable under conditions where the degree of dissociation of oxygen molecules is sufficiently low and oxygen atoms do not significantly affect the balance of charged particles (in particular, the rate of destruction of negative ions). At air pressures of the order of 1 atm, this corresponds to gas temperatures of the order of 1000 K and lower.

Another modification to the kinetic scheme [62] is an account of recombination. Again, this modification is not very relevant to the results reported in this work, however it will be useful for subsequent work. It should be stressed that due to

the lack of sufficient experimental information, the account of recombination cannot be introduced in an accurate way and should be considered rather as an order-of-magnitude estimate. The main mechanism of ion-ion recombination in air, reaction 9, at pressures of the order of 1 bar and higher is the ion-ion recombination with participation of neutral molecule(s), with the recombination coefficient in the range $(2-2.5)\times10^{-12}\,\mathrm{m^3\,s^{-1}}$ [120]. The rate constant of the binary ion-ion recombination is typically of the order of $10^{-13}\,\mathrm{m^3\,s^{-1}}$ (e.g., [112, 121]) and the contribution of this mechanism is small. At pressures of the order of 1 atm and higher, the coefficient of ion-ion recombination with participation of neutral molecule(s) may be estimated by means of the expression [122]

$$\beta_{ii}^{-1} = (\beta_{i3}N)^{-1} + \beta_{iL}^{-1}, \tag{B.2}$$

where β_{i3} is the three-body recombination rate constant and β_{iL} is the Langevin recombination coefficient. This expression has to be separately evaluated for each pair of positive (A^+) and negative (O^-, O_2^-, O_3^-) ions. The Langevin recombination coefficient is related to the mobilities of the recombining positive and negative ions, μ_α and μ_β, by the formula $\varepsilon_0\beta_{iL} = e\left(\mu_\alpha + \mu_\beta\right)$. The value of the three-body recombination rate constant for $T = 300$ K and low reduced electric field is assumed equal to $1.5\times10^{-37}\,\mathrm{m^6\,s^{-1}}$ for all three negative ion species; this value ensures a reasonably good agreement of the recombination coefficients for O_2^- and O_3^-, given by Eq. (B.2), with the experimental data shown in figures 6 and 7 of [120] on the recombination coefficient in air for a wide range of pressures. The temperature dependence of the three-body recombination rate constant varies from $T^{-5/2}$ (or T^{-3} for ions in parent gases [123]) at low pressures to $T^{-3/2}$ at pressures of around 1 atm [120]. Thus, one can set $\beta_{i3} = 1.5\times10^{-37}\,(300\,\mathrm{K}/T_{\alpha\beta})^{3/2}\ \mathrm{m^6\,s^{-1}}$, where $T_{\alpha\beta}$ is the effective reduced temperature of species α and β defined in Appendix C.

Electron-ion recombination, reaction 10, can occur via dissociative recombination of molecular ions, the recombination with participation of neutral molecules, and three-body recombination with the third body being the electron. The most effective dissociative electron-ion recombination process in air is the dissociative recombination of molecular ions O_2^+ and O_4^+. The rate constants of recombination of these ions are $\beta_{e2} = 2\times10^{-13}\,(300\,\mathrm{K}/T_e)^{0.7}\ \mathrm{m^3\,s^{-1}}$ [124] and $\beta_{e4} = 4\times10^{-12}\,(300\,\mathrm{K}/T_e)^{0.5}\ \mathrm{m^3\,s^{-1}}$ [125], respectively (here T_e is the electron temperature, which in this work was evaluated in terms of the electron mean energy with the use of the online version of the Bolsig+ solver [117] and the cross sections [118]). The total rate of electron-ion recombination, accounting for contributions of both these ion species, is $\beta_{e2}n_e n_{O_2^+} + \beta_{e4}n_e n_{O_4^+}$ and is represented in the considered model as $\beta_{ei}n_e n_{A^+}$, where n_{A^+} has the meaning of the sum $n_{O_2^+} + n_{O_4^+}$ and β_{ei} may be termed the electron-ion recombination coefficient.

One finds

$$\beta_{ei} = \frac{1}{1+z}\beta_{e2} + \frac{z}{1+z}\beta_{e4}, \tag{B.3}$$

where z is given by Eq. (B.1). Note that the second term on the rhs of Eq. (B.3), which describes the contribution of O_4^+ to the total recombination rate, can be appreciable even in cases where z is much lower than unity, since the recombination rate constant for this ion is much higher than that for O_2^+. (Note that the latter is a typical situation: rate constants of dissociative recombination for complex and cluster ions are by an order of magnitude higher than for diatomic ions.)

The coefficient of electron-ion recombination with participation of neutral molecules may be estimated by means of a formula similar to Eq. (B.2). The Langevin electron-ion recombination coefficient may be estimated in terms of the mobility μ_e of electrons, $\beta_{eL} = (e/\varepsilon_0)\,\mu_e$. Since the electron mobility is high (by two orders of magnitude higher than the ion mobility), the Langevin electron-ion recombination is negligible up to the gas pressures of about 100 atm. The three-body electron-ion recombination with the third body being a gas molecule has been studied in several gases, including CO_2 and H_2O. There are no data available on the three-body recombination of oxygen ions with electrons. In the experiment [126] on recombination of N_4^+ in nitrogen at $T_e = T$, the three-body process has not been observed up to the gas pressure of about 2 atm. It is also known (for CO_2) that the recombination coefficient for the three-body process decreases with increase of T_e much faster than that of the two-body process [127]. On the basis of this information, one can expect that the role of three-body electron-ion recombination with the third body being a gas molecule would not be very appreciable for air pressures up to several tens of atm, although this point requires future study. Thus, the electron-ion recombination with participation of neutral molecules will be neglected.

The rate constant of the three-body electron-ion recombination with a third body being the electron may be estimated as $1.4 \times 10^{-31}\,(T_e/300\,\mathrm{K})^{-4.5}\ \mathrm{m^6\,s^{-1}}$ [128]. This process comes into play at high electron densities, typically those exceeding $10^{24}\,\mathrm{m^{-3}}$, and may be accounted for by adding the corresponding term to the expression (B.3) if appropriate.

Appendix C

Effective reduced temperature of a pair of ion species in high electric fields

Let us consider the effective temperature T_α of an ion species α, which is defined by the equation $\frac{1}{2}m_\alpha\overline{(\mathbf{v}_\alpha - \mathbf{v}_{d\alpha})^2} = \frac{3}{2}kT_\alpha$ and characterizes the mean kinetic energy of the chaotic motion of the ions. Here $\mathbf{v}_\alpha$, m_α, and $\mathbf{v}_{d\alpha}$ are the particle velocity, particle mass, and average (drift) velocity of species α. This temperature may be evaluated by means of the Wannier formula in the form

$$\frac{3}{2}kT_\alpha = \frac{3}{2}kT + \frac{1}{2}Mv_{d\alpha}^2, \tag{C.1}$$

e.g., Eq. (6-2-13b) on p. 276 of [129]. Here M is the particle mass of the neutral gas. In the case of air, M is interpreted as a weighted average of N_2 and O_2 particle masses. It is natural to use the effective temperature T_α while evaluating Einstein's relation for the species α.

Let us consider the effective reduced temperature $T_{\alpha\beta}$ of species α and β, which characterizes the mean kinetic energy of relative motion of particles of species α and β and is defined by the equation $\frac{1}{2}m_{\alpha\beta}\overline{(\mathbf{v}_\alpha - \mathbf{v}_\beta)^2} = \frac{3}{2}kT_{\alpha\beta}$, where $m_{\alpha\beta} = m_\alpha m_\beta/(m_\alpha + m_\beta)$ is the reduced mass of the species. It can be shown that

$$\frac{3}{2}kT_{\alpha\beta} = \frac{3}{2}k\frac{m_\alpha T_\beta + m_\beta T_\alpha}{m_\alpha + m_\beta} + \frac{1}{2}m_{\alpha\beta}\left(\mathbf{v}_{d\alpha} - \mathbf{v}_{d\beta}\right)^2. \tag{C.2}$$

Note that the third factor in the first term on the rhs of Eq. (C.2) is the so-called reduced temperature of the species α and β, so the physical meaning of this equation is clear.

Note also that Eq. (C.2) is consistent with the well-known fact that the mean kinetic energy of relative motion of ions and neutrals is characterized by the effective

ion temperature: setting in (C.2) $v_{d\beta} = 0$, $m_\beta = M$, $T_\beta = T$, one obtains $T_{\alpha\beta} = T_\alpha$ as it should be.

Strictly speaking, the use of the effective reduced temperature $T_{\alpha\beta}$ for the evaluation of rate constants is justified in the case of binary ion-ion reactions. However, in the absence of better options it is natural to use these temperatures also in the case of three-body reactions, where the third body is a neutral particle, in the same way as the effective ion temperature is used for evaluation of rate constants of three-body ion-molecular reactions with the third body being a neutral particle. Note that in the particular case of ion-ion recombination reactions, the factor $(\mathbf{v}_{d\alpha} - \mathbf{v}_{d\beta})^2$ in (C.2) may be replaced by $(v_{d\alpha} + v_{d\beta})^2$.

Appendix D

Validation of the Local-Field and Quasi-Stationary Approximations

The fundamental mechanisms of gas discharges — ionization, drift, diffusion, recombination, and relaxations — have considerably different length and time-scales, and the conditions of the modelled setup will dictate what approximations are justified. In the hydrodynamic (drift-diffusion) description two main assumptions, or approximations, are made. The first is that the characteristic time for momentum transfer in collisions is assumed much shorter than the propagation time of any macroscopic characteristic. In particular, in a setup with a streamer, this would mean that the streamer head is at the same point during this characteristic time. The second assumption is that the characteristic distance of momentum transfer in collisions is much shorter than the space-variation of any macroscopic characteristic. This is also stated as inertia having a smaller influence than collision and for a setup with a streamer it means that the streamer properties are roughly the same over this characteristic distance. An analysis of the range of validity of the drift-diffusion approximation can be found in [130], where the assumption of negligible fluid inertia, as compared to the influence of collisions, is questioned for fields above 2000 Td.

The drift-diffusion equations comprise transport and kinetic coefficients that depend on the electric field. Here the validity of two approximations for these coefficients are studied. The Local-Field Approximation (LFA) related to length-scale variations and the Quasi-Stationary Approximation (QSA) related to time-scale variations. Validating the LFA will justify using the local electric field to calculate the transport and reaction rate coefficients. Validating the QSA will justify using the electric field at the considered time-instant to calculate the transport and reaction rate coefficients.

D.1 The Local-Field Approximation

The central issue is whether the space variation of the electric field is over length scales sufficiently large for the electron to collisionally relax fast enough to adjust the electron energy distribution function (EEDF) to the local value of the electric field. If it is, then the LFA is justified.

Collisional uniformization in air at standard temperature and pressure is related to the mean free path, for an electron in a weakly ionized plasma it is

$$\lambda_e = \frac{1}{n_h \bar{Q}_{eh}^{(1,1)}} \tag{D.1}$$

where $\bar{Q}_{eh}^{(1,1)}$ is the energy-averaged cross section for momentum transfer in electron-neutral collisions, plotted below in Fig. D.1, and n_h the number density of neutral particles. Each particle has its conservation and continuity equations and the length scale above which these equations are valid varies for each particle.

With the intention to obtain an expression for the length scale needed for electrons to relax to their equilibrium mean energy, the local energy balance written under the local-field quasi-stationary approximation is

$$j_e E = n_e \nu_{eh} \delta \frac{3}{2} k \left(T_e - T_h\right) \tag{D.2}$$

where n_e is the electron density, $j_e = e n_e v_d$ is the electron current density with $v_d = \mu_e E = eE/\left(m_e \nu_{eh}\right)$ relating drift speed (v_d) to mobility (μ_e) or ν_{eh} which is the number of electron-neutral collisions per second, δ is the fraction of electron energy lost per collision. In (D.2) the lhs is the electron energy gain per volume and time, due to the presence of an electric field, and the rhs is the electron energy loss per volume and time due to electron-neutral collisions. The fraction δ can be written as $\delta = 2\delta_u m_e/m_h$, where δ_u is the inelastic collision factor, i.e., a measure of how much the electron-neutral collisions deviate from being elastic collisions.

As expected, Fig. D.2a shows that the inelastic collision factor is two to four orders of magnitude larger than the elastic collision factor. The same figure also shows that the energy transferred to the electron per collision varies from less than 1% at 30 Td to 20% at 2000 Td typical of streamer propagation, meaning that at the higher fields fewer collisions are needed for the electron to relax to the mean energy.

The electron-neutral collision frequency can be written as $\nu_{eh} = n_h \bar{C}_e \bar{Q}_{eh}^{(1,1)}$, where $\bar{C}_e = \sqrt{8kT_e/\pi m_e}$ is the electron speed of chaotic motion, or, using (D.1), is written as

$$\nu_{eh} = \frac{\bar{C}_e}{\lambda_e}. \tag{D.3}$$

Using the foregoing relations, it follows from Eq. (D.2) that

$$E = \sqrt{\frac{12}{\pi}} \frac{k\sqrt{T_e\left(T_e - T_h\right)}}{e\lambda_u}, \tag{D.4}$$

where

$$\lambda_u = \lambda_e/\sqrt{\delta}. \tag{D.5}$$

The drift time of an electron over λ_u, namely $t_u = \lambda_u/v_d = \lambda_u/\left(\mu_e E\right)$, can be rewritten using (D.4), (D.5) and (D.3) to get

$$t_u = \frac{1}{\nu_{eh}\delta}\sqrt{\frac{16T_e}{3\pi\left(T_e - T_h\right)}}. \tag{D.6}$$

The number of collisions suffered by an electron during this time is $t_u\nu_{eh}$ and the corresponding energy lost by an electron during this time is

$$t_u\nu_{eh}\delta\frac{3}{2}k\left(T_e - T_h\right) = \frac{3}{2}kT_e\underbrace{\sqrt{\frac{16}{3\pi}}}_{1.3}\sqrt{\frac{T_e - T_h}{T_e}} \tag{D.7}$$

Given that the last two square-root multipliers on the rhs of (D.7) are of order unity, one can conclude that the energy lost by an electron during its drift over λ_u is comparable to its translational energy and therefore λ_u has the meaning of a length scale of the electron energy relaxation (spatial relaxation of the EEDF occurs on this length scale).

In Fig. D.2b it can be seen that the electron energy relaxation length scale λ_u does not exceed approximately $10\,\mu$m for all reduced fields of interest $E/n_h \geq 1\,$Td. For reduced fields of the order of 40 Td and higher, λ_u does not exceed approximately $1.5\,\mu$m. The reduced electric fields in active zones of gas discharges (e.g., in ionization regions of corona discharges or streamer heads of streamer discharges) are substantially higher than 40 Td and the local-field approximation is valid, unless the local scale of spatial variation of the electric field is of order of $1\,\mu$m or smaller, which is usually not the case. The reduced field outside active zones (e.g., in drift regions of corona discharges) may be smaller, however since there the local scale of spatial variation typically exceeds $10\,\mu$m, the LFA remains therefore valid.

Let L be a characteristic scale of variation of E. For $L \gg \lambda_u$, E does not vary significantly over the electron energy relaxation length and the exchange of energy is fast enough to adjust the EEDF to the local value of E. This is the condition of validity of the LFA. Both λ_e and λ_u are plotted in Fig. D.2b as functions of the reduced electric field.

The condition that needs to be satisfied for the LFA to be valid is [131],

$$\lambda_u\left|\frac{\mathbf{E}\cdot\boldsymbol{\nabla}E}{E^2}\right| \ll 1 \tag{D.8}$$

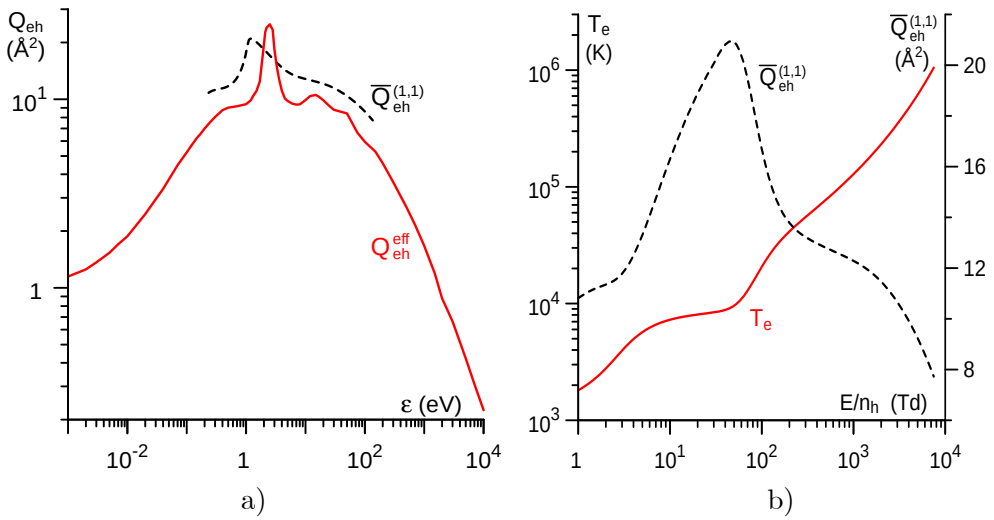

Figure D.1: a), solid: Q_{eh}^{eff} effective energy dependent collision cross-section between electron and artificial air (Phelps database, www.lxcat.net, retrieved on April 23, 2024). a), dashed: $\bar{Q}_{eh}^{(1,1)}$ averaged electron collision cross-section as a function of the electron mean energy (from Bolsig+ solver). b), solid: T_e electron temperature as a function of the reduced electric field. b), dashed: $\bar{Q}_{eh}^{(1,1)}$ averaged electron collision cross-section as a function of the reduced electric field.

where coefficient $|\mathbf{E}\cdot\boldsymbol{\nabla}E|/E^2$ is a measure of the spatial variation of the electric field in the numerical modelling at a particular point and time.

D.2 The Quasi-Stationary Approximation

The central issue is now whether the time variation of the electric field happens over time-scales large enough for the electron to collisionally relax fast enough to adjust the EEDF to the instantaneous value of the electric field. If it is, then the QSA is justified.

Let us introduce the electron mean free flight time $\tau_e = \nu_{eh}^{-1}$ and designate $\tau_u = \tau_e/\delta$, which will be seen to be the time-scale of the electron energy relaxation. Equation (D.6) may be rewritten as

$$t_u = \tau_u \frac{4}{\pi}\sqrt{\frac{T_e}{T_e - T_h}}. \tag{D.9}$$

Thus, τ_u is close to t_u the time of drift of an electron over λ_u. Energy lost by an electron during τ_u is given by an expression similar to Eq. (D.7):

$$\tau_u \nu_{eh}\delta\frac{3}{2}k\left(T_e - T_h\right) = \frac{3}{2}kT_e\sqrt{\frac{\pi}{3}}\frac{T_e - T_h}{T_e}. \tag{D.10}$$

Given that the last two multipliers on the rhs are of order unity, one can conclude that the energy lost by an electron during time τ_u is comparable to its translational energy

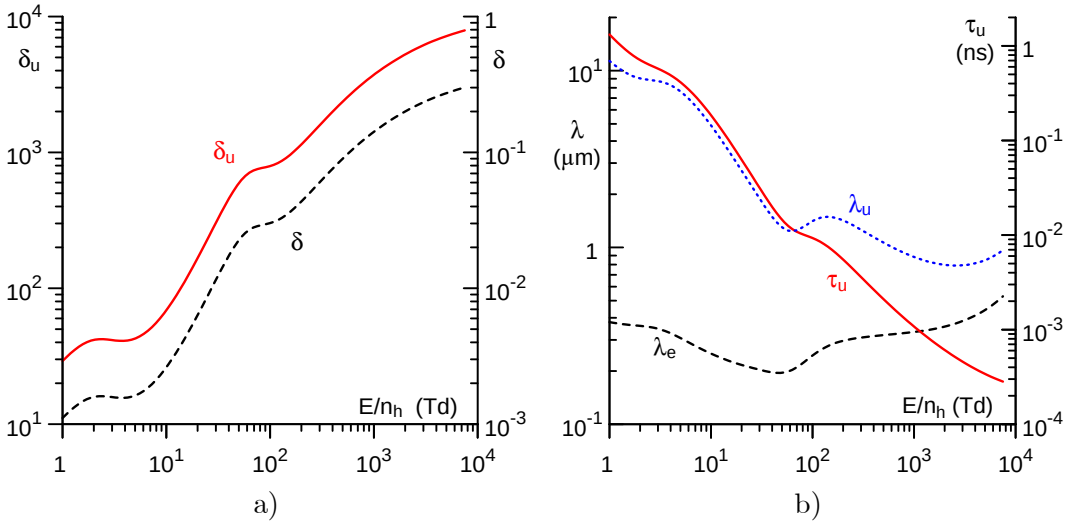

Figure D.2: a), solid: $\delta/(2m_e/M)$ inelastic collision factor. a), dashed: δ fraction of energy transferred per collision. b), solid: τ_u electron energy relaxation time. b), dashed: λ_e electron mean free path. b), dotted: λ_u electron energy relaxation length. Quantities are plotted as functions of the reduced electric field.

and therefore τ_u has the meaning of a time-scale of the electron energy relaxation (time relaxation of the EEDF occurs on this time-scale).

Let t be a characteristic time of variation of E. For $t \gg \tau_u$, E does not vary significantly during the electron energy relaxation time and the exchange of energy is fast enough to adjust the EEDF to the instantaneous value of E. This is the condition of validity of the QSA. The value for τ_u is plotted in Fig. D.2b as a function of the reduced electric field.

As can be seen in Fig. D.2b, the electron energy relaxation time τ_u does not exceed approximately 1 ns for all reduced fields $E/n_h \geq 1$ Td and is well below 0.1 ns for reduced fields of the order of 40 Td and higher. Hence, the QSA is justified for the vast majority of discharges in atmospheric-pressure air. Examples of exceptions are sub-nanosecond discharges and the post-discharge stage, where this approximation may fail.

The condition that needs to be satisfied for the QSA to be valid is [131],

$$\tau_u \left| \frac{dE/dt}{E} \right| \ll 1 \tag{D.11}$$

where coefficient $|dE/dt|/E$ is a measure of the time variation of the electric field in the numerical modelling at a particular point and time.

D.3 Validation in Simulations

In [132] condition (D.11) was studied in artificial air at 1 atm for different rates of change of the electric field. The electron Boltzmann equation was solved with and without an explicit term for the time-variation of the distribution function. Results show significant deviations between the exact and quasi-stationary EEDFs when the electric field rise-times from 0 to 50 Td were 1 ns or shorter. The deviations started right at the beginning of the electric field variation, resulting in significant deviations for the predominant low-energy electrons, i.e. below 2 eV. Deviations only became negligible at the end of the field rise-time. The authors show similar results for the electron mean energy and the electron power transfer, with the notable difference that the deviations are negligible already one order of magnitude before the terminus of the rise-time of 1 ns and two orders of magnitude earlier for a rise-time of 1 μs. The mentioned deviations raise the question whether streamers can be properly described by the QSA, since at their heads time variations are in the nanosecond range. The significant deviation of the EEDF at electron energies below 2 eV is related to the low fraction of electron energy transfer (δ) at low fields, see Fig. D.2a. This deviation however isn't critical in streamer modelling since at low energies very few electrons are present and therefore this deviation doesn't affect the gain and loss processes as much as at higher energies. This is the reason why the details of the EEDF at low energies are not that important, since energy-dependent quantities, like reaction rate constants, are very low at low energies. Furthermore, from [132] it can be seen that the mentioned rapid convergence in time of the exact and quasi-stationary results for the electron mean energy and power transfer, for rise-times of 1 ns and 1 μs, means that it is only during the initial instances, when the field increases to about 10% of its final value, that these quantities aren't suitably calculated in the quasi-stationary approximation, being this the time during which electrons have lower energy. If a higher electric field offset is used, there will also be a larger electron energy fraction transferred in collisions (δ), which favors a more rapid equilibrium of electron mean energy. In [133] electric field rise and fall times of 20 ns between 100 and 300 Td were studied in pure Nitrogen at a pressure of 1 torr and 300 K. In this work an approximate approach is used, based on the theory of perturbations using the parameter of the inequality in (D.11), which is presumed to be small. A comparison was made of this approximate approach with the exact and the quasi-stationary approach. For the calculated ionization rate constants, the quasi-stationary approach systematically over-estimated the values in rise-times and sub-estimated them in fall-times to about a factor of 2 to 3 relative to the exact value. This was to be expected, since at low pressures the QSA doesn't allow electrons to locally relax to a well defined energy value due to the reduced number of electron-

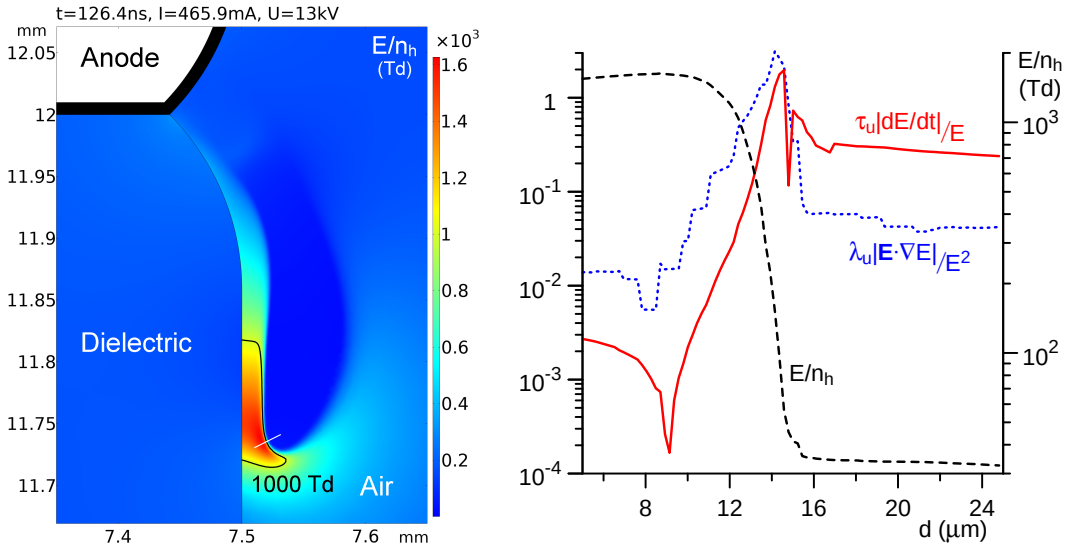

Figure D.3: Positive streamer over dielectric surface. a): E/n_h reduced electric field distribution. a), black line: contour for $E/n_h = 1000\,\mathrm{Td}$. a), white line: segment along which quantities in b) are calculated. b): Quantities plotted along the white line of a). b), dashed: reduced electric field. b), solid: $\tau_u \left|dE/dt\right| /E$ of (D.11). b), dotted: $\lambda_u \left|\mathbf{E}\cdot\boldsymbol{\nabla}E\right| /E^2$ of (D.8).

neutral collisions. For a more direct test as to whether a drift-diffusion description with the LFA-QSA is suitable for describing streamer dynamics at atmospheric pressure, Naidis in [134] took into account nonlocal effects in the calculation of rate constants following [133]. It was shown that the LFA-QSA can be used with practical accuracy to calculate the main characteristics of a streamer. It is known that the LFA-QSA is particularly bad at low pressure, for electrons emitted off electrodes and dielectrics by ion bombardment, and for describing electron transport in the sheath [135, 136], but at the pressure of 1 atm, used in the present work, the above mentioned constraints aren't expected to be important. For the purpose of verifying these assertions we check whether, in our calculations, the electric field's spatial and temporal variations are so high that the collision rates are unable to impart to the electrons their mean energy. This verification is done for the usual setup, see Fig. 4.1, subject to a high overvoltage and at an instant where there is already a positive streamer propagating in the gap close to a dielectric surface as seen in Fig. D.3a. The LFA and QSA conditions of (D.8) and (D.11) are checked for the white line at the streamer's head, shown in Fig. D.3a, along which gradients in space and time are expected to be more pronounced. Results of this verification are shown in Fig. D.3b. In Fig. D.4a and D.4b the validity of respectively the LFA and QSA is also checked in a larger region.

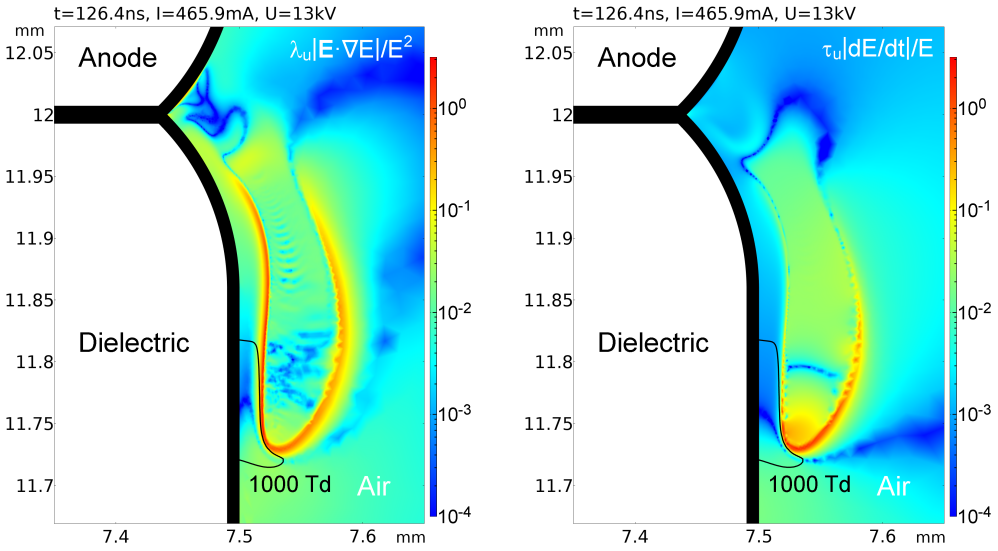

Figure D.4: Positive sreamer over dielectric surface. a), b), black line: contour for $E/n_h = 1000\,\mathrm{Td}$. a): $\lambda_u \left|\mathbf{E}\cdot\boldsymbol{\nabla}E\right|/E^2$ of (D.8). b): $\tau_u \left|dE/dt\right|/E$ of (D.11).

Results from Fig. D.3b show that in a narrow region about $1.5\,\mu$m wide, where the electric field decays approximately from 500 to 50 Td, the LFA isn't strictly valid, likewise the QSA isn't strictly valid in a narrow region about $0.5\,\mu$m wide where the electric field decays approximately from 200 to 50 Td. What mitigates these cautionary notes on the validity of LFA and QSA is the very small spatial extent over which they occur and the fact that they happen outside the bulk of the streamer where the main physical processes that affect the discharge, dominate. It was also verified that the high values of the electric field didn't lead to critical anisotropy of the EEDF, since the drift velocity was no larger than 30% of the thermal velocity.

One can conclude that the local-field quasi-stationary approximation is justified for the vast majority of discharges in atmospheric-pressure air, although analysis of space and time-scales of variation of the electric field may be needed in some cases.

Bibliography

[1] J.J.Thomson, *Conduction of electricity through gases*, 1st ed. (Cambridge University press, Ave Maria Lane, London, 1903).

[2] T. J. Hammons, V. F. Lescale, K. Uecker *et al.*, Proceedings of the IEEE **100**, 360 (2012).

[3] G. Shi, X. Cai, C. Sun *et al.*, in *12th IET International Conference on AC and DC Power Transmission (ACDC 2016)* (2016) pp. 1–6.

[4] P. Bordignon, in *2019 21st European Conference on Power Electronics and Applications (EPE '19 ECCE Europe)* (2019) pp. 1–1.

[5] C. Li, J. Fu, Y. Zi, and Y. Cao, IEEE Electrical Insulation Magazine **38**, 6 (2022).

[6] V. Madonna, P. Giangrande, and M. Galea, IEEE Trans. Transportation Electrification **4**, 646 (2018).

[7] M. Lizcano, in *SAE Aircraft High Voltage Workshop* (2018) mukliteo, WA, USA.

[8] E. Kuffel, W. S. Zaengl, and J. Kuffel, *High Voltage Engineering*, 2nd ed. (Newnes, Oxford, 2000).

[9] Y. Bourek, L. Mokhnache, N. N. Said, and R. Kattan, Electr. Pow. Syst. Research **81**, 2038 (2011).

[10] J. S. E. Townsend, *Electricity in Gases*, 1st ed. (Oxford, Clarendon Press, Broad street, Oxford, 1915).

[11] S. Nijdam, J. Teunissen, and U. Ebert, Plasma Sources Sci. Technol. **29**, 103001 (2020).

[12] I. Adamovich, S. Agarwal, E. Ahedo *et al.*, J. Phys. D: Appl. Phys. **55**, 373001 (2022).

[13] J. Omidi, Clean Energy **8**, 197 (2024), see https://academic.oup.com/ce/article-pdf/8/1/197/56289208/zkad085.pdf% BibitemShut NoStop

[14] J. M. Meek and J. D. Craggs, *Electrical Breakdown of Gases*, 1st ed. (Oxford, Clarendon Press, Oxford, 1953).

[15] L. B. Loeb and J. M. Meek, Journal of Applied Physics **11**, 459 (1940), see https://pubs.aip.org/aip/jap/article-pdf/11/7/459/18304683/459_1_online.pdf.

[16] H. Raether, *Electron avalanches and breakdown in gases*, 1st ed. (Butterworth & Co., 88 Kingsway, London, 1964).

[17] J. Qin and V. P. Pasko, J. Phys. D: Appl. Phys. **47**, 435202 (2014).

[18] A. Dubinova, *Modeling of streamer discharges near dielectrics*, Phd thesis 2 (research not tu/e / graduation tu/e), Applied Physics and Science Education (2016), phD Thesis in English.

[19] V. F. Tarasenko, G. V. Naidis, D. V. Beloplotov *et al.*, Plasma Physics Reports **46**, 320 (2020).

[20] Yu. P. Raizer, *Gas Discharge Physics* (Springer, Berlin, 1991).

[21] A. Pokryvailo, in *2017 IEEE 21st International Conference on Pulsed Power (PPC)* (2017) pp. 1–4.

[22] M. Robinson, J. Appl. Phys. **40**, 5107 (1969).

[23] N. L. Allen and A. Ghaffar, J. Phys. D: Appl. Phys. **28**, 331 (1995).

[24] H. C. Miller, IEEE Trans. Dielectr. Electr. Insul. **22**, 3641 (2015).

[25] A. S. Pillai and R. Hackam, J. Appl. Phys. **58**, 146 (1985).

[26] I. A. Bean, C. S. Adams, and T. Weber, IEEE Trans. Dielectr. Electr. Insul. **27**, 1982 (2020).

[27] T. S. Sudarshan and R. A. Dougal, IEEE Trans. Electr. Insul. **EI-21**, 727 (1986).

[28] Y. Meng, H. Xuan, Z. Deng *et al.*, J. Phys. D: Appl. Phys. **55**, 385203 (2022).

[29] Z. Jia, B. Zhang, X. Tan, and Q. Zhang, in *2009 Asia-Pacific Power and Energy Engineering Conference* (2009) pp. 1–4.

[30] X. Meng, L. Wang, H. Mei *et al.*, Polymers **14** (2022), https://dx.doi.org/10.3390/polym14050897.

[31] R. W. Macpherson, M. P. Wilson, I. V. Timoshkin *et al.*, IEEE Trans. Dielectr. Electr. Insul. **31**, 204 (2024).

[32] H. K. Meyer, R. Marskar, H. G. Osberg, and F. Mauseth, IEEE Trans. Dielectr. Electr. Insul. **30**, 2862 (2023).

[33] M. A. Baferani, C. Li, T. Shahsavarian *et al.*, IEEE Trans. Dielectr. Electr. Insul. **28**, 223 (2021).

[34] C. Li, T. Shahsavarian, M. A. Baferani *et al.*, IEEE Trans. Dielectr. Electr. Insul. **28**, 240 (2021).

[35] B. Zhang, Y. Li, D. Min *et al.*, J. Phys. D: Appl. Phys. **57**, 103001 (2023).

[36] S. T. Pai and J. P. Marton, Journal of Applied Physics **53**, 8583 (1982), see `https://pubs.aip.org/aip/jap/article-pdf/53/12/8583/18400427/8583_1_online.pdf`.

[37] G. Blaise and C. Le Gressus, J. Appl. Phys. **69**, 6334 (1991), see `https://pubs.aip.org/aip/jap/article-pdf/69/9/6334/18642767/6334_1_online.pdf`.

[38] T. Asokan and T. Sudarshan, IEEE Trans. Electr. Insul. **28**, 101 (1993).

[39] C. Li, J. Hu, and C. Lin, Scientific Reports **7**, 3271 (2017).

[40] J. Sun, S. Song, J. Zheng *et al.*, IEEE Trans. Dielectr. Electr. Insul. **29**, 1 (2022).

[41] Z. Li, J. Liu, Y. Ohki *et al.*, High Voltage **8**, 853 (2023), see `https://ietresearch.onlinelibrary.wiley.com/doi/pdf/10.1049/hve2.12340`.

[42] K. Nakai, A. Komuro, and H. Nishida, Physics of Plasmas **27**, 063518 (2020), see `https://pubs.aip.org/aip/pop/article-pdf/doi/10.1063/5.0006868/16052668/063518_1_online.pdf`.

[43] C. Ren, B. Huang, C. Zhang *et al.*, Plasma Sources Sci. Technol. **32**, 025004 (2023).

[44] M. Florkowski, Measurement **186**, 110170 (2021).

[45] H. K. H. Meyer, R. Marskar, and F. Mauseth, Plasma Sources Sci. Technol. **31**, 114006 (2022).

[46] X. Li, A. Sun, G. Zhang, and J. Teunissen, Plasma Sources Sci. Technol. **29**, 065004 (2020).

[47] D. J. M. Trienekens, S. Nijdam, and U. Ebert, IEEE Trans. Plasma Sci. **42**, 2400 (2014).

[48] F. Tochikubo and A. Komuro, Jap. J. Appl. Phys. **60**, 040501 (2021).

[49] B. Schober and U. Schichler, in *2022 9th International Conference on Condition Monitoring and Diagnosis (CMD)* (2022) pp. 225–230.

[50] L. Taibaoui, B. Zegnini, and A. Mahdjoubi, in *2022 19th International Multi-Conference on Systems, Signals & Devices (SSD)* (2022) pp. 1842–1847.

[51] N. Fahimi, H. R. Sezavar, and A. A. Shayegani-Akmal, IEEE Trans. Dielectr. Electr. Insul. **30**, 122 (2023).

[52] M. S. Benilov, P. G. C. Almeida, N. G. Ferreira *et al.*, J. Appl. Phys. **130**, 121101 (2021).

[53] L. C. Pitchford, L. L. Alves, K. Bartschat *et al.*, Plasma Processes Polym. **14**, 1600098 (2017).

[54] A. T. del Caz, V. Guerra, D. Gonçalves *et al.*, Plasma Sources Sci. Technol. **28**, 043001 (2019).

[55] M. A. Lieberman and A. J. Lichtenberg, *Principles of Plasma Discharges and Material Processing*, 2nd ed. (Wiley, New York, 2005).

[56] P. G. C. Almeida, M. S. Benilov, M. D. Cunha, and J. G. L. Gomes, Plasma Processes Polym. **14**, 1600122 (2017).

[57] M. J. Kushner, J. Phys. D: Appl. Phys. **38**, 1633 (2005).

[58] J. van Dijk, K. Peerenboom, M. Jimenez *et al.*, J. Phys. D: Appl. Phys. **42**, 194012 (2009).

[59] P. G. C. Almeida, R. M. S. Almeida, N. G. C. Ferreira *et al.*, Plasma Sources Sci. Technol. **29**, 125005 (2020).

[60] P. G. C. Almeida, M. S. Benilov, and M. J. Faria, J. Phys. D: Appl. Phys. **44**, 415203 (2011).

[61] A. Bourdon, V. P. Pasko, N. Y. Liu *et al.*, Plasma Sources Sci. Technol. **16**, 656 (2007).

[62] N. G. C. Ferreira, D. F. N. Santos, P. G. C. Almeida *et al.*, J. Phys. D: Appl. Phys. **52**, 355206 (2019).

[63] M. B. Zheleznyak, A. K. Mnatsakanyan, and S. V. Sizykh, High Temp. **20**, 357 (1982).

[64] G. V. Naidis, J. Phys. D: Appl. Phys. **38**, 2211 (2005).

[65] L. Papageorgiou, A. C. Metaxas, and G. E. Georghiou, J. Phys. D: Appl. Phys. **44**, 045203 (2011).

[66] P. Dordizadeh, K. Adamiak, and G. S. P. Castle, Plasma Sources Sci. Technol. **25**, 065009 (2016).

[67] A. Hopf, M. Rossner, F. Berger, and A. Kuchler, in *2020 IEEE Electrical Insulation Conference (EIC)* (IEEE, Virtual Event, 2020) pp. 118–123.

[68] Y. Zheng, B. Zhang, and J. He, Phys. Plasmas **18**, 123503 (2011).

[69] N. Monrolin, O. Praud, and F. Plouraboué, Phys. Plasmas **25**, 063503 (2018).

[70] M. S. Benilov, Sov. Phys. - Tech. Phys. **33**, 1267 (1988), see `https://fisica.uma.pt/Pub/Mikhail_Benilov/bib/1988d.pdf`.

[71] M. S. Benilov, Phys. Rev. E **77**, 036408 (2008).

[72] M. S. Benilov and M. D. Cunha, Phys. Rev. E **68**, 056407 (2003).

[73] N. G. C. Ferreira, G. V. Naidis, and M. S. Benilov, J. Phys. D: Appl. Phys. **54**, 255203 (2021).

[74] R. M. S. Almeida, P. G. C. Almeida, G. V. Naidis, and M. S. Benilov, Plasma Sources Sci. Technol. **32**, 105014 (2023).

[75] A. V. Phelps and Z. Lj. Petrović, Plasma Sources Sci. Technol. **8**, R21 (1999).

[76] D. Marić, M. Savić, J. Sivoš *et al.*, Eur. Phys. J. D **68**, 155 (2014).

[77] T. Kihara, Rev. Mod. Phys. **24**, 45 (1952).

[78] V. A. Lisovsky and V. D. Yegorenkov, J. Phys. D: Appl. Phys. **27**, 2340 (1994).

[79] R. V. Hodges, R. N. Varney, and J. F. Riley, Phys. Rev. A **31**, 2610 (1985).

[80] D. Marić, N. Škoro, G. Malović, and Z. L. Petrović, Plasma Sources Sci. Technol. **21**, 035016 (2012).

[81] P. J. Bruggeman, M. J. Kushner, B. R. Locke *et al.*, Plasma Sources Sci. Technol. **25**, 053002 (2016).

[82] G. V. Naidis, IEEE Trans. Dielectr. Electr. Insul. **22**, 2428 (2015).

[83] N. Druker, G. Goldwine, and E. Sher, Int. J. Engine Res. **22**, 341 (2021).

[84] T. You, X. Dong, W. Zhou *et al.*, IEEE Trans. Dielectr. Electr. Insul. **29**, 1633 (2022).

[85] J. Y. Kim, I. Kaganovich, and H.-C. Lee, Plasma Sources Sci. Technol. **31**, 033001 (2022).

[86] H. Noori and I. Jõgi, Phys. Lett. A **438**, 128111 (2022).

[87] R. Färber, Y. Lu, M. Balmelli *et al.*, J. Phys. D: Appl. Phys. **56**, 435204 (2023).

[88] R. Janalizadeh and V. P. Pasko, Plasma Sources Sci. Technol. **28**, 105006 (2019).

[89] G. F. Carrier and C. E. Pearson, *Partial Differential Equations: Theory and Technique* (Academic Press, London and New York, 1976).

[90] V. P. Pasko, R. Janalizadeh, and J. Jansky, Plasma Sources Sci. Technol. **32**, 075014 (2023).

[91] J. Dutton, J. Phys. Chem. Ref. Data **4**, 577 (1975).

[92] A. Pedersen, IEEE T. Power. Ap. Syst. **PAS-89**, 2043 (1970).

[93] M. Robinson, IEEE T. Power. Ap. Syst. **PAS-86**, 185 (1967).

[94] N. G. C. Ferreira, P. G. C. Almeida, M. S. Benilov *et al.*, IEEE Trans. Plasma Sci. **48**, 4080 (2020).

[95] F. W. Peek, Proc. Am. Inst. Electr. Eng. **31**, 717 (1912).

[96] A. Dubinova, D. Trienekens, U. Ebert *et al.*, Plasma Sources Sci. Technol. **25**, 055021 (2016).

[97] M. Saltzer, U. Gäfvert, B. Källstrand *et al.*, in *2011 Annual Report Conference on Electrical Insulation and Dielectric Phenomena* (IEEE, 2011) pp. 141–144.

[98] H. Ootera and K. Nakanishi, IEEE Trans. Pow. Deliv. **3**, 165 (1988).

[99] H. Fujinami, T. Takuma, M. Yashima, and T. Kawamoto, IEEE Pow. Eng. Rev. **9**, 62 (1989).

[100] T. S. Sudarshan, in *ATS Seminars, CERN, Switzerland* (2013) see https://indico.cern.ch/event/254522/.

[101] V. V. Timatkov, G. J. Pietsch, A. B. Saveliev *et al.*, J. Phys. D: Appl. Phys. **38**, 877 (2005).

[102] L. A. Lazaridis and P. N. Mikropoulos, IEEE Trans. Dielectr. Electr. Insul. **15**, 694 (2008).

[103] H. C. Miller, IEEE Trans. Electr. Insul. **24**, 765 (1989).

[104] M. S. Benilov and A. V. Lyashko, Sov. Phys. - Tech. Phys. **36**, 601 (1991), see https://fisica.uma.pt/Pub/Mikhail_Benilov/bib/1991b.pdf.

[105] M. S. Benilov and G. V. Naidis, J. Phys. D: Appl. Phys. **38**, 3599 (2005).

[106] M. S. Benilov, G. V. Naidis, Z. L. Petrovic *et al.*, J. Phys. D: Appl. Phys. **39**, 2959 (2006).

[107] M. S. Benilov, A. V. Lyashko, and V. I. Kovbasyuk, in *Proc. X Int. Conf. on MHD Electrical Power Generation (Dec. 1989, Tiruchirapalli, India)*, Vol. 2 (Tiruchirapalli, India, 1989) pp. X.105–X.109.

[108] G. J. M. Hagelaar, F. J. de Hoog, and G. M. W. Kroesen, Phys. Rev. E **62**, 1452 (2000).

[109] V. V. Gorin, A. A. Kudryavtsev, J. Yao *et al.*, Phys. Plasmas **27**, 013505 (2020).

[110] M. Sajben, AIAA J. **8**, 400 (1970).

[111] A. V. Filippov, I. N. Derbenev, N. A. Dyatko *et al.*, J. Exp. Theor. Phys. **125**, 246 (2017).

[112] I. A. Kossyi, A. Y. Kostinsky, A. A. Matveyev, and V. P. Silakov, Plasma Sources Sci. Technol. **1**, 207 (1992).

[113] L. A. Viehland and E. A. Mason, At. Data Nucl. Data Tables **60**, 37 (1995).

[114] N. Popov, Plasma Physics Reports **36**, 812 (2010).

[115] H. Böhringer, D. W. Fahey, W. Lindinger *et al.*, Int. J. Mass Spectrom. Ion Processes **81**, 45 (1987).

[116] R. S. Sigmond, J. Appl. Phys. **56**, 1355 (1984).

[117] G. J. M. Hagelaar and L. C. Pitchford, Plasma Sources Sci. Technol. **14**, 722 (2005).

[118] Phelps database, `www.lxcat.net` (retrieved Jan. 29, 2019).

[119] S. Pancheshnyi, J. Phys. D: Appl. Phys. **46**, 155201 (2013).

[120] J. Sayers and E. V. Appleton, Proc. R. Soc. Lond. A **169**, 83 (1938).

[121] A. Fridman, *Plasma Chemistry* (Cambridge University Press, Cambridge, UK, 2008).

[122] D. R. Bates and M. R. Flannery, J. Phys. B: At. Mol. Phys. **2**, 184 (1969).

[123] D. R. Bates, J. Phys. B: At. Mol. Phys. **13**, L623 (1980).

[124] C. H. Sheehan and J. P. St.-Maurice, J. Geophys. Res. Space Phys. **109**, A03302 (2004).

[125] J. L. Dulaney, M. A. Biondi, and R. Johnsen, Phys. Rev. A **37**, 2539 (1988).

[126] Y. Ikezoe, S. Matsuoka, and H. Nakamura, Chem. Phys. Lett. **177**, 366 (1991).

[127] I. M. Littlewood, M. C. Cornell, B. K. Clark, and K. J. Nygaard, J. Phys. D: Appl. Phys. **16**, 2113 (1983).

[128] B. Makin and J. C. Keck, Phys. Rev. Lett. **11**, 281 (1963).

[129] E. A. Mason and E. W. McDaniel, *Transport Properties of Ions in Gases* (Wiley, New York, 1988).

[130] Y. Zhu, X. Chen, Y. Wu *et al.*, Plasma Sources Sci. Technol. **30**, 075025 (2021).

[131] M. J. Kushner, in *Nonequilibrium Processes in Partially Ionized Gases*, Vol. 220, edited by M. Capitelli and J. N. Bardsley (Plenum Press, New York, 1990) pp. 63–90, in NATO ASI Series B: Physics.

[132] A. Tejero-del Caz, V. Guerra, N. Pinhão *et al.*, Plasma Sources Sci. Technol. **30**, 065008 (2021).

[133] N. Aleksandrov, N. Dyatko, and I. Kochetov, Fizika Plazmy **21**, 806 (1995).

[134] G. V. Naidis, Tech. Phys. Letters **23**, 493 (1997).

[135] D. P. Lymberopoulos and D. J. Economou, J. Res. Natl. Inst. Stand. Technol. **100**, 473 (1995).

[136] G. K. Grubert, M. M. Becker, and D. Loffhagen, Phys. Rev. E **80**, 036405 (2009).